Studies on Luminescence and Quenching Mechanisms in Phosphors for Light Emitting Diodes

Cover Photograph: Luminescent materials generated in the preparation of this thesis. Photographs made by the author.

Printed by Datawyse B.V.

Bachmann, Volker Michael
Studies on Luminescence and Quenching Mechanisms
in Phosphors for Light Emitting Diodes
(Studies aan luminescentie- en doofmechanismen in
fosforen voor licht emitterende diodes)
Volker Michael Bachmann, Utrecht: Universiteit Utrecht,
Condensed Matter and Interfaces, Debye Instituut.
Proefschrift Universiteit Utrecht. Met een samenvatting
in het Nederlands
ISBN: 978-90-3934600-6

Studies on Luminescence and Quenching Mechanisms in Phosphors for Light Emitting Diodes

Studies aan luminescentie- en doofmechanismen in fosforen voor licht emitterende diodes

(met een samenvatting in het Nederlands)

Proefschrift

ter verkrijging van de graad van doctor aan de Universiteit Utrecht op gezag van de rector magnificus, prof. dr. W. H. Gispen, ingevolge het besluit van het college voor promoties in het openbaar te verdedigen op woensdag 12 september 2007 des middags te 12.45 uur

door

Volker Michael Bachmann

geboren op 21 juni 1977 te Leipzig, Duitsland

Promotoren: Prof. dr. A. Meijerink
Prof. dr. C. R. Ronda

The work described in this thesis is financially supported by Philips Technologie GmbH Forschungslaboratorien, Aachen, Germany.

Rot, Orange, Gelb und Grün sind im Regenbogen drin,
Blau und Indigo geht‘s weiter auf der Regenbogenleiter,
Und dann kommt das Violett, sieben Farben sind‘s komplett.

(Reinhard Lakomy/Monika Ehrhardt)

Content

Chapter 1: Introduction

This thesis is concerned with luminescent materials, known as phosphors, which function as color converter in light emitting diodes (LEDs). It presents optical investigations on new and known materials. The aim is to study and explain the mechanisms behind luminescence properties and the luminescence quenching processes. This information is crucial in the development of better phosphors in the prospering field of solid state lighting. In this introductory chapter background information to different aspects of white LEDs and luminescence is given, as well as a summary of the results.

1.1 A short history of Solid State Lighting

Today we are on the bridge to the age of sold state lighting. Using artificial light to lengthen the day beyond the time of sunset goes back thousands of years. For a long the time the light generated was of thermal origin. Ancient mankind created light by burning wood. A historical summary of the development of light sources is given by Žukauskas et al. in the book "Introduction to Solid-State Lighting" [1]. The following milestones in lighting are taken from this reference.

[…] The limelight was the first solid-state lighting device. It was introduced by Thomas Drummond in 1826 and consisted of a cylinder of calcium oxide (lime). It was brought to a state of glittering radiance by a oxyhydrogen flame from an blowpipe. This device used a novel emission effect – candoluminescence – which was discovered by Goldsworthy Gurney in 1820. In candoluminescence ions are thermally excited, which leads to emission in addition to the blackbody incandescence. […]

Today we know many different types of luminescence: electroluminescence, photoluminescence, chemoluminescence, bioluminescence, and triboluminescence to name a few. Even before electricity became a commodity, new possibilities were found in making light.

[…] Sir Humphry Davy was the first to demonstrate an arc between two carbon rods (discharge) and a glowing wire which was heated by electric current (incandescence). Thereby he discovered around 1800 the principles of electric lighting only shortly after the Italian physicist Alessandro Volta invented an early type of battery. Already in the seventeenth century the principle of luminous discharge of static electricity was discovered. Although there was a lot work done since the invention of Davy a change from utilizing a flame to electric powered lighting was not achieved until the invention of the dynamo by Z. T. Gramme in the 1870s. The inconvenience of having to use the non-continuous power supply of a battery prevented an earlier breakthrough of the then new technology in lighting. […]

It was Paul Jablochkoff who fabricated the first arc based electric lighting device in 1876. Thomas Alva Edison got a patent granted in 1879 for a filament (or incandescent) lamp [2]. He started out with a carbonized-paper filament which was replaced after 1903 by a tungsten filament [3]. At almost

the same time Peter Cooper Hewitt introduced the first gas discharge lamp (mercury vapor lamp). This was the basis for the fluorescent lamp that was introduced in 1938. GE and Westinghouse Electric Corporation used the UV radiation emitted by the low pressure mercury plasma to excite fluorescent powders coated on the inside of a glass tube. At present fluorescent tubes are the most efficient source for generating white light for general lighting applications. The competition from white light emitting diodes is however increasing and will change the future of lighting.

1.2 Light Emitting Diodes

The phosphors discussed in this thesis are designed for application in (white) Light Emitting Diodes. This section will present some background information on LEDs. The type of luminescence found in LEDs is a special form of electroluminescence, also known as injection luminescence. It represents the most efficient subgroup of electroluminescence. The process of charge carrier injection is the basis of operation in all LEDs used in semiconductor-based solid-state lamps [1]. The first to observe this phenomenon was H.J. Round in 1907 [4]. He injected charge carriers into silicon carbide via a metal contact and observed the emission of yellowish light. Injection luminescence started to receive more attention after Holonyak and Bevacqua invented the red LED in 1962 [5].
The performance of an LED is typically characterized by its radiant efficiency [1]

(eq. 1-1) $$\eta_e = \eta_{ext}\,\eta_f$$

where η_{ext} is the external quantum efficiency and η_f is the feeding efficiency. The external quantum efficiency η_{ext} is the product of three components: internal quantum efficiency (radiative efficiency) η_{rad}; injection efficiency η_{inj}; and the light-extraction efficiency (optical efficiency) η_{opt}.

(eq. 1-2) $$\eta_{ext} = \eta_{inj} \times \eta_{rad} \times \eta_{opt}$$

The feeding efficiency is the ratio of the energy of the photon emitted $h\nu$ and the total energy an electron-hole-pair acquires from the power source when passing through the LED

(eq. 1-3) $$\eta_f = \frac{h\nu}{qV}$$

where V is the forward voltage drop across the LED and q is the elementary charge [1].
In a direct-gap semiconductor the internal quantum efficiency is defined as ratio of the radiative recombination rates to total recombination rates (radiative and non-radiative).

(eq. 1-4) $$\eta_{rad} = \frac{\tau}{\tau_r} = \frac{1}{1 + \tau_r / \tau_{nr}}$$

In its simplest design, an LED consists of a p-type semiconductor and an n-type semiconductor of the same kind (p-n homojunction). Either one or both of the conductive regions can act as radiative-recombination zone. In modern high-power LEDs a much more sophisticated design is used since this simple design has a number of disadvantages. These are [1]:

- Light generated from the active region is reabsorbed in the conductive regions, which reduces the light extraction efficiency η_{opt}
- High internal quantum efficiency is obtained only in one conductive region (mostly p-type), which requires low injection levels in the n-type region. Asymmetric doping levels can solve this but will lead to increased re-absorption in the highly doped region
- Highly doped regions can contain more impurities serving as centers of additional non-radiative recombination

Modern high-power LEDs are made of three different types of layers. One speaks of a heterostructure LED. Each type has a different band gap E_g. A typical design comprises an n-type conductive layer with E_{g1}, an active layer with E_{g2}, a p-type electron blocking layer (EBL) with E_{g3}, and a p-type conductive layer with E_{g1}. For the different band gaps the following relation applies (compare Figure 1-1):

(eq. 1-5) $$E_{g3} > E_{g1} > E_{g2}$$

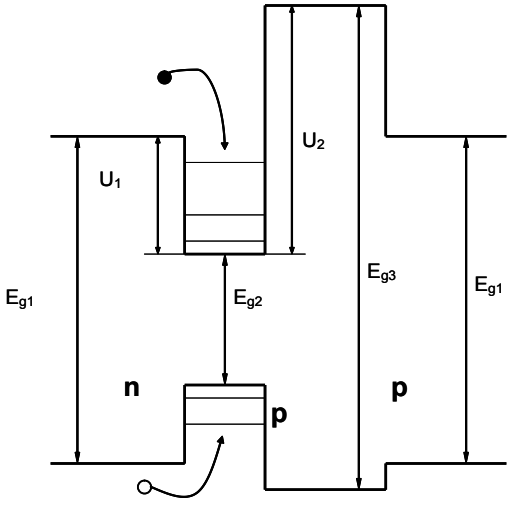

Figure 1-1: Band alignment diagram of an electroluminescent structure based on a quantum well with an electron blocking layer (asymmetric QW).

1.3 White light LEDs

The history of white light LEDs starts with the invention of the blue emitting InGaN-based LED by Nakamura in 1991 [6]. The development of the high-power LED in the years after this [7] was the technological basis to achieve the goal of an efficient white light solid-state lighting device. Starting at very low efficiencies, the white light LEDs of today have already surpassed incandescent and halogen lamps in their luminous efficiency and are on the road to exceed the efficiency of a fluorescent tube lamp (for many years the most efficient white light source). Low power LEDs (< 1 W power consumption) have already demonstrated higher efficiencies, up to 150 lm/W. Figure 1-2 shows a graph that compares the efficiency of different light sources with the efficiency development of LEDs over time.
The standard white light phosphor converted LED (pc-LED) consists of a yellow emitting phosphor (YAG:Ce^{3+} [8], also see chapter 5 and 6) besides

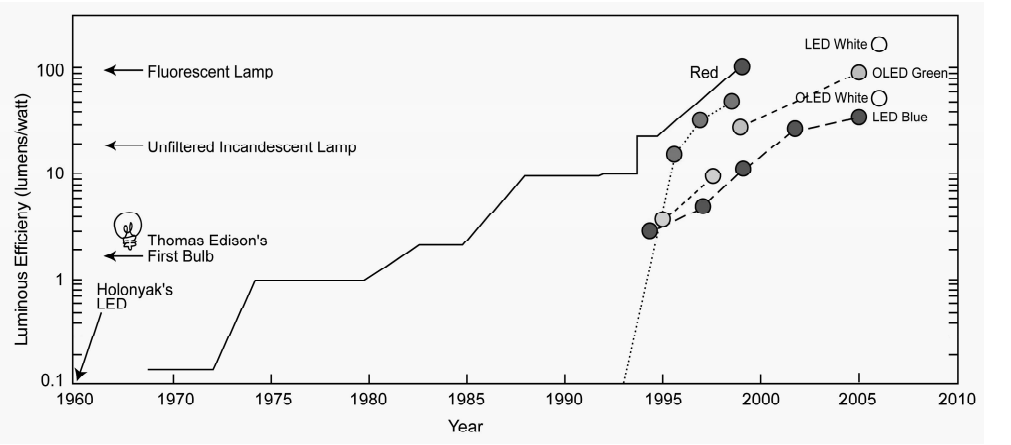

Figure 1-2 Comparison of the efficiency of different light sources with the efficiency development of LEDs over time.

the blue emitting chip. The phosphor can be seen as a yellow layer when looking into LED. The mixture of blue and yellow light is perceived as white light by the human eye. The disadvantage of this one phosphor solution is the high color temperature. The light is perceived as bluish-white, cool light. Figure 1-3 shows a schematic design of this type of white LED. To guide the light into a certain direction a mirror is placed around the chip. Bound to the chip is a phosphor layer which partially absorbs the blue light emitted by the chip. The absorbed light is converted to yellow light to mix with the blue to yield white light (see Figure 1-4).

With the increase in efficiency and the exploration of new application markets a demand for white LEDs with a lower color temperature (more reddish, warm white light) arose. This is especially true since today's white LEDs are capable (in terms of light output) of replacing conventional (incandescent) light sources for home lighting. To achieve this, a red component has to be added to the light emitted by the pc-LED. The first warm white LEDs were based on an mixture of YAG:Ce^{3+} [8] and CaS:Eu^{2+} [9]. Recently many new materials have been proposed for the use as color converters. A very promising approach was published by Mueller-Mach et al. [10]. They report on the use of nitride and oxonitride based phosphors of red and yellowish green emission color, respectively. Both host lattices use Eu^{2+} as activator

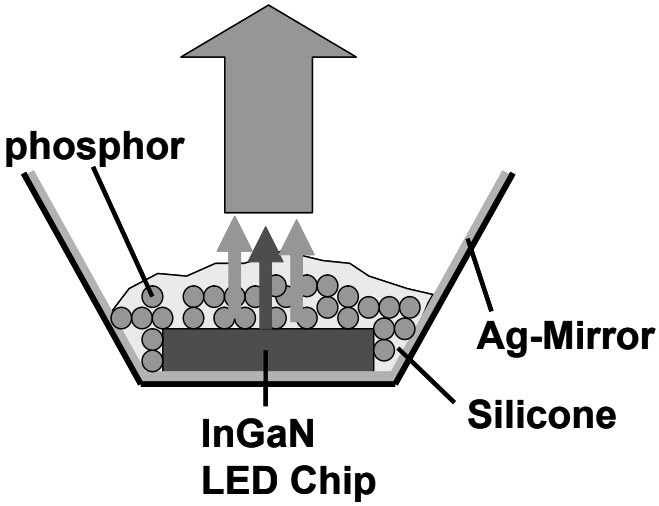

Figure 1-3 Schematic design of a phosphor coated LED: a one phosphor solution with an InGaN based chip and a YAG:Ce^{3+} phosphor.

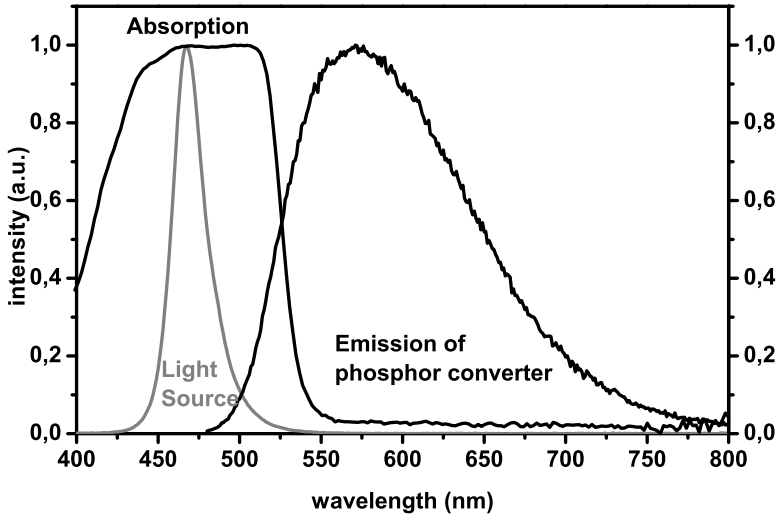

Figure 1-4 Absorption and emission spectrum of YAG:Ce^{3+} (black lines) and emission spectrum of an InGaN based LED chip (gray line).

ion. Those new materials, especially the red emitting $M_2Si_5N_8:Eu^{2+}$ (M = Ca, Sr, Ba) exceed sulphide based and some oxide based materials in terms of quantum efficiency, stability against hydrolysis and in thermal stability. The oxonitride material $SrSi_2O_2N_2:Eu^{2+}$ (also described in chapters 2 & 3 of this thesis) emits in the green spectral region which is an advantageous addition to the yellow light because it increases the color rendering index (CRI) R_a. This index defines the ability of a light source to illuminate an object and how its illumination makes a color appear to the human eye compared to the sun as light source. The CRI of sunlight is defined as 100.

The future of LED lighting will be bright. This is true in two different ways: It will be bright in the sense that the light output generated by one LED chip will continue to increase. In analogy to Moore's law on the development of the computational power of processor chips there is Haitz's law on the light output of LED chips. It states that each decade the prices of LEDs fall by a factor of 10 while the performance increases by a factor of 20. That means that the LED brightness doubles every 18 to 24 month, a development that already holds up for about 30 years. Considering this, LEDs will soon be able to exceed the performance of presently used light sources and will potentially replace these light sources in the near future. This is the second way in which the future is bright. At the beginning of the LED era they were used in niche markets only; mainly as indicator lights or in remote controls (LEDs in the non-visible IR range of the spectrum) for e.g. TV sets. This has changed drastically in the last years. LEDs entered the market in almost all branches of the lighting industry: automotive lighting, shop lighting, city beautification, signage (traffic lights), backlighting for LCD displays, for outdoor equipment or home lighting. Today most LEDs are still used in portable devices but they will find their way into the lamps in our homes soon.

The steady development of LEDs has consequences for the phosphors that are applied. Today's high power LEDs have chip temperatures of around 150 °C. High power LEDs (> 1 W power consumption) are needed for home lighting but with increasing power consumption the junction temperature of the chip will further increase. Thermal stability and thermal quenching of the luminescence are therefore central issues for newly developed LED phosphors. All materials presented in this thesis were investigated for their thermal quenching behaviour and form an important aspect in the discussion on the applicability of each

of the phosphors. A second criterion is that to be used in LEDs, the phosphor has to be efficiently excitable in the near UV to blue spectral range to absorb the light emitted by the LED. The long lifetime of an LED chip (more than 30 000 h) poses strict demands for chemical resistivity. If the phosphor applied degrades due to hydrolysis or oxidation it will have a negative effect on the performance of the whole LED package. The large interest in phosphors for white emitting LEDs is also reflected in the lively research activities resulting in an increasing amount of publications and patents in this field.
Most phosphors proposed for the use in LEDs contain Eu^{2+} or Ce^{3+} as activator ions. These activator ions can show optically allowed absorption and emission bands in the near-UV and visible spectral range. As a result, the absorption of the LED pump light is strong enough and the emission is fast enough to prevent ground state depletion. In addition, optical transitions involve the 5d-orbitals. Since these orbitals participate in the chemical bonds of the activator ions, the position of the lowest excited 5d-levels (from where the emission occurs) is strongly dependent on the local surroundings and can be varied by changing the lattice around the dopant (see chapters 3 & 6 for examples). Further information on 4f-5d transitions will be given in section 1.5.

1.4 Rare earth elements

The history of the rare earth elements (also called lanthanides) started almost 220 years ago in 1788 when Geijer reported on a black stone found close to the Swedish town of Ytterby [11]. The stone was called Yttria. Later on Klaproth found a stone he named Ceria (1803). After decades of careful analysis, for example by Gadolin, both materials turned out to contain a number of different but chemically very similar elements, which made it hard to isolate them. It took about 100 years until all lanthanides were obtained in a pure form. From the mineral Ceria the light lanthanides lanthanum, cerium, didymium, samarium, europium and gadolinium were separated [12]. Didymium was later on found to be a mixture of praseodymium and neodymium. The mineral Yttria was found to contain the elements terbium, erbium, ytterbium, holmium, thulium, dysprosium and lutetium [12].

In this thesis the luminescence of three rare earth (RE) elements, cerium, europium and ytterbium, is used. Before discussing the optical properties, it is interesting to give some background information on these special elements.

1.4.1 Cerium

Cerium was first discovered by Klaproth (Germany) and later independently by Berzelius and Hisinger (Sweden) in 1803. It was named after the asteroid Ceres, which was discovered two years earlier. The pure metal was first prepared by Hillebrand and Norton in 1875. The two most common sources of cerium today are monazite [(Ce, La, Th, Nd, Y)PO_4] and bastnasite [(Ce, La, Y)CO_3F]. The pure metal is prepared via metallothermic reduction or via electrolysis. The most common oxidation states are +3 and +4. A metal comprising the former oxidation state is also referred to as cerous, in the latter state as ceric.
In this thesis cerium is used as a trivalent ion and its luminescence properties are exploited. Besides this, cerium is used in several other fields of science and technology. In metallurgy it is used in the production process of malleable iron, stainless steel, in the production of permanent magnets and as alloy to tungsten electrodes for gas tungsten arc welding. The motion picture industry uses cerium in carbon-arc lighting. In the chemical industry cerium(III) and cerium (IV) compounds are used as catalysts, coloring agents in enamel, in self cleaning ovens and as selective absorber of ultraviolet light in glass.

1.4.2 Europium

Spectral lines of europium were first observed by Paul Emile Lecoq de Boisbaudran in1890 in a samarium-gadolinium mixture. The discovery is credited to Eugene Anatole Demarcay who in 1901 was the first one able to separate europium from samarium. The name is a dedication to Europe and makes the element, besides americium, one of only two elements named after a continent. It took several more years for the pure metal to be prepared. Like most rare-earth elements europium is found in minerals. Technically important are bastnasite and monazite. Spectral lines have been found in the spectrum of the sun and certain stars. Europium is the most reactive of the

rare earth elements. It is found in the oxidation states +2 and +3, where the divalent ion is the more often occurring. This is in contrast to all the other rare earth ions, which are mostly stable as trivalent ion.
The usage of divalent and trivalent europium is restricted in relation to its unique luminescence properties. Europium activated phosphors are used in cathode ray tubes, in fluorescent tubes, in scintillators, as safeguard feature in banknotes [13], and in markers for a variety of medical applications. For further information the reader is referred to the review article by Jüstel et al. [14].

1.4.3 Ytterbium

It took until 1878 that the Swiss chemist Galissard de Marignac was able to separate an element he called ytterbia. Only in 1937 for the first time the pure metal was prepared by Klemm and Bonner. The metals quality was not good enough to determine chemical and physical properties. A pure enough material allowing a more extensive characterization was made in 1953.
Ytterbium is found in minerals as part of a mixture of rare earths. The minerals monazite, euxenite and xenotime comprise small amounts of this element. In these compounds ytterbium is mainly found having the oxidation state +3. Only few materials containing divalent ytterbium are known. This thesis will present two new Yb^{2+} containing materials.
Ytterbium can be used to improve the mechanical properties of stainless steel. It is part of alloys which are used as high quality permanent magnets. The isotope ^{169}Yb is a rarely used source for γ-radiation in nuclear medicine. Ytterbium(III)fluoride is used in dental applications to increase contrast for x-ray images and to improve the caries protection due to the constant release of fluoride. In combination with other RE ions it can show upconversion (for examples with Ho^{3+} [15], Tm^{3+} [16] and Er^{3+} [17] as co-dopants) and is able to convert infrared radiation into visible light.

1.5 4f-5d luminescence

Lanthanide ions are well known for their efficient luminescence due to intraconfigurational $4f^h$ transitions. The luminescence from the lanthanides discussed in this thesis is of a different origin. All three lanthanide ions show

absorption and emission bands related to $4f^{n-1}5d \rightarrow 4f^{n}$ transitions. Since the transitions involve different orbitals one speaks of *inter*configurational transitions. These transitions are parity allowed and give rise to intense absorption bands. This distinguishes them from the other trivalent RE ions.
The f-d absorption and emission bands of lanthanide ions are usually situated in the (vacuum)ultraviolet part of the spectrum. Low energy 5d-levels are found for lanthanide ions with a relatively low electron affinity. This includes the divalent lanthanides (Eu^{2+}, Yb^{2+}, Sm^{2+} and Tm^{2+}) and trivalent lanthanides which have a relatively high stability in the tetravalent state (Ce^{3+}, Tb^{3+} and Pr^{3+}). Ce^{3+} has one electron in the 4f orbital. Since there are no higher energy f-levels besides the splitted groundstate it can only show 4f-5d absorption and emission. Figure 1-5 gives schematic overview of the d-band positions for Ce^{3+} ($4f^1$) and Eu^{2+} ($4f^7$) and the excited 4f levels within the d-band for the Eu^{2+} ion.
The 5d-orbitals are extended and participate in the chemical bonding. Therefore the 4f-5d transitions are highly influenced by the local surroundings (the host lattice). The position of the 5d-level is mainly influenced by two

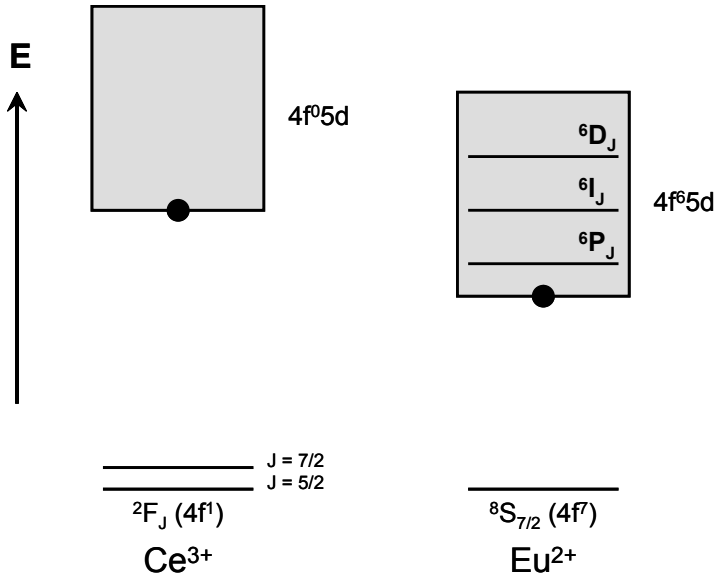

Figure 1-5 Schematic overview of the d-band positions for Ce^{3+} and Eu^{2+} and the excited 4-f levels within the d-band for the Eu^{2+} ion.

factors: the nephelauxetic effect and the crystal field splitting [18]. The word nephelauxetic stands for (electron) cloud expanding. It can be understood considering the covalency between two atoms. For materials like rock salt the difference in electronegativity (EN) is large and the material has ionic atom bonding. The electrons reside on either Cl^- or the Na^+ ions. Bonds between the same elements, e.g. H_2, involve atoms with identical EN and the bond is covalent. The electron cloud is shared between the two atoms. For a decreasing EN difference in the bonding between two different atoms the covalence increases. As the covalency of the bonding with the surrounding ligands increases, the energy for the 5d state of the lanthanide shifts to lower energy, while the 5d electron is more delocalized (nephelauxetic effect) over the ligands as a result of the covalent bonding. The shift involves the barycenter of the 5d state (the average energy of all crystal field components). The crystal field splitting can be understood by considering the static electric field resulting from the charged ligands surrounding the lanthanide ion (although a better understanding can be obtained from a molecular orbital diagram). Replacing O^{2-} by N^{3-} results in a higher formal charge of the ligands and will increase the crystal field splitting. This will result in a lowering of the lowest emitting d-level and shift the d-f emission to longer wavelengths. As an example, the oxide $Ba_2SiO_4:Eu^{2+}$ shows green emission [19] while the nitride $Ba_2Si_5N_8:Eu^{2+}$ shows red emission [10]. Additionally, an energy difference is found between the excitation and the emission energy: the so called Stokes' shift. This effect originates from the ions relaxation in the excited state. It is very important for the luminescence quenching behavior. Figure 1-6 depicts schematically the influence of those three factors on the 4f-5d transitions.
Also the size (ionic radius) of the host lattice cation, for which the lanthanide ion substitutes, plays a role. Generally speaking, the crystal field splitting is larger when substituting for a smaller cation, leading to a lowering of the 5d-level. For ions built in on too large sites the crystal field splitting will decrease which in turn raises the energy of the lowest 5d-level [20]. The positions of the 5d-levels of RE elements are related to each other within one host lattice. Nowadays it is possible to predict the position of different RE d-levels from knowing the position for one ion, for instance the Ce^{3+} d-level. After pioneering work by Blasse, a systematic analysis for the full series of lanthanides has been published by Dorenbos. In a series of papers a

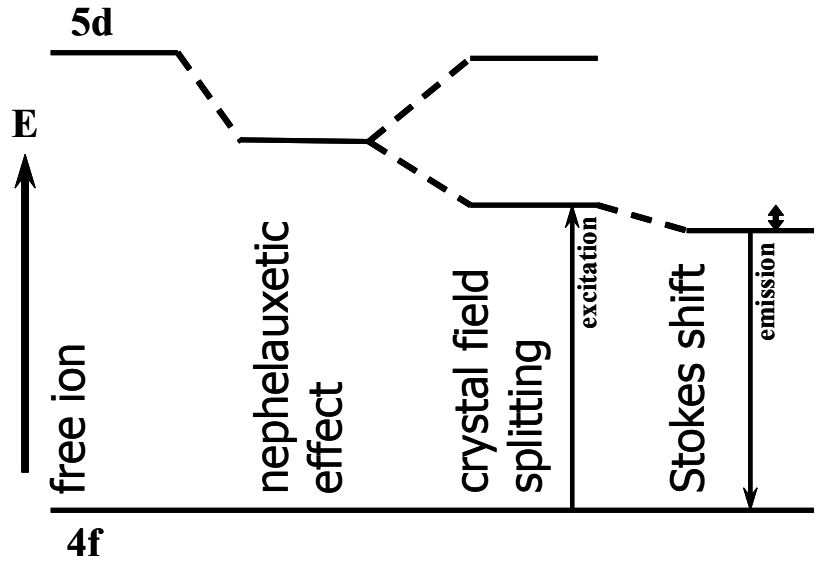

Figure 1-6 The influence of nephelauxetic effect, crystal field splitting and Stokes shift on the 4f-5d transition of the free ion.

comprehensive analysis of the f-d luminescence properties of the divalent and trivalent lanthanides is given [21].
Important for the use of RE elements is also their luminescence decay time. For the 5d-4f emission of Ce^{3+}, Eu^{2+} and Yb^{2+} it was found that decay times differ by several orders of magnitude. For Ce^{3+} typical decay times are in the ns range [22], for Eu^{2+} in the µs range [23] and for Yb^{2+} in the ms range [24]. Poort et al. established a dependence of the decay time of Eu^{2+} on the position of the emission band [25]. The position of the 5d-levels for other trivalent RE ions except Ce^{3+} are mainly in the VUV range of the electromagnetic spectrum. They are not investigated in this thesis. The interested reader is referred to the work of van Pieterson [26].

1.6 Summary

This thesis can be divided into two different parts. Part one comprises chapters 2, 3 and 4 which are on oxonitridosilicate (sion) and aluminooxonitridosilicate (sialon) materials doped each with Eu^{2+} or Yb^{2+}.

Part two comprises chapters 5 and 6 which are on Yttrium Aluminum Garnet (YAG) doped with Ce^{3+} and/or Gd^{3+}.
In chapter 2 the optical properties of $SrSi_2O_2N_2$ doped with divalent Eu^{2+} and Yb^{2+} are investigated. The Eu^{2+} doped material shows efficient green emission peaking at around 540 nm that is consistent with $4f^6 5d \rightarrow 4f^7$ transitions of Eu^{2+}. Due to the high quantum yield (90%) and high quenching temperature (>500 K) of the luminescence $SrSi_2O_2N_2:Eu^{2+}$ is a promising material for application in phosphor converted LEDs. The Yb^{2+} luminescence is markedly different from Eu^{2+} and is characterized by a larger Stokes' shift and a lower quenching temperature. The anomalous luminescence properties are ascribed to impurity trapped exciton emission. Based on temperature and time dependent luminescence measurements, a schematic energy level diagram is derived for both Eu^{2+} and Yb^{2+} relative to the valence and conduction bands of the oxonitridosilicate host material.
Chapter 3 describes the possibilities of color tuning of the LED phosphor $Sr_{1-x-y-z}Ca_xBa_ySi_2O_2N_2:Eu_z^{2+}$ ($0 \leq x, y \leq 1$; $0.005 \leq z \leq 0.16$). The emission color can be tuned in two ways: by changing the Eu^{2+} concentration and by substitution of the host lattice cation Sr^{2+} by either Ca^{2+} or Ba^{2+}. The variation of the Eu^{2+} concentration shows a red shift of the emission upon increasing the Eu-concentration above 2%. The red shift is explained by energy migration and energy transfer to Eu^{2+} ions emitting at longer wavelengths. Along with this (desired) red shift there is an (undesired) lowering of the quantum efficiency and the thermal quenching temperature due to concentration quenching. Partial substitution of Sr^{2+} by either Ca^{2+} or Ba^{2+} also results in a red shifted Eu^{2+} emission. For Ca^{2+} this is expected and the red shift is explained by an increased crystal field splitting for Eu^{2+} on the (smaller) Ca^{2+} cation site. For Ba^{2+} the red shift is surprising. Often, a blue shift of the fd emission is observed in case of substitution of Sr^{2+} by the larger Ba^{2+} cation. The Eu^{2+} emission in the pure $BaSi_2O_2N_2$ host lattice is indeed blue shifted. Temperature dependent luminescence measurements show that the quenching temperature drops upon substitution of Sr by Ca, while for Ba substitution the quenching temperature remains high. Color tuning by partial substitution of Sr^{2+} by Ba^{2+} is therefore the most promising way to shift the color point of LEDs while retaining a high relative quantum yield and high luminescence quenching temperature.

To conclude the first part of this thesis chapter 4 investigates the optical properties of $SrSi_2AlO_2N_3$ doped with Eu^{2+} and Yb^{2+} for a potential application in LEDs. The Eu^{2+} doped material shows emission in the green, peaking around 500 nm. The emission is ascribed to the $4f^65d^1$ to $4f^7$ transition on Eu^{2+}. In view of the too low quantum efficiency and the thermal quenching temperature around the operation temperature of high power LEDs the phosphor is less suitable for the use in phosphor converted LEDs. The Yb^{2+} emission shows the same anomalously red-shifted emission compared to the one of Eu^{2+}, as reported in chapter 2, which is characterized by a larger FWHM, a larger Stokes' Shift and lower thermal quenching temperature as well. The emission is ascribed to self-trapped exciton emission. The Yb^{2+} activated phosphor is found to be unsuitable for use in phosphor converted LEDs.

The second part of this thesis is on YAG doped with gadolinium and/or cerium. In chapter 5 we report on the luminescence temperature quenching in YAG:Ce. For a wide range of Ce-concentrations (between 0.033% and 3.3%) the temperature dependence of the emission intensity and the luminescence life times are reported. The intrinsic quenching temperature of the Ce-luminescence is shown to be very high (>680 K). The lower quenching temperatures reported in the literature are explained by thermally activated concentration quenching (for highly doped systems) and the temperature dependence of the oscillator strength (for low doping concentrations). In addition, high resolution spectra are reported which provide insight in the position of the zero-phonon transition (20 450 cm^{-1}), the Stokes' shift (2400 cm^{-1}), the energy of the dominant phonon mode (200 cm^{-1}) and the Huang-Rhys parameter (S=6). These parameters can serve as input for comparison with *ab initio* calculations on the position of and relaxation in the excited 5d state of Ce^{3+} in YAG.

Finishing this thesis, for the widely applied white light LED-phosphor $Y_3Al_5O_{12}$:Ce (YAG:Ce) the influence of partial substitution of Y by Gd on the Ce^{3+} luminescence and temperature quenching is reported in chapter 6. Low Ce-doping concentrations (0.03 and 0.3%) are used to avoid concentration quenching or radiative reabsorption. The luminescence shows a pronounced redshift from 536 nm (for YAG:Ce) to 579 nm (for $Y_{0.25}Gd_{0.75}Al_5O_{12}$:Ce) while the quenching temperature decreases. The results are explained by an

increase in the crystal field splitting and Stokes' shift upon substitution of Y^{3+} by Gd^{3+} ions in the YAG host lattice. In spite of the lower luminescence quenching temperature, (Y,Gd)AG:Ce is a promising phosphor for realizing white light LEDs with a lower color temperature.

References

1 A. Žukauskas, M.S. Shur, R. Gaska, Introduction to Solid-State Lighting, Wiley-Interscience Publication (2002) chapter 4.
2 T.A. Edison, U.S. patent No. 223,898 of 1879.
3 A. Just, F. Hanaman, German patent No. 154,262 of 1903.
4 H.J. Round "A note on Carborundum" Electrical World 49 (6) (1907) 309.
5 N. Holonyak Jr., S.F. Bevacqua, Appl. Phys. Lett. 1 (4) (1962) 82.
6 S. Nakamura, Jpn. J. Appl. Phys. 30 (1991) L1705.
7 S. Nakamura, G. Fasol, The blue Laser Diode: GaN Based Light Emitters and Lasers, (Springer, Berlin) (1997) 343.
8 P. Schlotter, J. Baur, Ch. Hielscher, M. Kunzer, H. Obloh, R. Schmidt, J. Schneider, Mater. Sci. Eng. B 59 (1999) 390.
9 Y. Hu, W. Zhuang, H. Ye, S. Zhang, Y. Fang, X. Huang, J. Lumin. 111 (2005) 139.
10 R. Mueller-Mach, G. Mueller, M.R. Krames, H.A. Höppe, F. Stadler, W. Schnick, T. Juestel, P. Schmidt, phys. stat. sol. (a) 202 (2005) 1721.
11 B. Geijer, Annalen für die Freunde der Naturlehre 9 (1788) 229.
12 W.H. Brock, The Norton History of Chemistry (1st ed. W.W. Norton & Company, 1993).
13 F. Suyver and A. Meijerink, Chemisch2Weekblad 98 (2002) 12.
14 T. Jüstel, H. Nikol, C. Ronda, Angew. Chem. Int. Ed. 37 (1998) 3084.
15 X. Luo, W. Cao, Mater. Lett. 61(17) (2007) 3696.
16 W. Xu, X. Xu, F. Wu, G. Zhao, Z. Zhao, G. Zhou, J. Xu, Opt. Commun. 272(1) (2007) 182.
17 Y. Wei, F. Lu, X. Zhang, D. Chen, Mater. Lett. 61(6) (2007) 1337.
18 G. Blasse, A. Bril, Philips Tech. Rev. 31 (1970) 303.
19 J.S. Kim, Y.H. Park, S.M. Kim, J.C. Choi, H.L. Park, Solid State Commun. 133(7) (2005) 445.
20 G. Blasse, B.C. Grabmaier, Luminescent materials (1994) Springer Verlag, Berlin.
21 P. Dorenbos, J. Lumin. 91 (2000) 155 and P. Dorenbos, J. Lumin. 104 (2003) 239.
22 G. Blasse, A. Bril, Appl. Phys. Lett. 11(2) (1967) 53.
23 T. Hoshina, J. Phys. Soc. Japan 48 (1980) 1261.
24 S. Lizzo, A. Meijerink, G. Blasse, J. Lumin. 59 (1994) 185.

25 S.H.M. Poort, A. Meijerink, G. Blasse, J. Phys. Chem. Solids, 58(9) (1997) 1451.
26 L. van Pieterson, Proefschrift Universiteit Utrecht, 2001.

Chapter 2: Luminescence properties of $SrSi_2O_2N_2$ doped with divalent rare earth ions

The optical properties of $SrSi_2O_2N_2$ doped with divalent Eu^{2+} and Yb^{2+} are investigated. The Eu^{2+} doped material shows efficient green emission peaking at around 540 nm that is consistent with $4f^6 5d \rightarrow 4f^7$ transitions of Eu^{2+}. Due to the high quantum yield (90%) and high quenching temperature (>500 K) of the luminescence $SrSi_2O_2N_2:Eu^{2+}$ is a promising material for application in phosphor converted LEDs. The Yb^{2+} luminescence is markedly different from Eu^{2+} and is characterized by a larger Stokes' shift and a lower quenching temperature. The anomalous luminescence properties are ascribed to impurity trapped exciton emission. Based on temperature and time dependent luminescence measurements, a schematic energy level diagram is derived for both Eu^{2+} and Yb^{2+} relative to the valence and conduction bands of the oxonitridosilicate host material.

2.1 Introduction

An exciting new development in the field of luminescent materials is the search for new phosphors for the conversion of the near UV or blue emission from (In,Ga)N LEDs into visible light. In the past, luminescence research has mainly focused on conventional phosphors for the conversion of 254 nm UV radiation from a mercury discharge into visible light. Research has contributed to the development of a mature product with stable and efficient (90 % quantum efficiency) phosphors and at present work on phosphors for fluorescent tubes is aimed at incremental improvements in the stability, morphology, and efficiency of existing phosphors. Luminescence conversion of near UV or blue light into longer wavelength radiation applied in state-of-the-art white LED lamps poses new challenges in phosphor research especially in view of the small energy difference between pump and emission wavelength. In the search for new phosphors for inorganic LEDs, luminescent materials with high charge densities between activator and its surroundings are investigated. Doping such materials with Ce^{3+} or Eu^{2+} can lead to strong absorption in the near UV to blue spectral range combined with efficient emission in the visible. For example, oxides like $Y_3Al_5O_{12}:Ce^{3+}$ (YAG:Ce) or sulfides like $CaS:Eu^{2+}$ are currently applied in phosphor converted LEDs (pcLEDs) as luminescence converters [1,2]. Nevertheless, pronounced temperature quenching of luminescence and low chemical stability restricts their use in LED lighting applications where a long device lifetime under harsh conditions is required.

Oxonitridosilicates, known as siones, represent a class of solid compounds, which can be formally derived from oxosilicates by partial substitution of oxygen by nitrogen. They can combine attractive material properties like high mechanical hardness and strength, also exceptional thermal and chemical stability is reported [3]. Higher condensed siones are known to be highly covalent and stable towards oxidation and hydrolysis [3]. The $SrSi_2O_2N_2$ host lattice we are about to report was developed in a synthesis approach that earlier led to efficient nitridosilicate phosphors $M_2Si_5N_8:Eu^{2+}$ (M = Sr, Ba) [4-6]. The strong interest in this class of novel materials is reflected by a number of publications published in the last few years on the

system Ln-Si-O-N (Ln = La, Gd, Y) in general [7] and the title compound in detail [8-12]. This chapter describes the synthesis and continuative studies on the optical properties of luminescent materials based on the $SrSi_2O_2N_2$ host lattice doped with divalent rare earth ions, viz. Eu^{2+} and Yb^{2+}. The luminescence properties are investigated and the luminescence mechanism is discussed. The luminescence characteristics of the Eu^{2+} doped $SrSi_2O_2N_2$ are shown to be very promising for application in pcLEDs. This is substantiated by a recent paper on an all-nitride phosphor-converted white light emitting diode using the Eu^{2+} doped title compound [13].

2.2 Experimental methods

All samples were synthesized by a conventional solid-state reaction. Mixtures of $SrCO_3$ (Philips Lighting Components, 99.9%), $Si_3N_{4-x}(NH)_{3/2x}$ ($x \approx 1$,made by thermal decomposition of $Si(NH)_2$ as described in [14], O content < 2wt%), and the rare earth dopants Eu_2O_3 (Alfa Aesar, REacton 99.999%) or Yb_2O_3 (Auer-Remy, 99.99%) were prepared by ball milling and fired for 2 to 4 hours at 1200 to 1500 °C in a reducing atmosphere (H_2/N_2) in a tube furnace. After milling the raw product powders were washed with water and isopropanol. XRD analysis was done on a Philips diffractometer PW 1729 at RT, using Cu K_α radiation.
Luminescence spectra were recorded between 4 K and 300 K on a Spex Fluorolog 2 spectrofluorometer equipped with a helium flow cryostat. The set-up is described in detail in Ref. [15]. To study thermal quenching between 300 and 600 K luminescence spectra were measured on a modified spectrofluorimeter system FL900 of Edinburgh Instruments using a Xe-lamp as excitation source. The spectra were measured with a spectral resolution of 0.5 to 1.0 nm. The complete set-up was described earlier [16]. Luminescence lifetime measurements were measured using a Lambda Physik dye laser pumped by a Lambda Physik LPX100 excimer laser (operating at 308 nm) for pulsed excitation at 450 nm using a Coumarin 47 dye. Luminescence decay curves were measured using a 0.25 m Acton Research monochromator and an RCA C31034 photomultiplier tube in combination with a Tektronix 2430 Digital Oscilloscope.

2.3 Experimental results

2.3.1 Crystal Structure

Phase purity of $SrSi_2O_2N_2$ samples was checked by means of x-ray powder diffraction. The crystal structure is similar to the structure of $CaSi_2O_2N_2$ [17]. Both compounds represent a new class of layered materials with layers of $(Si_2O_2N_2)^{2-}$ that consist exclusively of $SiON_3$-tetrahedrons. The N atom bridges three Si atoms while the O atom is bound terminally to the Si atom. There are four types of sites for the Sr^{2+} ions each surrounded by six oxygen atoms in a distorted trigonal prismatic manner [18]. The XRD patterns of the $SrSi_2O_2N_2$ phases described in this chapter show similarities to the pattern assigned to a high temperature (HT) phase of $SrSi_2O_2N_2$ in [19].

2.3.2 $SrSi_2O_2N_2:Eu^{2+}$

The room temperature excitation and emission spectra of the Eu^{2+}-doped $SrSi_2O_2N_2$ are shown in Figure 2-1. The emission spectrum shows a single emission band peaking at 539 nm. The position and width of the emission band differs from that reported for a $SrSi_2O_{2-\delta}N_{2+2/3\delta}$:Eu ($\delta$~1) compound with a similar XRD pattern [12] and is comparable with the emission spectrum of a phase that was described as the high temperature modification of $SrSi_2O_2N_2$:Eu [11]. The emission band is assigned to the $4f^65d^1 \rightarrow 4f^7$ (fd) transition on Eu^{2+}. The Stokes' Shift (SS) of the fd emission can be estimated by taking twice the energy difference between the zero phonon line energy and the energy of the emission maximum [20]. The spectral position of the zero phonon line was taken to be the point of intersection of absorption and emission spectrum, $\lambda_{0\text{-}0}$ = 494 nm (2,51 eV). This yields a value of 0.42 eV for the Stokes' shift, which is a typical value for the fd emission from Eu^{2+} [20,21]. For example, in aluminates, silicates and phosphate host lattices, SSs are reported between 0.25 and 1 eV for fd emission from Eu^{2+} [20,21]. The full width at half maximum (FWHM) of the emission band is 0.3 eV and is slightly smaller than the FWHM as is commonly observed for Eu^{2+} fd emission [22]. The position of the emission band is at longer wavelengths than for Eu^{2+} in oxo-silicates [23] showing Eu^{2+}

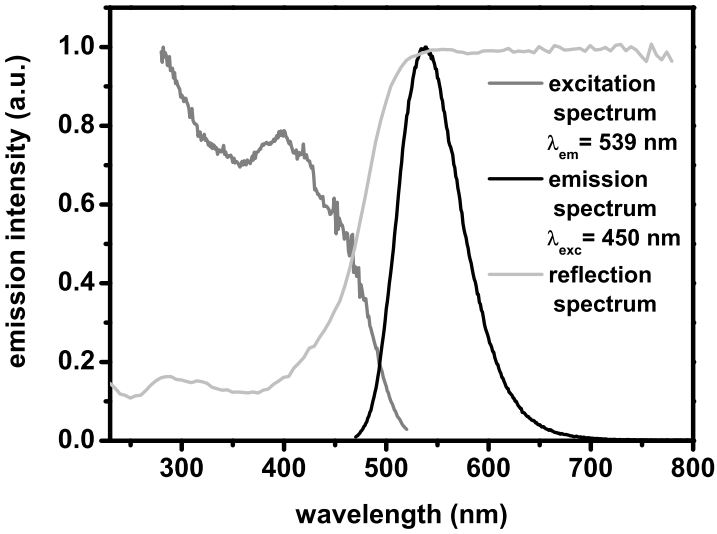

Figure 2-1 Luminescence excitation (gray line) for 539 nm emission, emission (black line) for 450 nm excitation and diffuse reflection spectrum (light gray line) of $SrSi_2O_2N_2:Eu^{2+}$ 2%, recorded at 298 K.

emission typically in the blue spectral region [24]. One of a few exceptions is $(Ba,Sr)_2SiO_4:Eu^{2+}$ which emits in the green to yellow spectral range, viz. 520-580 nm [21]. The shift of the emission to longer wavelength is ascribed to a higher degree of covalency between the activator ion and its surroundings (nephelauxetic effect) [25]. For $SrSi_2O_2N_2:RE^{2+}$ the bonding situation is comparable to orthosilicates like $M_2SiO_4:RE^{2+}$ where the RE-dopant is coordinated by only O-atoms as well [25]. However, due to the higher degree of condensation of the $SrSi_2O_2N_2$ lattice, the stability against hydrolysis is much higher compared to alkaline earth orthosilicates.

The decay time of the fd emission of Eu^{2+} is short since the transition involved is parity allowed. Typical values are around 1 µs [24]. In Figure 2-2a the luminescence decay curves for the Eu^{2+} emission are shown for various temperatures between 4 and 723 K. All decay curves show a single-exponential decay behavior. Between 4 and 450 K the decay time $\tau_{1/e}$ is 1.15 µs, close to the typical value for the fd emission from Eu^{2+}. It has been shown that the radiative decay time of the Eu^{2+} fd emission decreases with increasing energy of the emission maximum in agreement with the theoretical relation between the radiative transition probability and the energy of electric

dipole transition [24]. The radiative decay rate A_R (= 1/ $\tau_{1/e}$) is proportional to the third power of the energy of the emission band (σ, energy in cm^{-1}) [24]:

(eq. 2-1) $$A_R(\mathrm{Eu}) = \frac{1}{\tau} = 5.06\mathrm{x}10^{-8}\left|\langle 5d|r|4f\rangle\right|^2 \chi\sigma^3$$

where $\langle 5d|r|4f\rangle$ is the radial overlap integral and χ equals $(n(n^2+2)^2)/9$ and corrects for the dependence of A_R on the refractive index n [24]. With $\langle 5d|r|4f\rangle = 0.81$ [24] and $n = 1.75$ (estimated from the refractive index reported for similar oxonitridosilicate [26-28] the value for $\chi = 5$ and the calculated radiative life time is 0.94 µs. This is very close to the experimentally observed decay time (1.15 µs) and the error is within the uncertainty range caused, for example, by the fact that the refractive index for $SrSi_2O_2N_2$ is not known exactly giving an uncertainty of about 10% in χ. The observation that the experimentally observed luminescence life time is very close to the predicted radiative life time in the temperature regime 4 - 450 K indicates that in this temperature range the luminescence quantum efficiency of the Eu^{2+} emission is close to unity.

Above 450 K the luminescence decay time decreases as is shown in Figure 2-2b. The decrease in the luminescence decay time above 450 K is accompanied by a decrease in the emission intensity indicating that non-

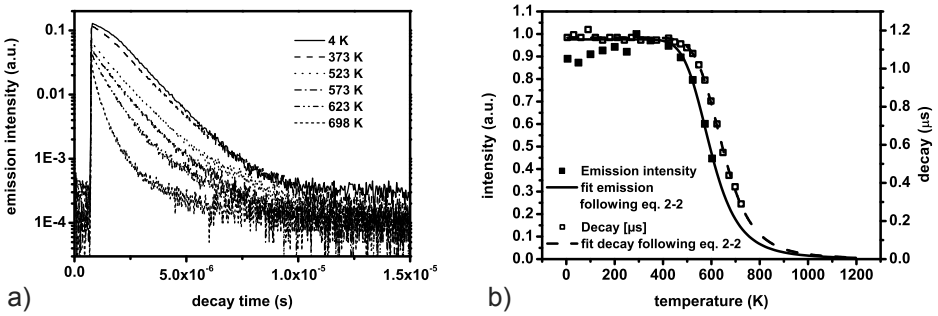

Figure 2-2 a)Temperature dependent decay curves of the Eu^{2+} emission (for 539 nm emission under 450 nm excitation) in $SrSi_2O_2N_2$:Eu^{2+} 2%; b)Temperature dependence of the integrated emission intensity (black squares) and luminescence decay times (open squares) derived from the curves in Fig. (a). The lines through the data points are fits to Eq. 2-2.

radiative relaxation sets in above 450 K. In Figure 2-2b both the temperature dependence of the luminescence lifetime and the luminescence intensity are plotted. For the plot of the emission intensity care has been taken to take changes in the absorption due to thermal broadening into account. An analysis based on the thermal broadening of the absorption band and the Kubelka-Munk model for the reflection shows that the changes in the reflection over the temperature investigated is less than 5% and will not significantly influence the measured luminescence intensity. From the temperature dependence of the luminescence decay time and the emission intensity, the luminescence quenching temperature (temperature at which the luminescence intensity has decreased to half its initial values) is estimated to be about 600 K. Current high brightness LEDs can reach temperatures around 450 K. At this temperature the thermal quenching of the fd luminescence of Eu^{2+} in $SrSi_2O_2N_2$ is marginal.

The mechanism for the quenching of the fd luminescence of Eu^{2+} may be either quenching by thermally activated cross-over from the $4f^65d$ excited state to the $4f^7$ ground state or thermally activated photoionization from the $4f^65d$ state to the conduction band. The former mechanism is historically the most widely used explanation and for a proper analysis of the temperature dependence of the luminescence intensity the Struck-Fonger model can be used [29]. More recently, it has been shown that in several host lattices thermally induced ionization of the 5d electron is responsible for the quenching of the Eu^{2+} fd luminescence [30]. Especially for host lattices where the SS for the fd emission is small and yet the quenching temperature for the luminescence is low, it is clear that thermally induced ionization from the fd state to the conduction band is responsible for the temperature quenching of the luminescence. Confirmation has been obtained by temperature dependent photoconductivity experiments [31]. In the present composition, the SS is small and the luminescence quenching temperature is relatively high and there is no clear proof for either of the mechanisms being responsible for the temperature quenching. Based on the results for Yb^{2+} (vide infra) it is likely that the 5d state of Eu^{2+} is close to the conduction band edge and that thermally activated ionization from the $4f^65d$ state is responsible for the temperature quenching of the luminescence. In this case the temperature dependence of the luminescence intensity and decay time are described by

a modified Arrhenius equation. This equation is easily derived by taking the radiative and thermally activated non-radiative decay into account.

(eq. 2-2) $$\tau(T) = \frac{\tau_0}{1 + \tau_0 \cdot C \cdot e^{\frac{-E_A}{k \cdot T}}} \; ; \; I(T) = \frac{I_0}{1 + D \cdot e^{\frac{-E_A}{k \cdot T}}}$$

where $\tau(T)$ and $I(T)$ are luminescence decay time and intensity at temperature T [K] respectively, τ_0 and I_0 the decay time and intensity at 0 K, C is a rate constant for the thermally activated escape as is D which contains I_0 as well, E_A is the activation energy for this process which is the energy gap between the Eu^{2+} $4f^6 5d^1$-excited level and the bottom of the conduction band and k is the Boltzmann constant. The intensity measured at 4 K was normalized to 1. In Figure 2-2b the best fits to this equation are shown for both the emission and the luminescence decay time. The energy gap E_A for the best fits of emission intensity and decay time is 0.6 eV (marked as 2 in Figure 2-4). For the emission intensity D and I_0 are 2.76×10^4 and 0.976 respectively. For the decay time C and τ_0 are 4.24×10^{10} and 1.16 μs respectively.

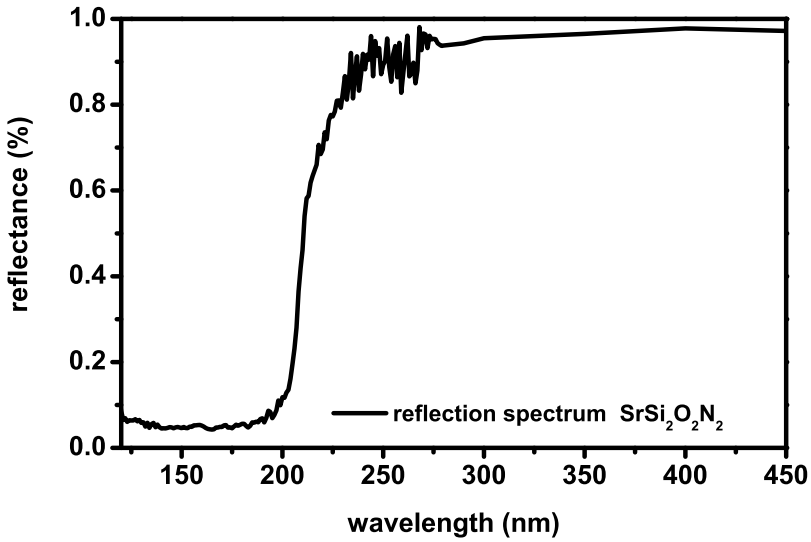

Figure 2-3 Diffuse reflection spectrum of undoped $SrSi_2O_2N_2$ (T=298 K). See Ref. [6] for experimental details.

The optical band gap of the $SrSi_2O_2N_2$ host lattice can be obtained from the reflection spectrum of the undoped host lattice. In Figure 2-3 the reflection spectrum is shown. The band edge is situated at 220 nm, which shows that the band gap is around 5.6 eV. Together with the information of the energy difference between the lowest $4f^6 5d$ state and the $4f^7$ ground state (for which the energy of the zero-phonon line, 2.5 eV, marked as 1 in Figure 2-4, is used) a complete energy level diagram for the Eu^{2+} ion in the $SrSi_2O_2N_2$ host lattice can be derived. The diagram is shown on the left hand side in Figure 2-4. In this diagram the $4f^7$ ground state is situated 2.5 eV above the top of the valence band. Note that, although useful as a schematic picture, one should realize that in this type of diagrams energies from results for relaxed and unrelaxed excited configurations are combined in one diagram.
The temperature dependent luminescence properties show that luminescence quenching does not set in below 500 K. A high quenching temperature is important, especially in high brightness LEDs where the temperature of the phosphor can increase to about 450 K. The presently used phosphors in white light LEDs suffer from luminescence temperature quenching at these elevated

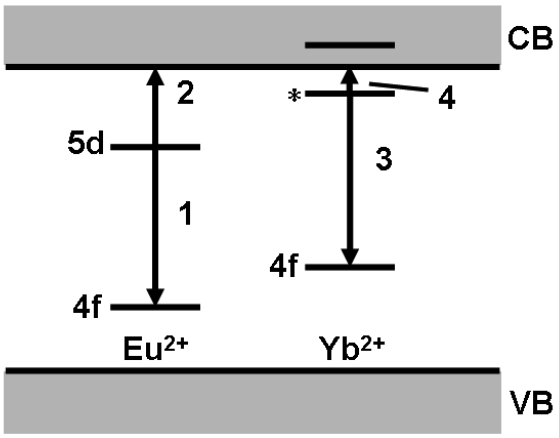

Figure 2-4 Energy level diagram for Eu^{2+} (left hand side) and Yb^{2+} (right hand side) in $SrSi_2O_2N_2$ derived from luminescence masurements. (emissive state of the trapped exciton emission of Yb^{2+}) See also text.*

temperatures. The absence of luminescence quenching below 500 K in combination with the high luminescence quantum yield (90 % for $SrSi_2O_2N_2$: Eu^{2+} 2%) implies that this material is very promising for application as a luminescence converter in phosphor converted LEDs [13].

2.3.3 $SrSi_2O_2N_2:Yb^{2+}$

The luminescence properties of Eu^{2+} and Yb^{2+} are often quite similar for the same host lattice [22,32-35]. In general, the $4f^{13}5d$ excited state of Yb^{2+} is at a slightly higher energy (~ 0.1 eV) than the $4f^{6}5d$ excited state of Eu^{2+} resulting in a slightly blue shifted fd emission for Yb^{2+}. In Figure 2-5 the excitation, emission and reflection spectra are depicted for Yb^{2+}-doped $SrSi_2O_2N_2$. The lowest energy fd excitation band is around 450 nm, very similar to the position of the lowest energy fd excitation band for Eu^{2+}. Comparing the excitation and reflection spectra of the Eu^{2+} and Yb^{2+} doped sample one must come to the conclusion that the crystal field splitting of Yb^{2+} must be larger the one for Eu^{2+}. This can be seen in the much more pronounced fine structure for the two Yb^{2+} spectra. Reasons for the larger crystal field splitting are the larger effective nuclear charge and the smaller atomic radius of Yb^{2+} at the same formal charge compared to Eu^{2+}. The Yb^{2+} emission band, however, is strongly red shifted (λ_{max}=620 nm for Yb vs. 540 nm for Eu) and both the FWHM (0.32 eV for Yb vs. 0.30 for Eu) and the Stokes' shift (0.54 eV for Yb vs. 0.42 eV for Eu) are larger than for the Eu^{2+} emission band. This type of anomalous red-shifted emission has been reported before for Yb^{2+}. For example, in the fluorite host lattices CaF_2 and SrF_2 it has been observed that for CaF_2 the fd luminescence of Eu^{2+} and Yb^{2+} are quite similar but in SrF_2 the emission for Yb^{2+} is red shifted (rather than slightly blue shifted) and the emission is characterized by a larger SS and FWHM and a lower luminescence quenching temperature [36]. The anomalous luminescence properties for Yb^{2+} are explained by considering the position of the lowest energy fd state. The anomalous emission is observed when the lowest energy fd state is situated in the conduction band. When the fd state is at energies higher than the conduction band edge, excitation into the fd state is followed by photoionization and trapping of the electron close to the lanthanide impurity forming an impurity trapped exciton state. Luminescence is observed

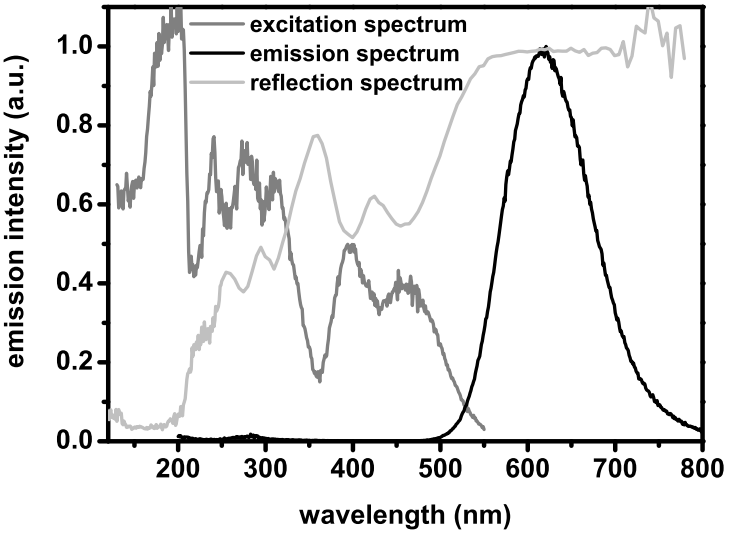

Figure 2-5 Excitation spectrum (gray line) for 615 nm emission, emission spectrum (black line) under 450 nm excitation and diffuse reflection spectrum (light gray line) of $SrSi_2O_2N_2:Yb^{2+}$ 2%. All spectra have been recorded at 298 K.

from this impurity trapped exciton state. Convincing evidence for this model was obtained by performing photoconductivity experiments [37,38]. In host lattices where Yb^{2+} or Eu^{2+} show the anomalous emission, excitation into the lowest energy fd band gave a clear photoconductivity confirming that the lowest energy fd state is situated in the conduction band. At present there are a number of oxide and fluoride host lattices in which impurity trapped exciton emission is observed for Yb^{2+} and Eu^{2+} [39]. Moine and co-workers describe in Ref. [36] and [40] the temperature dependence of Yb^{2+} emission in SrF_2. The present results on Eu^{2+} and Yb^{2+} doped $SrSi_2O_2N_2$ show that in this oxonitridosilicate the lowest fd state is below the conduction band for Eu^{2+} and above the conduction band edge for Yb^{2+}, similar to the situation found for SrF_2.

Luminescence decay times have been measured for the Yb^{2+} emission between 4 and 640 K. In Figure 2-6a the luminescence decay curves are shown for several temperatures. All decay curves are single-exponential. In Figure 2-6b the luminescence decay times derived from fitting the curves of Figure 2-6a to a single exponential function are plotted as a function of temperature.

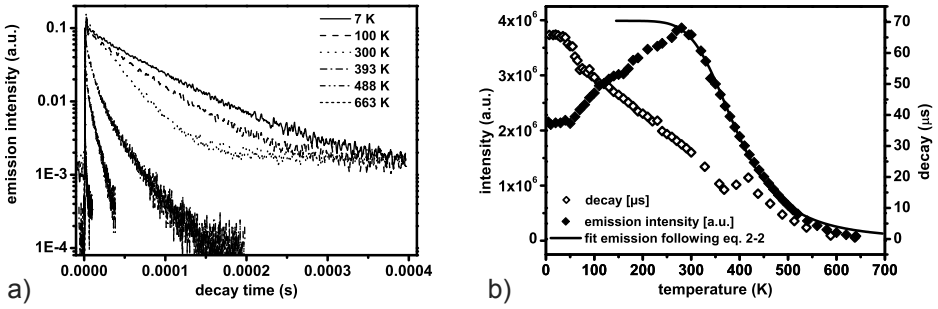

Figure 2-6 a) Temperature dependent decay of the Yb^{2+} emission (for 615 nm emission under 450 nm excitation) $SrSi_2O_2N_2:Yb^{2+}$ 2%; b)Temperature dependence of the integrated emission intensity (black diamonds) and luminescence decay times (open diamonds) derived from the curves in a). The line through the data points is a fit to Eq. 2-2.

The luminescence decay time at 4 K is 65 µs. This is shorter than the low temperature decay time of the fd emission from Yb^{2+} (typically 10 ms) and is in line with the low temperature decay times for impurity (Yb) trapped exciton emission (typically 50-500 µs). The relatively short luminescence decay time supports the assignment of the Yb-emission to impurity trapped exciton emission. Above 50 K the luminescence decay time decreases as is shown in Figure 2-6b. There are two possible reasons for this effect. First, thermal quenching may set in leading to an increase in the non-radiative relaxation rate and therefore to a decrease of the overall decay time. Second, the thermal population of higher energy levels with faster decay times can explain this decrease. To distinguish between the two scenarios we studied the emission intensity in the same temperature range as the decay time. If non-radiative relaxation is responsible, the intensity is expected to decrease in the same manner as the decrease in decay time. Contrary to this, we found an increase of the emission intensity starting above 50 K. This increase continues when heating the sample further until a decrease in the emission intensity is observed above 280 K. Based on this observation it is evident that thermal population of a higher energy level with a faster decay time is responsible for the decrease of the luminescence life time between 50 and

280 K. The increase in emission intensity concurrent with the decrease in lifetime has been observed before and is explained by a constant non-radiative decay channel at low temperatures. An increase in the radiative decay rate is in that case accompanied by an increase in luminescence intensity since the radiative decay channel is favored over the non-radiative channel. Above 280 K thermal quenching sets in and decreases the emission intensity and causes a further decrease of the decay time. To calculate the activation energy of the thermal quenching we used the emission intensities measured between 280 K and 640 K. The best-fit following eq. 2-2 gives an activation energy E_A of 0.3 eV. From this fit the values for I_0 and D are 4×10^6 and 2441 respectively. Together with the information of the energy difference between the emitting impurity trapped exciton state (marked as * in Figure 2-4) and the $4f^{14}$ ground state (for which the energy of the zero-phonon line, 2.3 eV, marked in Figure 2-4 as 3, is used) a complete energy level diagram for Yb^{2+} in the $SrSi_2O_2N_2$ host lattice can be derived. As shown in Figure 2-4 on the right hand side of the diagram the $4f^{14}$ ground state is located 3.0 eV above the valence band.

2.4 Conclusions

The temperature dependence and lifetimes are reported for the f-d luminescence of Eu^{2+} and Yb^{2+} in $SrSi_2O_2N_2$. For Eu^{2+} a very efficient $4f^6 5d \rightarrow 4f^7$ emission at relatively long wavelength in the green spectral range (around 540 nm) is observed. The quenching temperature of the emission is high (no quenching below 500 K) and makes $SrSi_2O_2N_2$:Eu^{2+} a promising phosphor for high power phosphor converted LEDs [13]. For Yb^{2+} an anomalous emission is observed around 615 nm, which is characterized by a large Stokes' shift and a low quenching temperature. The emission is ascribed to an Yb^{2+} trapped exciton luminescence. Based on the luminescence measurements an energy diagram is derived in which the positions of local states of Eu^{2+} and Yb^{2+} are included as well as bottom and top of conduction and valence band of the oxonitridosilicate host. For Eu^{2+} the lowest energy fd state is below the edge of the conduction band whereas for Yb^{2+} the lowest fd state is positioned within the conduction band.

References

1 P. Schlotter, J. Baur, Ch. Hielscher, M. Kunzer, H. Obloh, R. Schmidt, J. Schneider, Mater. Sci. Eng. B 59 (1999) 390.

2 Y. Hu, W. Zhuang, H. Ye, S. Zhang, Y. Fang, X. Huang, J. Lumin. 111 (2005) 139.

3 W. Schnick, Int. J. Inorg. Mat. 3 (2001) 1267.

4 H. Huppertz, W. Schnick, Acta Crystallogr. C 53 (1997) 1751.

5 T. Schlieper, W. Milius, W. Schnick, Z. Anorg. Allg. Chem. 621 (1995) 1380.

6 H.A. Höppe, H. Lutz, P. Morys, W. Schnick, A. Seilmeier, J. Phys. Chem. Solids 61 (2000) 2001.

7 J.W.H. van Krevel, On new rare-earth doped M-Si-Al-O-N materials, Ph.D. thesis (Universiteitsdrukkerij TU Eindhoven, Eindhoven, 2000).

8 V. Bachmann, T. Jüstel, C.R. Ronda, P.J. Schmidt, European Patent EP04106286.0.

9 P. Schmidt, T. Jüstel, W. Mayr, H.-D. Bausen, W. Schnick, H. Höppe, World Patent WO 2004/036962 A1.

10 H. Tamaki, S. Kakashima, World Patent WO 2004/039915 A1.

11 T. Fiedler, F. Jermann, World Patent WO 2005/030905 A1.

12 Y.Q. Li, A.C.A. Delsing, G. de With, H.T. Hintzen, Chem. Mater. 17 (2005) 3242.

13 R. Mueller-Mach, G. Mueller, M.R. Krames, H.A. Höppe, F. Stadler, W. Schnick, T. Juestel, P. Schmidt, phys. stat. sol. (a) 202 (2005) 1721.

14 H. Lange, G. Wötting, G. Winter, Angew. Chem. 103 (1991) 1606.

15 J.F. Suyver, J. J. Kelly, A. Meijerink, J. Lumin. 104, 3 (2003) 187.

16 T. Jüstel, J.-C. Krupa, D.U. Wiechert, J. Lumin. 93 (2001) 179.

17 H.A. Höppe, F. Stadler, O. Oeckler, W. Schnick, Angew. Chem. 116, 41 (2004) 5656.

18 W. Schnick, private communication.

19 W.H. Zhu, P.L. Wang, W.Y. Sun, D.S. Yan, J. Mater. Sci. Lett. 13 (1994) 560-562.

20 A. Meijerink, G. Blasse, J. Lumin. 43 (1989) 283.

21 S.H.M. Poort, H. M. Reijnhoudt, H. O. T. van der Kuip, G. Blasse, J. Alloys Comp. 241, (1996) 75.

22 P. Dorenbos, J. Lumin., 104, 4 (2003) 239.

23 W.M. Yen, M.J. Weber, Inorganic Phosphors, CRC Press, 2004.

24 S.H.M. Poort, A. Meijerink, G. Blasse, J. Phys. Chem. Solids 58, 9 (1997) 1451.

25 P. Schmidt, T. Jüstel, C. Clausen, W. Mayr, Meeting Abstracts volume 2002-1 of the 201st Meeting of The Electrochemical Society, Abstract No. 1195.

26 D. Criado, Pereyra, M.I. Alayo, Materials Characterization 50 (2003) 167.

27 K. Worhoff, L.T.M. Hilderink, A. Driessen, P.V. Lambeck, Proceedings ECS, 2001-7, 191.
28 M. Serenyi, M. Racz, T. Lohner, Vacuum 61 (2001) 245.
29 C.W. Struck, W.H. Fonger, J. Lumin. 10 (1975) 1.
30 E. v.d. Kolk, P. Dorenbos, C.W.E. van Eijk, S.A. Basun, G.F. Imbusch, W.M. Yen, Pys. Rev. B 71 (2005) 165120/1.
31 U. Happek, S.A. Basun, J. Choi, J.K. Krebs, M. Raukas, J. Alloys Comp. 303– 304 (2000) 198.
32 S. Lizzo, A. Meijerink, G. Blasse, J. Lumin. 59 (1994) 185.
33 S. Lizzo, A. Meijerink, G.J. Dirksen, G.Blasse, J. Lumin. 63 (1995) 223.
34 S. Lizzo, A.H.Velders, A. Meijerink, G.J. Dirksen, G. Blasse, J. Lumin. 65 (1995) 303.
35 J.W.M. Verwey, G.J. Dirksen, G. Blasse, J. Phys. Chem. Solids 53, 3 (1992) 367.
36 B. Moine, B. Courtois, C. Pedrini, J. Lumin. 48&49 (1991) 501.
37 B. Moine, C. Bruna, C. Pedrini, J. Lumin. 45 (1990) 248.
38 M. Raukas, S.A. Basun, W. van Schaik, U. Happek, W.M. Yen, Mat. Science Forum, 239-241 (1999) 249.
39 P. Dorenbos, J. Phys: Condensed Matter 15 (2003) 2645.
40 B. Moine, C. Pedrini, D.S. McClure, H. Bill, J. Lumin. 40&41 (1988) 299.

Chapter 3: Color point tuning for $Sr_{1-x-y-z}Ca_xBa_ySi_2O_2N_2:Eu_z^{2+}$ ($0 \leq x, y \leq 1$; $0.005 \leq z \leq 0.16$)

Color point tuning is an important challenge for improving white light LEDs. In this chapter the possibilities of color tuning with the efficient LED phosphor $Sr_{1-x-y-z}Ca_xBa_ySi_2O_2N_2:Eu_z^{2+}$ ($0 \leq x, y \leq 1$; $0.005 \leq z \leq 0.16$) are investigated. The emission color can be tuned in two ways: by changing Eu^{2+} concentration and by substitution of the host lattice cation Sr^{2+} by either Ca^{2+} or Ba^{2+}. The variation of the Eu^{2+} concentration shows a red shift of the emission upon increasing the Eu-concentration above 2%. The red shift is explained by energy migration and energy transfer to Eu^{2+} ions emitting at longer wavelengths. Along with this (desired) red shift there is an (undesired) lowering of the relative quantum efficiency and the thermal quenching temperature due to concentration quenching. Partial substitution of Sr^{2+} by either Ca^{2+} or Ba^{2+} also results in a red shifted Eu^{2+} emission. For Ca^{2+} this is expected and the red shift is explained by an increased crystal field splitting for Eu^{2+} on the (smaller) Ca^{2+} cation site. For Ba^{2+} the red shift is surprising. Often, a blue shift of the fd emission is observed in case of substitution of Sr^{2+} by the larger Ba^{2+} cation. The Eu^{2+} emission in the pure $BaSi_2O_2N_2$ host lattice is indeed blue shifted. Temperature dependent luminescence measurements show that the quenching temperature drops upon substitution of Sr by Ca, while for Ba substitution the quenching temperature remains high. Color tuning by partial substitution of Sr^{2+} by Ba^{2+} is therefore the most promising way to shift the color point of LEDs while retaining the high quantum yield and high luminescence quenching temperature.

3.1 Introduction

The market for white light emitting LEDs is expanding rapidly. From niche applications, like flashlights and traffic lights, white light LEDs are now finding their way into general lighting applications. This has an impact on phosphor research. Research on phosphors for lighting used to be focused on the conversion of 254 nm UV radiation from a mercury discharge into visible light. Today these phosphors, used in fluorescent tubes, are mature products, which are stable and highly efficient (90% quantum efficiency). Present work aims at incremental improvements in efficiency, morphology, price and stability of existing phosphors. With the invention of the near UV to blue emitting InGaN based LEDs by Nakamura [1] in 1991 and the development of high power LEDs (HP-LEDs) [2] in the same spectral region, the need for new phosphors arose. These phosphors have to efficiently absorb in the near UV to blue spectral range and emit in the visible. The energy difference between excitation and emission wavelength is small which is good for the energy efficiency, but it lowers the choice of activator ions that can be used and research is mainly focused on Eu^{2+} and Ce^{3+}. For an LED phosphor to be applied in commercial products several criteria have to be met such as: high efficiency in light conversion, high thermal quenching temperature, and the possibility to adjust the color point, e.g. by means of varying the chemical composition. Host lattices with a high degree of covalency and/or a large crystal field splitting at the site for which Ce^{3+} or Eu^{2+} substitute, can lead to efficient visible emission while absorbing light in the near UV to blue range of the electromagnetic spectrum. Presently oxides like $Y_3Al_5O_{12}:Ce^{3+}$ or sulfides like $CaS:Eu^{2+}$ are applied in phosphor converted LEDs (pcLEDs) as luminescent converters [3,4].

An important property of white light LEDs is the color temperature. The combination of the blue light from the LED and the yellow emission from the most widely applied YAG:Ce phosphor yields a relatively cool white light. For general lighting applications it is essential to make pc-LEDs that emit a warmer white light. A shift of the emission to the orange/red spectral region is needed to realize this.

There are several concepts for changing the emission color of a luminescent material. In inorganic luminescent compounds two different ways of realizing

the color tuning need to be differentiated. First, changing the amount of dopant in a host lattice and second, changing the host lattice itself. For the first case different origins are known for the observed color change with changing the amount of dopant. In case of Tb^{3+}-doped materials a color change from blue to green for increasing dopant concentrations is well-known [5]. For low Tb concentrations blue emission from the higher laying $^5D_3$ level can be seen. For higher dopant concentrations the lower excited level ($^5D_4$) is populated through cross-relaxation between Tb-neighbors, shifting the emission color to the green spectral region [6]. In Sr_2CeO_4 color shifting from the blue to red has been reported by doping with Eu^{3+} [7]. The color tuning is caused by energy transfer to the Eu^{3+} ion. The second concept in color tuning is changing the composition of the host lattice. A good overview on the possibility to tailor the photoluminescence of $Y_3Al_5O_{12}$:Ce given by Pan et al. [8]. Replacing Y^{3+} by Lu^{3+}, La^{3+}, Gd^{3+} and Al^{3+} by Ga^{3+}, In^{3+} are shown to shift the Ce^{3+} 5d-4f emission [8]. Partial substitutions between the ions Ca^{2+}, Sr^{2+} and Ba^{2+} is also utilized as a method for color point tuning. To name just two examples, You et al. reported on the tunable color emission in a $Ba_{1-x}Sr_xY_2S_4$:Eu^{2+} phosphor [9]. Exchanging Sr^{2+} by Ca^{2+}, Chen et al. reported a red shift in $SrAl_2O_4$:Eu [10]. In all these cases the energy of the excited 5d state of Eu^{2+} or Ce^{3+} is influenced by changes in the local surroundings.

The Eu^{2+} ion shows emission in the visible range in many lattices due to $4f^65d \rightarrow 4f^7$ transitions. Upon excitation an electron is promoted from a 4f-orbital to a 5d-orbital (4f-5d-absorption). The energy of the emitting lowest energy $4f^65d$ state depends on the covalency of the host lattice (nephelauxetic effect) and the crystal field splitting [11]. A new class of phosphor materials is the oxonitridosilicates, known as sions. The N^{3-} in this lattice is a soft Lewis base, which results in a high covalency. This affects the energy of the 4f-5d absorption and emission transitions for Eu^{2+} and Ce^{3+} ions when introduced to these host lattices. Higher condensed sions are known to be highly covalent and stable towards oxidation and hydrolysis [12]. We, among others, reported recently on $SrSi_2O_2N_2$:Eu^{2+} [13-17]. For this lattice the Eu^{2+} absorption and emission are in the visible range of the spectrum. The material was developed earlier in a synthesis approach leading to the highly efficient nitridosilicate phosphor $M_2Si_5N_8$:Eu^{2+} (M = Sr, Ba) [18-20]. The conversion efficiency, determined as relative quantum efficiency, is above 90% and the thermal

quenching temperature for the emission is high. Mueller-Mach et al. reported on the use of $SrSi_2O_2N_2:Eu^{2+}$ and $M_2Si_5N_8:Eu^{2+}$ (M = Ca, Sr, Ba) in pcLEDs [21] and show that these materials are promising for application.
This chapter reports on the possibility to tune the emission color for the LED phosphor $SrSi_2O_2N_2:Eu^{2+}$ in two different ways: first by varying the concentration of the Eu^{2+} dopant and second by replacing Sr^{2+} (partly or completely) by Ca^{2+} or Ba^{2+}. Structural changes, luminescence quenching temperatures and quantum efficiencies were examined to determine the influence of doping $SrSi_2O_2N_2:Eu^{2+}$. Temperature dependent luminescence and decay time measurements were done to understand the mechanisms responsible for the color change and the quenching behavior and to determine the most promising way to design new compositions that can serve as efficient phosphors in white light LEDs with a warmer color.

3.2 Experimental methods

Samples were synthesized using a conventional solid-state reaction. As starting materials were used: $SrCO_3$ (Philips Lighting Components, 99.9%), $CaCO_3$ (Philips Lighting Components, 99.9%), $BaCO_3$ (Philips Lighting Components, 99.9%), $Si_3N_{4-x}(NH)_{3/2x}$ ($x \approx 1$, made by thermal decomposition of $Si(NH)_2$ as described in [22], O content < 2wt%), and the rare earth dopant Eu_2O_3 (Alfa Aesar, REacton 99.999%). Mixtures of these materials were prepared by ball milling and firing for 2 to 4 hours at 1200 to 1500 °C in reducing atmosphere (H_2/N_2) in a tube furnace. When fired in a reducing atmosphere and being doped to a divalent lattice site, europium will be built into the host lattice as Eu^{2+}. After milling the raw product powders were washed with water and iso-propanol. XRD analysis was done on a Philips diffractometer PW 1729 at RT, using Cu K_α radiation. For the samples with a partial substitution of Sr by Ca or Ba, a shift of the lines in the diffraction pattern is observed due to a change in the lattice constants. Only for Ba and Ca contents larger 0.5 phase mixing rather than solid solution is observed.
Luminescence spectra were recorded between 4 K and 300 K on a Spex Fluorolog 2 spectrofluorimeter equipped with a helium flow cryostat. To study thermal quenching between 300 and 600 K the same spectrofluorimeter was equipped with a homemade heating cell. Both types of measurements

used a Xe-lamp as excitation source. The spectra were measured with a spectral resolution of 0.5 to 1.0 nm. This setup is described in detail in Ref. [23]. On a different setup quantum efficiencies were measured relative to a sample of YAG:Ce for which the absolute quantum efficiency is known to be 70%. This set-up was described before in Ref. [24]. Luminescence lifetime measurements were done using the third harmonic (355 nm) of a Quanta-ray DCR YAG:Nd laser as the excitation source. Luminescence decay curves were measured using a 0.25 m Acton Research monochromator and an RCA C31034 photomultiplier tube in combination with a Tektronix 2430 Digital Oscilloscope. For temperature dependent measurements the same type of cryostat and heating cell as described above are used.

3.3 Results and Discussion

3.3.1 Crystal Structures

The phase purity of the end compositions $CaSi_2O_2N_2$, $SrSi_2O_2N_2$, and $BaSi_2O_2N_2$ were checked using x-ray powder diffraction. For the first two compositions a precise structure analysis was published [25,26]. The structures of the two materials are similar but not isotypic. They were found to consist of alternating layers of Ca^{2+} or Sr^{2+} and layers of $(Si_2O_2N_2)^{2-}$. The latter type of layers is built exclusively on $SiON_3$-tetrahedrons. The N atoms bridge three of the Si atoms, while the O atoms are terminally bound to the Si atom. The O atoms coordinate in both cases the divalent cations Ca and Sr. There are four different Ca^{2+} and Sr^{2+} crystallographic sites in the lattice. $CaSi_2O_2N_2$ was found to have a monoclinic unit cell with lattice parameters a = 732.4(2), b = 1365.6(3), c = 1048.3(2) pm, β = 102.04(3) °. It belongs to space group $P2_1$ (No. 4). $SrSi_2O_2N_2$ was found to have a triclinic unit cell with the lattice parameters a = 708.02(2), b = 723.06(2), c = 725.54(2) pm, α = 88.767(3) °, β = 84.733(2) °, γ = 75.905(2) °. It belongs to space group *P*1 (No. 1).

For $BaSi_2O_2N_2$ structural investigations show that this compound has a layered structure like the two materials described above [27,28]. A precise description of the crystal structure is still lacking but the lattice parameters have been determined. The Ba-compound consists of an orthorhombic unit

cell with the lattice parameters a = 533.5(3), b = 482.9(2), c = 1437.8(7) pm. In this lattice there is only one crystallographic site for Ba^{2+}. This will have an impact on the luminescence spectra, which will be discussed later.
The x-ray diffraction patterns that were recorded for the various compositions of $Sr_{1-x-y-z}Ca_xBa_ySi_2O_2N_2:Eu_z^{2+}$ ($0 \leq x, y \leq 1$; $0.005 \leq z \leq 0.16$) are consistent with the crystal structures described above. By co-doping Ba or Ca in $SrSi_2O_2N_2$ a small shift of the diffraction peaks is observed due to a change in the lattice parameters as a result of the difference in ionic radius of Ca (smaller) or Ba (larger) with respect to Sr. The x-ray diffraction patterns will be shown and discussed in detail in connection with the luminescence properties below.

3.3.2 $Sr_{1-x}Eu_xSi_2O_2N_2$

The influence of the Eu^{2+} concentration on the luminescence properties was investigated by varying the Eu-concentration between 0.5 and 16%. Excitation and emission spectra show bands related to 4f-5d transitions as is commonly seen for Eu^{2+} doped luminescent materials. Figure 3-1 shows the excitation, emission and reflection spectrum at room temperature for the sample with 2% Eu^{2+}. As can be seen from the reflection spectrum, the host material doped with Eu^{2+} shows strong absorption in the blue spectral range of the spectrum which is consistent with a yellow daylight color. Excitation at 450 nm gives a green band emission centered around 539 nm. It differs in position and width from the emission band reported for $SrSi_2O_2N_{2+⅔\delta}:Eu^{2+}$ ($\delta \sim 1$) with the same XRD pattern [17]. This is probably due to the higher Eu^{2+} concentration (10%) in the case of the reference [17]. The influence of the Eu^{2+} concentration will be discussed later. The presently reported emission spectrum is the same as the emission spectrum given for the phase of the high temperature modification of $SrSi_2O_2N_2$:Eu in Ref. [16]. The emission band is assigned to the $4f^65d^1 \rightarrow 4f^7$ (5d-4f) transition on Eu^{2+}.
When comparing our highest doped sample (16% vs. 10% in the reference) a further red shift of the emission maximum as well as a pronounced shoulder on the low energy side of the spectrum in Ref. [17] is noticed. This has a large impact on the position of the color point in the CIE chromaticity coordinate diagram. Possibly this shift and the shoulder originate from trace mounts of

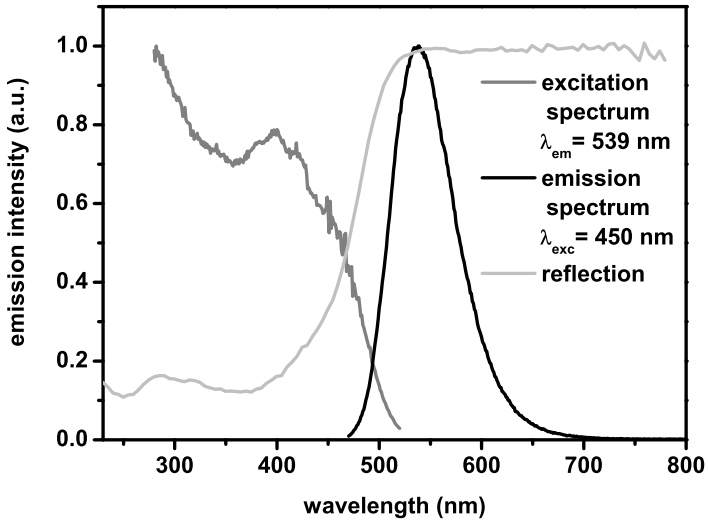

Figure 3-1 Luminescence excitation (gray line) for 539 nm emission, emission (black line) for 450 nm excitation and diffuse reflection spectrum (light gray line) of $SrSi_2O_2N_2:Eu^{2+}$ 2%, recorded at 298 K.

$Sr_2Si_5N_8:Eu^{2+}$, a red emitting phosphor [18-20], which are below the detection level of XRD.

An important parameter for LED phosphors is the luminescence quenching temperature. This is especially important in high power LEDs where the phosphor temperature can increase up to 450 K. In Figure 3-2a the temperature dependence of the Eu^{2+} emission spectra excited at 450 nm can be seen for the sample doped with 2% Eu^{2+}. In addition to monitoring the temperature dependence of the emission intensity, also the temperature dependence of the luminescence decay time was measured. For 355 nm excitation the luminescence decay curves for various temperatures are depicted in Figure 3-2b. All curves show single exponential decay behavior. The decay time at RT was measured to be 1.15 µs, which is a typical value found for green Eu^{2+} emission [29]. Integrated emission intensities from Fig. 3-2a and luminescence decay times derived from Fig. 3-2b are plotted as a function of temperature in Figure 3-2c. The lines through the data points represent a fit to equation 3-1 [13]:

(eq. 3-1)
$$\tau(T) = \frac{\tau_0}{1 + C \cdot e^{\frac{-E_A}{kT}}}; I(T) = \frac{I_0}{1 + D \cdot e^{\frac{-E_A}{kT}}}$$

Figure 3-2
a) Emission spectra of $SrSi_2O_2N_2$:Eu^{2+} 2% excited at 450 nm for various temperatures;

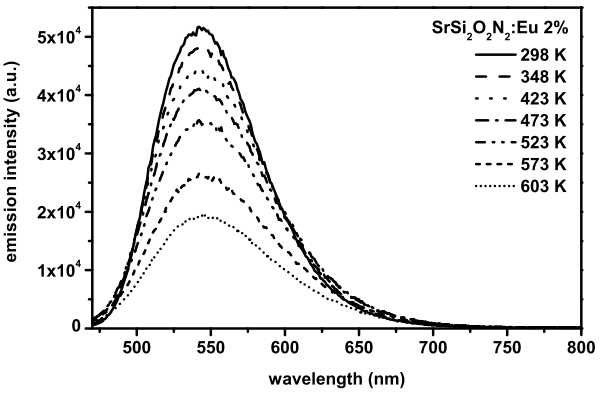

b) Luminescence decay curves of the Eu^{2+} emission (for 539 nm emission under 450 nm excitation) in $SrSi_2O_2N_2$:Eu^{2+} 2% for various temperatures;

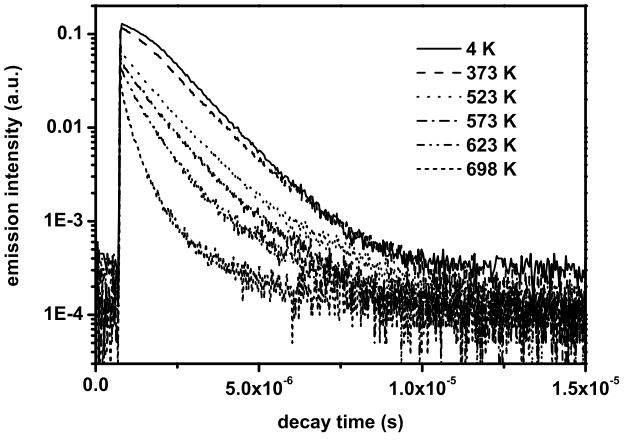

c) Temperature dependence of the integrated emission intensity (black squares) and luminescence decay times (open squares) derived from the curves in Fig. (b); the lines through the data points are fits to eq. 3-1.

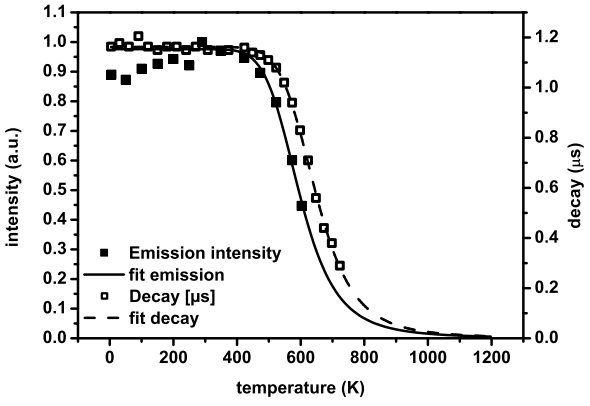

where τ(T) and I(T) are luminescence decay time and intensity at temperature T (K) respectively, τ_0 and I_0 the decay time and intensity at low temperatures (only radiative decay), C and D are the rate constants for the thermally activated escape, E_A is the activation energy connected with this process (the energy gap between the lowest energy Eu^{2+} $4f^6 5d^1$-excited level and the bottom of the conduction band) and k is the Boltzmann constant. The intensity at 4.2 K was set to 1. The experimental data are well described by eq. 3-1 and the plots were used to determine the temperature at which intensity drops to 50% of its initial value ($T_{50\%}$). From both the temperature dependence of the integrated emission intensity and the luminescence decay time, the $T_{50\%}$ for the sample doped with 2% Eu^{2+} is calculated to be around 600 K.

By varying the concentration of Eu^{2+} in the host lattice, the influence of energy migration and energy transfer processes on the (temperature) quenching and the color point can be studied. The dependence of the relative (room temperature) quantum efficiency and decay time for $Sr_{1-x}Eu_xSi_2O_2N_2$ (x = 0.005 – 0.16) is shown in Figure 3-3. The decay times in Fig. 3-3a result from single exponential fits to the decay curves depicted in Figure 3-3b. Decay times are constant around 1 μs for concentrations $x \leq 0.02$ and decrease for higher dopant concentrations. It is well known that energy migration due to energy transfer between Eu^{2+} ions followed by energy transfer to traps or quenching sites leads to a faster luminescence decay. Based on the decrease of the emission intensity and the luminescence life time for concentrations higher than 2% we conclude that the critical concentration for energy migration (x_c) for Eu^{2+} is at $x_c = 0.02$. The quantum efficiency is found to have a maximum at $x = 0.02$. One would expect the quantum efficiency to be at a constant level up to critical concentration and to only decrease, in analogy to the decay time, for higher doping levels. The observation of a maximum at 2% implies the presence of competing absorption processes by non-luminescent defects or impurities. At low Eu^{2+} concentrations (smaller than 2%) a significant part of the exciting radiation will be absorbed by these impurities or defects and will not result in Eu^{2+} emission, thus explaining the lower quantum efficiency

Turning to the influence of Eu^{2+} concentration on the color point the following observation is made. For concentrations up to 2% Eu^{2+} the color point is almost stable (no shift in the emission spectrum). Upon doping the host lattice with higher amounts of Eu^{2+} a continuous red shift is observed.

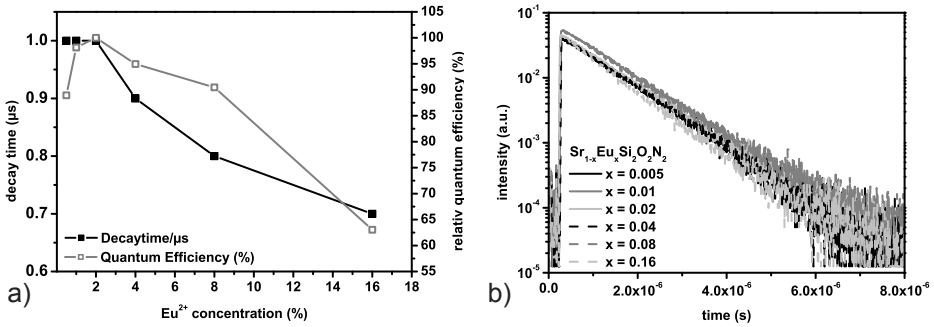

Figure 3-3 a) Dependence of decay time (black squares) derived from Fig. 3-3b and relative quantum efficiency (open gray squares) on the concentration of Eu^{2+} in $SrSi_2O_2N_2$ b) Luminescence decay curves of the Eu^{2+} emission (for 539 nm emission under 450 nm excitation) in $SrSi_2O_2N_2$:Eu^{2+} for the given concentrations.

There are two possible causes for the shift in color point: first, re-absorption and second, energy transfer between different Eu^{2+}-sites. In the case of re-absorption, the high energy part of the emission (resonant with the low energy part of the excitation spectrum) is reabsorbed thus shifting the emission spectrum to the red. In the case of energy transfer between Eu^{2+} ions, energy is transferred to Eu^{2+} emitting at lower energy, possibly via multiple energy transfer steps between Eu^{2+} ions (energy migration). To determine which process is responsible, the concentration dependence of the luminescence life time is considered. In the case of (multiple) reabsorption steps, the experimentally observed luminescence life time lengthens. The emission of photons is delayed by the reabsorption steps. In the case of energy transfer, the luminescence life time is shortened, especially on the shorter wavelength side of the emission spectrum. Due to this energy transfer process there is an additional decay channel that shortens the life time of the excited state. The results in Fig. 3-3b show a shortening of the life time upon increasing the Eu^{2+} concentration. This shows that the shift in color point is mainly caused by energy transfer processes, although a contribution from reabsorption cannot be excluded. Please note that the shift in color point is seen for Eu^{2+} concentrations larger 2%.

The presence of four different crystallographic sites can potentially cause a larger shift of the color point upon increasing the concentration. If the

emission bands of Eu^{2+} on the different sites are different, the energy will be transferred to the Eu^{2+} ions emitting at longer wavelengths (lower energy) upon increasing the concentration. From structure analysis it is known that of four crystallographic sites that can be occupied by Eu^{2+}, two sets of two have a similar surrounding [26]. To distinguish between the two types, emission spectra were recorded for a low concentration of Eu^{2+} (0.5%) at 4.2 K (Fig. 3-7a). It was not possible to distinguish between the two Eu^{2+} sites by means of optical spectroscopy indicating that the excitation spectra for the four different sites are similar and result in broad overlapping and unstructured excitation and emission bands bands. The emitting d-level positions for the different sites are too close to each other in energy to be clearly distinguished, even at low temperatures. Nevertheless some evidence for the presence of different sites can be found. In Figure 3-4 excitation spectra are depicted for of low-doped (0.5%) and high-doped (8%) samples. Excitation spectra were recorded for the high energy tail and the low energy tail of the emission (each at 5% of the maximum emission intensity). Monitoring the excitation spectrum for 480 nm and 640 nm emission for the sample with low Eu^{2+} concentration a difference in the region around 300 nm is observed, indicating a difference in the splitting of the $4f^6 5d$ excited states for the different sites. Monitoring the excitation spectra for the high Eu^{2+} concentration at for emission at 488 nm and 666 nm no significant differences in the excitation spectra are noticed since emission results mainly from the Eu^{2+} ions emitting at the longest wavelength upon excitation of all different Eu^{2+} ions (via energy transfer).

Figure 3-5 shows the emission spectra for $SrSi_2O_2N_2$ doped with various amounts of Eu^{2+}. It shows that varying the Eu^{2+} concentration can be used for tuning the color point. The spectral shift that can be realized is 8 nm (band maximum shifts from 539 nm at 0.5% Eu^{2+} to 547 nm at 16% Eu^{2+}). The shift in emission color is however accompanied by a reduction in the relative quantum efficiency due to concentration quenching. At room temperature the relative quantum efficiency for the 16% sample has dropped to 63%. This restricts the application of higher doped $SrSi_2O_2N_2$:Eu^{2+} phosphors. The thermal quenching behavior is also affected by increasing the concentration. Due to thermal broadening at elevated temperatures the spectral overlap between excitation and emission band increases upon raising the temperature.

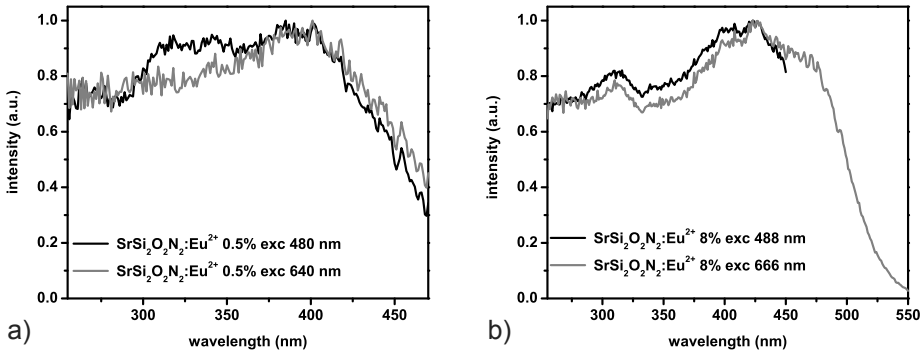

Figure 3-4 Excitation spectra for low-doped (a) and high-doped (b) $SrSi_2O_2N_2$ one of each taken at the high-energy side of the emission spectrum (black line) (in (a) at λ_{emi} = 480 nm; in (b) at λ_{emi} = 488 nm) and on the low-energy side of the emission spectrum (gray line) (in (a) at λ_{emi} = 640 nm; in (b) at λ_{emi} = 666 nm).

This leads to faster energy migration and stronger concentration quenching. The influence is however limited and the thermal quenching temperatures for the highest dopant concentrations are still acceptable ($T_{50\%}$ is 537 K and 471 K for 8% and 16% Eu^{2+}, respectively). Figure 3-6 shows the emission intensities of the samples containing 2, 8 and 16% Eu^{2+} as function of temperature. Intensities at 300 K were each normalized to unity. The thermal quenching of 4f-5d luminescence of 2% Eu^{2+} in $SrSi_2O_2N_2$ is marginal at typical LED operation temperatures ($T_{50\%}$ = 600 K). It also exhibits a high quantum efficiency of above 0.9, which makes this phosphor suitable for the use in pc-LEDs as proposed in Ref. [21]. In Table 3-1 optical and thermal properties for the different Eu^{2+} concentrations in $SrSi_2O_2N_2$ are summerized.

3.3.3 $Sr_{0.98-x-y}Ca_xBa_yEu_{0.02}Si_2O_2N_2$

3.3.3.1 $Ca_{0.98}Eu_{0.02}Si_2O_2N_2$ and $Ba_{0.98}Eu_{0.02}Si_2O_2N_2$

A second method to shift the position of the Eu^{2+} emission band is to replace part of the Sr^{2+} ions with a larger (Ba^{2+}) or smaller (Ca^{2+}) cations. This method is well established [30,31]. To understand the influence of partial replacement of Sr^{2+} by the other alkaline earth ions, it is good to compare the luminescence

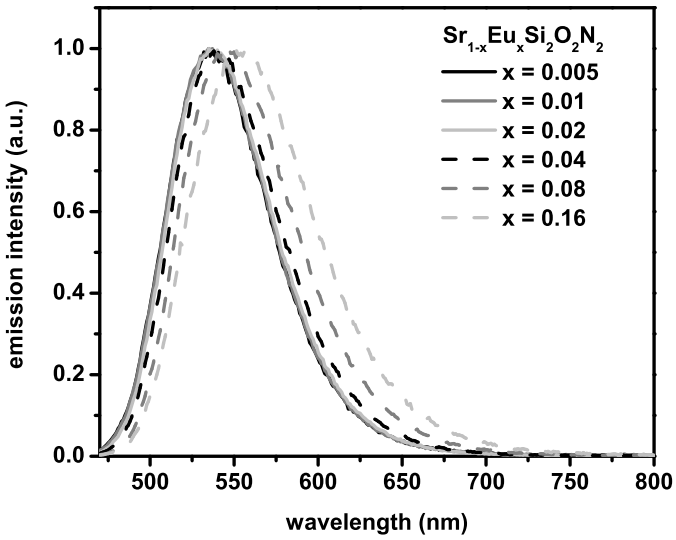

Figure 3-5 Normalized emission spectra for $Sr_{1-x}Eu_xSi_2O_2N_2$ (x = 0.005 – 0.16) at RT all excited at λ_{exc} = 450 nm.

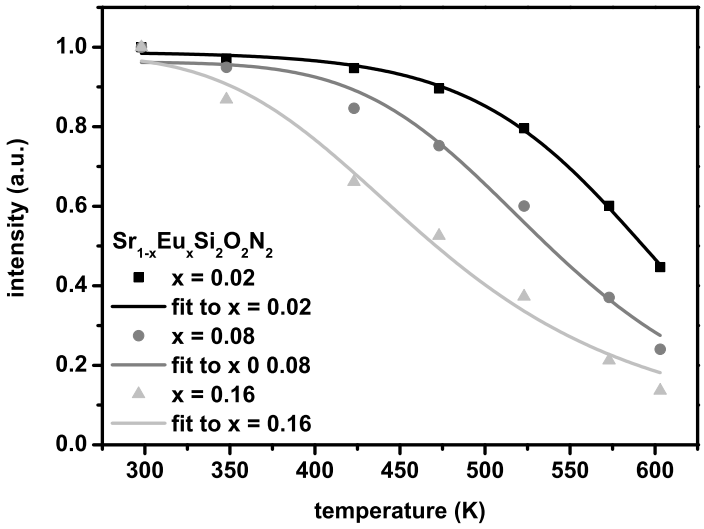

Figure 3-6 Temperature dependence of the integrated emission intensity (black squares for 2% Eu^{2+}, gray circles for 8% Eu^{2+}, light gray triangles for 16% Eu^{2+}); the lines through the data points are fits to eq. 3-1.

spectra of Eu^{2+} in the pure host lattices for all three alkaline earth ions. The ionic radii of the ions (in six-fold coordination) are 114 pm for Ca^{2+}, 131 pm for Eu^{2+}, 132 pm for Sr^{2+} and 149 pm for Ba^{2+} [26]. In Figure 3-7a the excitation and emission spectra are shown of the three compositions $BaSi_2O_2N_2$, $SrSi_2O_2N_2$ and $CaSi_2O_2N_2$ each doped with 2% Eu^{2+} measured at low temperature (4.2 K). The emission maxima are at 494 nm, 537 nm and 560 nm for the Ba, Sr and Ca compound, respectively. The onset of the $4f^65d$ band in the excitation spectra shifts to higher energies going from Ca to Ba. The room temperature luminescence of Eu^{2+} in the three compounds has also been reported in Ref. [17]. The results are similar, but differences in band width and in shape are found. The band widths are narrower in the presently reported spectra, which may originate from a better phase purity.

The shift to higher energies of the 4f-5d emission from Ca to Ba is due to two effects. First, the crystal field splitting of the d-manifold is smaller for Eu^{2+} on a larger cation site. As a result the position of the lowest energy 5d state (the emitting state) shifts to higher energies from Ca^{2+} to Sr^{2+} to Ba^{2+} host lattices, assuming that the barycenter is not affected. The energy of the

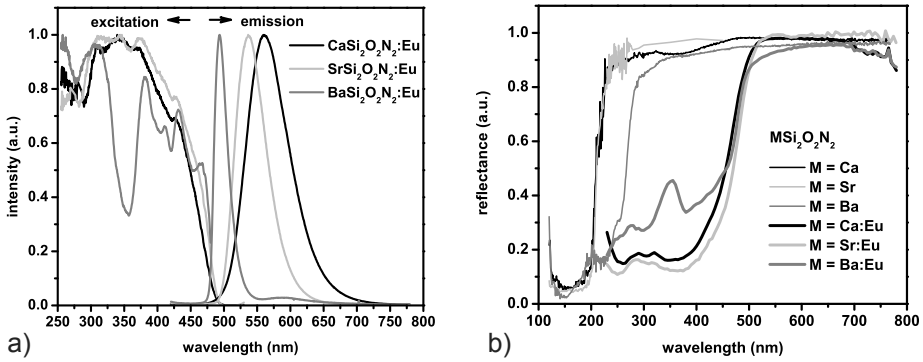

Figure 3-7 a) Excitation and emission spectra of $CaSi_2O_2N_2$ (black line), $SrSi_2O_2N_2$ (light gray line), and $BaSi_2O_2N_2$ (gray line) each doped with 2% Eu^{2+} taken at 4 K; emission spectra were taken at 450 nm excitation wavelength; excitation spectra were taken at the emission maxima (see Table II); b) diffuse reflection spectra of undoped (thin lines) and 2% Eu^{2+} doped (thick lines) $CaSi_2O_2N_2$ (black), $SrSi_2O_2N_2$ (light gray), and $BaSi_2O_2N_2$ (gray).

Table 3-1 Color coordinates, relative quantum efficiency (%), max. emission wavelength all at RT, quenching temperature $T_{50\%}$ (K); all for excitation wavelength of 450 nm for $Sr_{1-x}Eu_xSi_2O_2N_2$ (x = 0.005 – 0.16).

composition	x	y	QE (%)	λ_{max} (nm)	$T_{50\%}$ (K)
$SrSi_2N_2O_2$:Eu 0.5%	0.330	0.621	89	535	-
$SrSi_2N_2O_2$:Eu 1.0%	0.330	0.621	98	535	-
$SrSi_2N_2O_2$:Eu 2%	0.337	0.619	100	538	600
$SrSi_2N_2O_2$:Eu 4%	0.352	0.611	95	541	-
$SrSi_2N_2O_2$:Eu 8%	0.384	0.590	90	546	537
$SrSi_2N_2O_2$:Eu 16%	0.419	0.562	63	554	471

barycenter is lower for Eu^{2+} in a more covalent host lattice. The covalency of the oxonitridosilicates is expected to be similar, although the covalency of the Ba-compound is probably higher. A second reason for the shift of the emission to lower energies from Ba to Sr to Ca is the Stokes' shift. The Stokes' shift is largest for the Eu^{2+} emission in the Ca-compound and smallest in the Ba-compound. The width of the emission band becomes larger as the Stokes' shift increases. These observations are typical for the luminescence of Eu^{2+} in (isostructural) alkaline earth compounds. The results are explained by considering the relaxation in the $4f^65d$ excited state. There is increasing evidence that, contrary to most luminescent ions and molecules, the equilibrium distance in the excited state of Eu^{2+} is smaller than for the ground state [32-34]. As a result, the contraction in the $4f^65d$ excited state is largest when Eu^{2+} is substituted on a small cation site (like Ca^{2+}) and this will result in the largest relaxation and shift of the parabolas in the configurational coordinate diagram. On the other hand, when Eu^{2+} replaces a large cation (like Ba^{2+}) a reduction of the distance between Eu^{2+} and the coordinating anions will be unfavorable since the site is already too large for Eu^{2+}. The small relaxation results in a small shift of the parabolas in the configurational coordinate diagram which is reflected in the luminescence spectra by a small Stokes' shift, narrow bands and a high luminescence quenching temperature. Even though the compounds investigated are not isostructural, the differences

in the luminescence spectra for Eu^{2+} in the three compounds can be explained by the model discussed above. The temperature quenching behavior for the Eu^{2+} emission will be discussed below.

A second difference that can be observed, is that the excitation spectrum for the Eu^{2+} emission in $BaSi_2O_2N_2$ shows relatively narrow bands and structure that is explained by the splitting of the $4f^6$ core in the $4f^65d$ excited state into the different ^7F_J components [34]. The width of the lowest energy excitation band (between 375 and 475 nm) is about 5900 cm^{-1}, slightly larger than the theoretical ^7F_J splitting of 5000 cm^{-1}. The fact that the structure cannot be observed for Eu^{2+} in the Ca- and Sr- compound is probably due to the presence of four different crystallographic sites, each with slightly different excitation spectra. The overlapping spectra of the four different types of Eu^{2+} ions results in a broad band. In addition, the larger width of the excitation band (due to the larger relaxation in the excited state as discussed above) will also contribute to the absence of a well-resolved structure in the excitation spectra for Eu^{2+} in $CaSi_2O_2N_2$ and $SrSi_2O_2N_2$. The diffuse reflection spectra of the three compositions each doped with 2% Eu^{2+} are

Table 3-2 Summary of luminescence and thermal properties for $CaSi_2O_2N_2$, $SrSi_2O_2N_2$, $BaSi_2O_2N_2$ each doped with 2% Eu^{2+}.

property	$CaSi_2O_2N_2$	$SrSi_2O_2N_2$	$BaSi_2O_2N_2$
emission maximum	560 nm	537 nm	494 nm
absorption maximum	355 nm	360 nm	380 nm
onset absorp. undoped	210 nm	210 nm	260 nm
Stokes shift [a]	0.64 eV	0.43 eV	0.14 eV
FWHM	0.29 eV	0.23 eV	0.12 eV
onset quenching (decay)	380 K	450 K	420 K
quenching temp. $T_{50\%}$	440 K	600 K	600 K

[a] As determined from the emission and excitation maxima. A more careful analysis for the low temperature spectra will yield a smaller Stokes shift, see also Ref. [34].

shown in Fig. 3-7b. The spectra are consistent with the excitation spectra. To determine the bandgap of the three alkaline earth oxonitridosilicates, diffuse reflection spectra were also recorded for the undoped compounds. Figure 3-7b depicts the reflection spectra. The absorption onset is at 260 nm (4.8 eV) for $BaSi_2O_2N_2$ and 210 nm (5.9 eV) for $CaSi_2O_2N_2$ and $SrSi_2O_2N_2$. In Table 3-2 the luminescence properties are collected for comparison.

3.3.3.2 $Sr_{0.98-x}Ca_xEu_{0.02}Si_2O_2N_2$ ($0 \leq x \leq 1$)

A high flexibility in the color point tuning may be achieved by continuously varying the fraction x in $Sr_{0.98-x}Ca_xEu_{0.02}Si_2O_2N_2$ between 0 and 0.98. It is known from references [25] and [26] that the structures for the Ca- and the Sr-compounds are similar although not isotypic. To investigate the structural changes upon increasing the Ca-content, x-ray powder diffractograms were recorded. In Fig. 3-8 the diffractograms are shown. The overall pattern does not change up to a Ca fraction of 0.5. Upon increasing the Ca content the diffraction peaks shift to larger angles. This indicates that solid solutions are formed. The shift of the diffraction peaks to larger angles is consistent with a contraction of the lattice parameters due to the smaller ionic radius of Ca^{2+} in comparison to Sr^{2+}. For Ca^{2+} fraction of 0.5 and higher there may be a mixture of two structures rather than a solid solution.
In Figure 3-9 the Eu^{2+} emission spectra are shown for various compositions. The emission band continuously shifts to longer wavelengths as the fraction of Ca^{2+} is increased. Along with the spectral shift, the width of the emission band and the Stokes' shift increase. By varying the Ca to Sr ratio, the maximum of the emission band can be tuned precisely to any wavelength between 537 and 560 nm.
The thermal quenching of the luminescence is important for applications. To study the influence of the replacement of Sr by Ca on the luminescence quenching, the intensity of the Eu^{2+} emission and the luminescence decay time were measured as a function of temperature for $CaSi_2O_2N_2$ with 2% Eu^{2+}. In Figure 3-10 the results are shown. The luminescence decay time and the emission intensity steadily decrease between 300 and 600 K. The decay time of 1 µs at RT is typically found for Eu^{2+} activated phosphors emitting in the green spectral region [29]. The plot of the decay times and the emission intensities

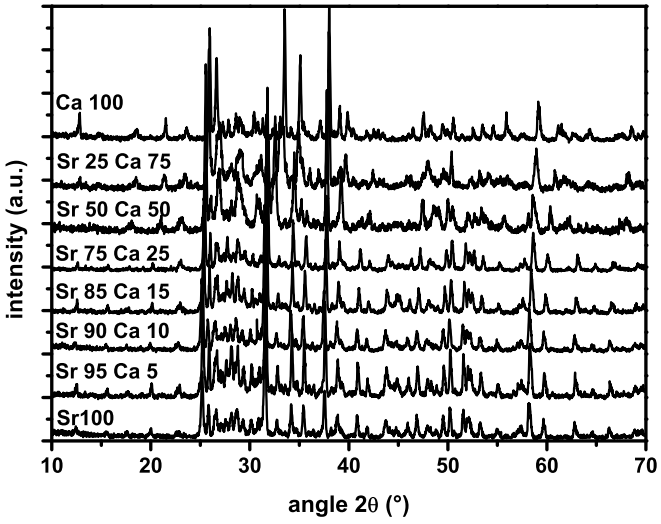

Figure 3-8 XRD Patterns of $Sr_{1-x}Ca_xSi_2O_2N_2:Eu^{2+}$ 2% (x = 0 – 1) taken with Cu Kα radiation at RT.

as a function of temperature (Fig. 3-10) shows that the onset of the thermal quenching is around 300 K and $T_{50\%}$ is around 440 K. One would expect the temperature dependence of the intensity and the luminescence decay time to be the same, both being affected in a similar manner by thermally induced non-radiative decay processes. The results show that the intensity starts to drop in a lower temperature range than the decay time. Possibly, this can be due to thermally activated non-radiative relaxation from a higher f-d state, before thermal equilibrium is reached. In spite of the discrepancy between the temperature dependence of the luminescence life time and intensity, it is clear that the luminescence quenching temperature is much lower than for the Eu^{2+} emission in $Sr_{0.98}Eu_{0.02}Si_2O_2N_2$ and that it is too low for an application of $Ca_{0.98}Eu_{0.02}Si_2O_2N_2$ in high power LEDs. For two intermediate compositions also the temperature dependence of the emission intensity was measured. The results are shown in Figure 3-11. For the sample with x = 0.25 the quenching temperature $T_{50\%}$ is 557 K and for x = 0.5 $T_{50\%}$ is 500 K. This shows that also the quenching temperature of the emission gradually decreases upon raising the fraction of Ca.

For all compositions the relative luminescence quantum efficiency was determined at 300 K. For values of x between 0 and 0.5 the quantum efficiency

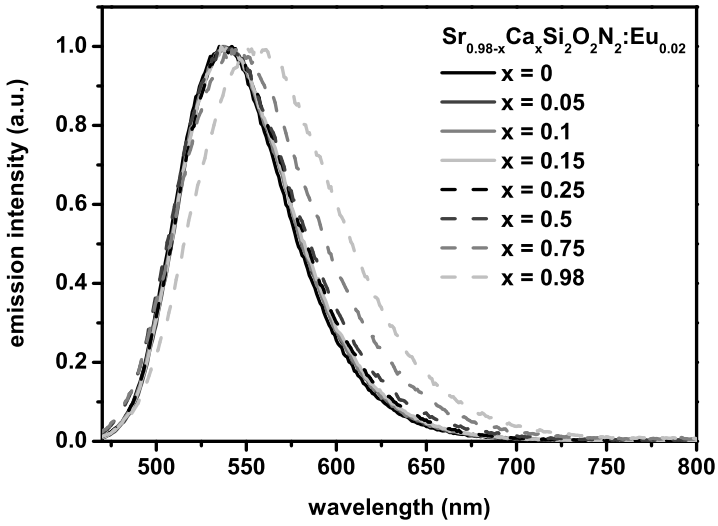

Figure 3-9 Normalized emission spectra for $Sr_{1-x}Ca_xSi_2O_2N_2:Eu^{2+}$ 2% (x = 0 – 1) at RT all excited at λ_{exc} = 450 nm.

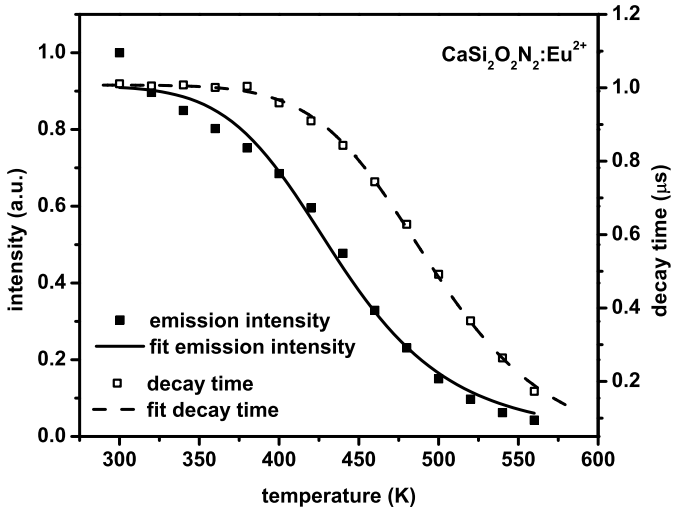

Figure 3-10 Temperature dependence of the integrated emission intensity (black squares) and luminescence decay times (open squares) in $CaSi_2O_2N_2:Eu^{2+}$ 2% all excited at λ_{exc} = 450 nm; the lines through the data points are fits to eq. 3-1.

at room temperature is unchanged high. For the samples with x = 0.75 and x = 1.0 a lower quantum efficiency is measured (89 and 83%, respectively). All the results are tabulated in Table 3-3. The table shows that the luminescence properties gradually change from those of $Ca_{0.98}Eu_{0.02}Si_2O_2N_2$ to those of $Sr_{0.98}Eu_{0.02}Si_2O_2N_2$. Up to a fraction of x = 0.5 the relative quantum efficiency and thermal quenching temperature are high and meet the criteria for application in pc-LEDs. Above x = 0.5 the relative quantum efficiency and luminescence quenching temperature drop to values that are too low for commercial application. Based on this, one can conclude that Ca-doping can be used for color point tuning in $Sr_{0.98}Eu_{0.02}Si_2O_2N_2$ up to a fraction of 0.5. Note however that the spectral shift that can be achieved is limited (from 538 nm for x = 0 to 543 nm for x = 0.5).

3.3.3.3 $Sr_{0.98-x}Ba_xEu_{0.02}Si_2O_2N_2$ ($0 \leq x \leq 1$)

The Eu^{2+} emission band for $BaSi_2O_2N_2$:Eu is shifted to shorter wavelengths (495 nm) in comparison to the Eu^{2+} emission band for $SrSi_2O_2N_2$:Eu

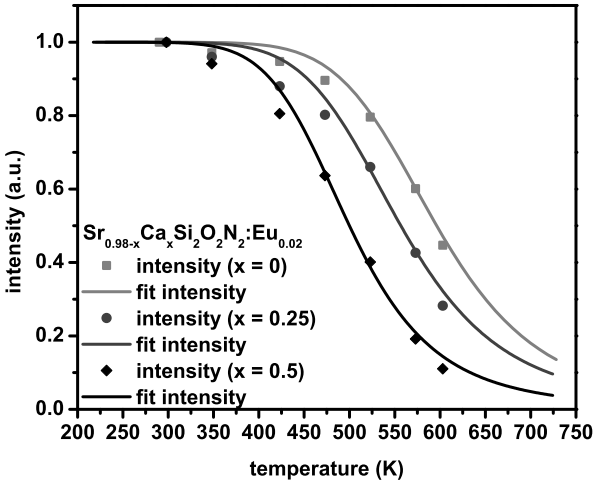

Figure 3-11 Temperature dependence of the integrated emission intensity $Sr_{1-x}Ca_xSi_2O_2N_2$:Eu^{2+} 2% (x = 0, 0.25, 0.5), all excited at λ_{exc} = 450 nm; the lines through the data points are fits to eq. 3-1.

Table 3-3 Color coordinates, relative quantum efficiency (%), max. emission wavelength all at RT, quenching temperature $T_{50\%}$ (K); all for excitation wavelength of 450 nm for $Sr_{1-x}Ca_xSi_2O_2N_2:Eu^{2+}$ 2% (x = 0 – 1).

composition	x	y	QE (%)	λ_{max} (nm)	$T_{50\%}$ (K)
$SrSi_2N_2O_2$:Eu 2%	0.337	0.619	100	538	600
(Sr,Ca5%)$Si_2N_2O_2$:Eu 2%	0.342	0.616	98	538	-
(Sr,Ca10%)$Si_2N_2O_2$:Eu 2%	0.345	0.614	100	538	-
(Sr,Ca15%)$Si_2N_2O_2$:Eu 2%	0.349	0.611	100	536	-
(Sr,Ca25%)$Si_2N_2O_2$:Eu 2%	0.351	0.608	100	542	557
(Sr,Ca50%)$Si_2N_2O_2$:Eu 2%	0.354	0.601	100	543	500
(Sr,Ca75%)$Si_2N_2O_2$:Eu 2%	0.378	0.581	89	546	-
$CaSi_2N_2O_2$:Eu 2%	0.419	0.556	83	555	440

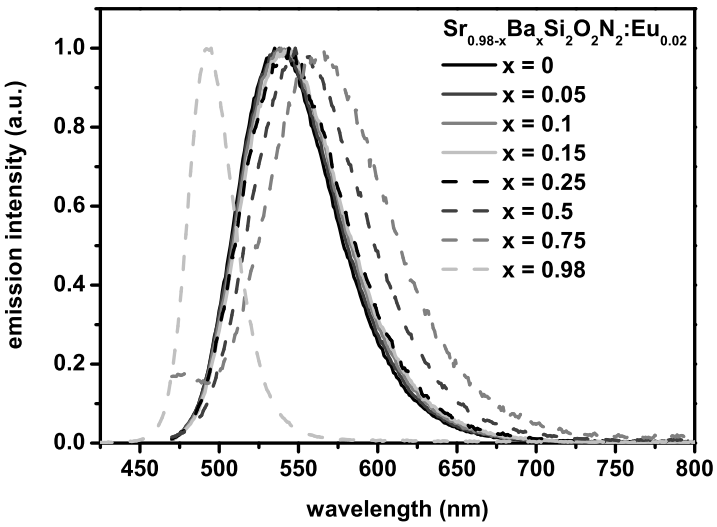

Figure 3-12 Normalized emission spectra for $Sr_{1-x}Ba_xSi_2O_2N_2:Eu^{2+}$ 2% (x = 0 – 1) at RT all excited at λ_{exc} = 450 nm.

(538 nm). To investigate the influence of partial replacement of Sr by Ba, a concentration series was investigated for $Sr_{0.98-x}Ba_xEu_{0.02}Si_2O_2N_2$ with x = 0.05, 0.1, 0.15, 0.25, 0.5, 0.75 and 1. In Figure 3-12 the emission spectra are shown. Up to a concentration of x = 0.75 there is a continuous red shift of the emission band to longer wavelengths from 538 nm for x = 0 to 564 nm for x = 0.75. However, for x = 1 there is a sudden blue shift of the emission band maximum to 495 nm.

To understand this unexpected behavior, the x-ray diffraction patterns are considered. The XRD patterns for the various compositions are depicted in Fig. 3-13. The patterns show that even for small amounts of Ba-doping there is a shift in the reflexes to smaller angles. This is accompanied by changes in the intensity ratios between the strongest reflections. The shifts to smaller angles shows that the lattice parameters increase upon replacing part of the Sr-ions with the (larger) Ba-ions, as expected for a solid solution of Sr and Ba. Intensity changes can be ascribed to differences in the scattering power between Sr and Ba. A drastic change is observed between the XRD patterns for x = 0.75 and x = 1: the XRD pattern for x = 1 corresponds to a different crystal structure, the structure of $BaSi_2O_2N_2$ (as discussed in section 3.3.1). Based on the XRD patterns we conclude that upon replacing Sr by Ba, the crystal structure of the Sr-compound is preserved up to a fraction of 0.75 for Ba^{2+}. The transition to solid solutions with the Ba-phase occurs for a fraction between 0.75 and 1 (the exact fraction cannot be determined from the present data). The luminescence measurements show that for the solid solutions $Sr_{0.98-x}Ba_xEu_{0.02}Si_2O_2N_2$ the emission shifts to longer wavelengths as the fraction x of Ba increases. This behavior seems to be opposite to the expected blue shift in view of the larger lattice parameters due to the larger size of Ba^{2+} ion. The red shift may be explained by the fact that the $SrSi_2O_2N_2$ structure is preserved while a part of the Sr^{2+} ions is replaced by the larger Ba^{2+} ions. To accommodate these larger cations, the bond lengths between Sr^{2+} (or Eu^{2+}) and the anions may not increase or even become slightly smaller, thus increasing the crystal field splitting, causing a red shift of the emission. Also, the shrinking of the bondlengths between Eu^{2+} and the coordinating anions will not be hampered in the excited $4f^65d$ state. Only after the transition (for x = 1) to a different crystal structure in which the cation-anion bondlengths are larger (determined by the Ba^{2+} ion) the substitution of Eu^{2+} on this (larger)

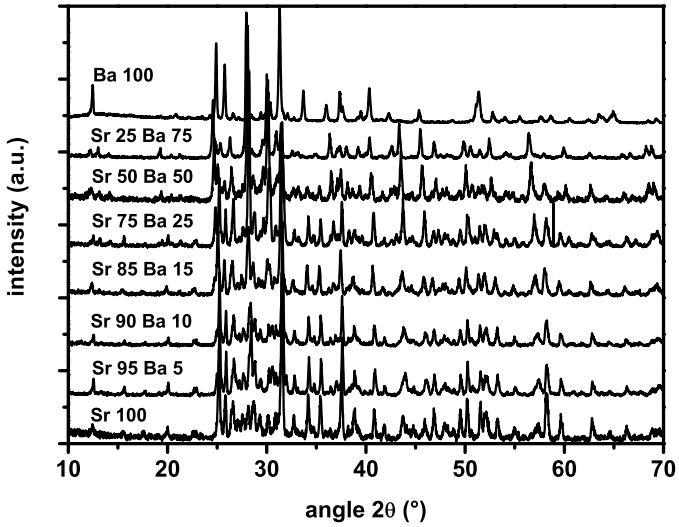

Figure 3-13 XRD Patterns of $Sr_{1-x}Ba_xSi_2O_2N_2:Eu^{2+}$ 2% (x = 0 – 1) taken with Cu Kα radiation at RT.

cation site will result in a blue shifted emission due to a smaller crystal field splitting and a smaller relaxation in the $4f^6$5d excited state for Eu^{2+}. To validate this hypothesis, it will be useful to have an accurate crystal structure determination for $BaSi_2O_2N_2$ with information on the coordination and bondlengths to the anions for the Ba^{2+} ion.

To evaluate the potential as color converter in LEDs the thermal quenching behavior has been measured for a number of compositions. For the Eu^{2+} emission in $Ba_{0.98}Eu_{0.02}Si_2O_2N_2$ both the emission intensity and the decay times between 300 and 600 K were measured. All decay curves were found to be single exponential. In Figure 3-14 emission intensity and decay time are plotted as function of temperature. The intensity at 300 K was normalized to 1. The room temperature decay time was found to be 0.47 µs. This decay time is shorter than expected for a radiative decay for Eu^{2+} emission with a maximum at 495 nm [29]. The shorter life time may be explained by the low quantum efficiency at room temperature. The relative quantum yield is only 78% indicating that there is already non-radiative decay at 300 K. If this is the case, the life time of 0.47 µs contains a radiative and a non-radiative component and the radiative decay rate can estimated to be 0.65 µs which is slightly shorter than the expected value (~0.8 µs at 490 nm) [29]. The results

in Fig. 3-14 show that the onset of thermal quenching is above 300 K and the value of $T_{50\%}$ for both curves is found to be around 600 K. In this chapter we have not studied the quenching mechanism in detail. For $Sr_{0.98}Eu_{0.02}Si_2O_2N_2$ we have recently shown that luminescence quenching occurs through thermally activated ionization from the $4f^65d$ excited state to the conduction band. This may very well be the quenching mechanism for the Eu^{2+} emission in $Ba_{0.98}Eu_{0.02}Si_2O_2N_2$ as well, but this aspect has not been further investigated here. An excellent overview on the quenching mechanisms for the Eu^{2+} emission has been published by Dorenbos [35].

To investigate the luminescence temperature quenching for the mixed (Sr,Ba) compounds, the temperature dependence of the emission intensities for the samples containing 25 and 50% Ba^{2+} was measured. The results are shown in Fig 3-15. For comparison the temperature dependence of the emission intensity of the pure Sr-compound is also included. The intensity at 300 K was normalized to unity for all three samples. From Figure 3-15 it is clear

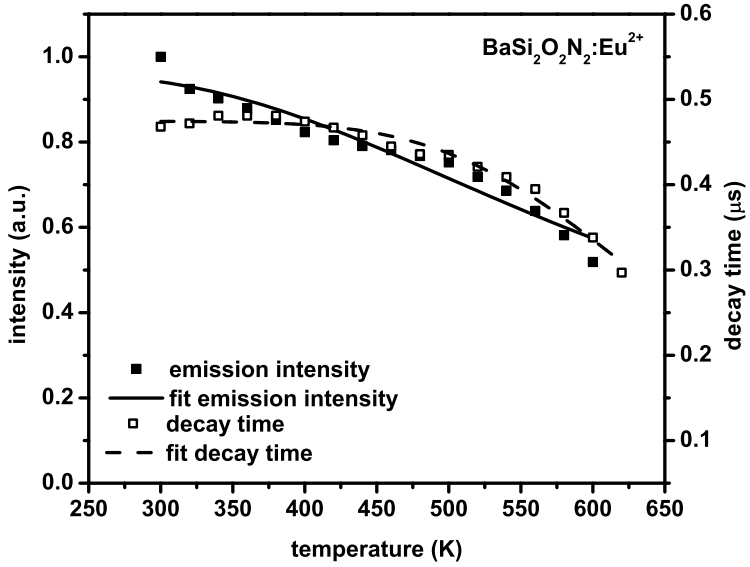

Figure 3-14 Temperature dependence of the integrated emission intensity (black squares) and luminescence decay times (open squares) in $BaSi_2O_2N_2$:Eu^{2+} 2% all excited at λ_{exc} = 450 nm; the lines through the data points are fits to eq. 3-1.

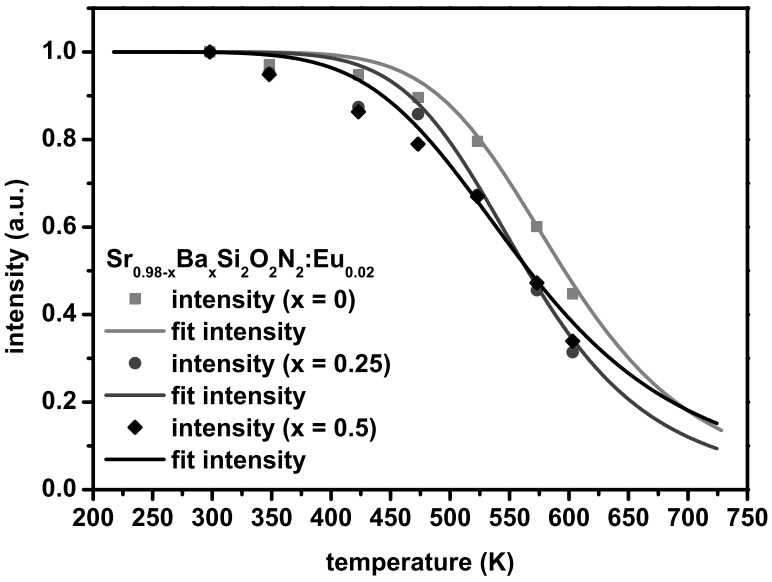

Figure 3-15 Temperature dependence of the integrated emission intensity $Sr_{1-x}Ba_xSi_2O_2N_2:Eu^{2+}$ 2% (x = 0, 0.25, 0.5), all excited at λ_{exc} = 450 nm; the lines through the data points are fits to eq. 3-1.

that the quenching temperature $T_{50\%}$ is reduced from 600 K for $SrSi_2O_2N_2$:Eu to 560 K for the two Ba-doped materials. These quenching temperatures are however still high enough for application in high power LEDs where the temperature of the phosphor is between 450 and 500 K. The relative quantum efficiencies at RT for the Eu^{2+} emission in the mixed Ba-Sr compositions are also high (~100%). From that it is concluded that small amounts of Ba^{2+} doped into $SrSi_2O_2N_2$:Eu are useful for tuning the color point. The shifting of the color point can be achieved while preserving a high quantum efficiency and a high thermal quenching temperature. The spectral range over which the emission maximum can be tuned is 538 nm to 548 nm. Table 3-4 contains a summary of emission maxima, color points, quantum efficiencies and thermal quenching parameters for $Sr_{0.98-x}Ba_xEu_{0.02}Si_2O_2N_2$.

3.4 Conclusions

The ability to tune the emission color of a luminescent material is of great importance for practical applications. Here the color tuning for the efficient

Table 3-4 Color coordinates, relative quantum efficiency (%), max. emission wavelength all at RT, quenching temperature $T_{50\%}$ (K); all for excitation wavelength of 450 nm for $Sr_{1-x}Ba_xSi_2O_2N_2:Eu^{2+}$ 2% (x = 0 – 1).

composition	x	y	QE (%)	λ_{max} (nm)	$T_{50\%}$ (K)
$SrSi_2N_2O_2$:Eu 2%	0.337	0.619	100	538	600
(Sr,Ba5%)$Si_2N_2O_2$:Eu 2%	0.343	0.614	100	538	-
(Sr,Ba10%)$Si_2N_2O_2$:Eu 2%	0.351	0.610	99	539	-
(Sr,Ba15%)$Si_2N_2O_2$:Eu 2%	0.358	0.606	97	544	-
(Sr,Ba25%)$Si_2N_2O_2$:Eu 2%	0.361	0.602	87	544	560
(Sr,Ba50%)$Si_2N_2O_2$:Eu 2%	0.401	0.573	99	548	560
(Sr,Ba75%)$Si_2N_2O_2$:Eu 2%	0.434	0.528	73	564	-
$BaSi_2N_2O_2$:Eu 2%	0.076	0.440	78	495	600

oxonitridosilicate phosphor $SrSi_2O_2N_2:Eu^{2+}$ is reported with a focus on the use of this material in high power white light LEDs. To change the color of the emission two concepts were followed: (1) varying the concentration of the Eu^{2+} dopant and (2) changing the host lattice composition by replacing Sr^{2+} with either Ca^{2+} or Ba^{2+}.

Upon raising the Eu^{2+} concentration above 2% a red shift in the emission is observed from 535 nm (0.5% Eu^{2+}) to 554 nm (16% Eu^{2+}). This is ascribed to energy migration and energy transfer between the dopant ions. Increasing the concentration of Eu^{2+} however also results in a decrease of the quantum efficiency and luminescence quenching temperature, which makes this concept not suitable for color tuning aimed at application in white light LEDs.

The concept of color tuning by changing the host lattice was found to be very promising. Replacing part of the host lattice cation Sr^{2+} with Ca^{2+} shows a red shift in the emission while retaining the high (90%) quantum efficiency. The luminescence quenching temperature is however lower for the Eu^{2+} emission in the mixed (Sr,Ca) compounds. Admixture of Ba^{2+} to the host lattice shows an unexpected red shift of the Eu^{2+} emission. For the mixed composition with

up to 50% Ba^{2+}, the high quantum efficiency and a high thermal quenching temperature are maintained for the red-shifted Eu^{2+} luminescence. Based on this, Ba^{2+} substitution is a promising method for shifting the emission of $SrSi_2O_2N_2$:Eu to longer wavelengths.

References

1 S. Nakamura, Jpn. J. Appl. Phys. 30 (1991) L1705.

2 S. Nakamura, G. Fasol, The blue Laser Diode: GaN Based Light Emitters and Lasers, (Springer, Berlin) (1997) 343.

3 P. Schlotter, J. Baur, Ch. Hielscher, M. Kunzer, H. Obloh, R. Schmidt, J. Schneider, Mater. Sci. Eng. B 59 (1999) 390.

4 Y. Hu, W. Zhuang, H. Ye, S. Zhang, Y. Fang, X. Huang, J. Lumin. 111 (2005) 139.

5 G.C. Kim, H.L. Park, T.W. Kim, Mat. Res. Bull. 36 (2001) 1603.

6 G. Blasse, B.C. Grabmaier, Luminescent Materials (1994) Springer, Berlin.

7 R. Sankar, G.V. Subba Rao, J. Electrochem. Soc. 147 (7) (2000) 2773.

8 Y. Pan, M. Wu, Q. Su, J. Phys. Chem. Sol. 65 (2004) 845.

9 Y.C. You, J.S. Choi, Y.R. Do, T.W. Kim, H.L. Park, Solid State Commun. 99 (12) (1996) 961.

10 L.T. Chen, C.S. Hwang, I.L. Sun, I.G. Chen, J. Lumin. 118 (2006) 12.

11 V. Bachmann, A. Meijerink, C. Ronda, submitted to J. Lumin.

12 W. Schnick, Int. J. Inorg. Mat. 3 (2001) 1267-1272.

13 V. Bachmann, T. Jüstel, A. Meijerink, C. Ronda, P.J. Schmidt, J. Lumin. 121 (2006) 441.

14 P. Schmidt, T. Jüstel, W. Mayr, H.-D. Bausen, W. Schnick, H. Höppe, World Patent WO 2004/036962 A1.

15 H. Tamaki, S. Kakashima, World Patent WO 2004/039915 A1.

16 T. Fiedler, F. Jermann, World Patent WO 2005/030905 A1.

17 Y.Q. Li, A.C.A. Delsing, G. de With, H.T. Hintzen, Chem. Mater. 17 (2005) 3242.

18 H. Huppertz, W. Schnick, Acta Crystallogr. C 53 (1997) 1751.

19 T. Schlieper, W. Milius, W. Schnick, Z. Anorg. Allg. Chem. 621 (1995) 1380.

20 H.A. Höppe, H. Lutz, P. Morys, W. Schnick, A. Seilmeier, J. Phys. Chem. Solids 61 (2000) 2001.

21 R. Mueller-Mach, G. Mueller, M.R. Krames, H.A. Höppe, F. Stadler, W. Schnick, T. Juestel, P. Schmidt, phys. stat. sol. (a) 202 (2005) 1721.

22 H. Lange, G. Wötting, G. Winter, Angew. Chem. 103 (1991) 1606.

23 J.F. Suyver, J.J. Kelly, A. Meijerink, J. Lumin. 104, 3 (2003) 187.

24 T. Jüstel, J.-C. Krupa, D.U. Wiechert, J. Lumin. 93 (2001) 179.
25 H.A. Höppe, F. Stadler, O. Oeckler, W. Schnick, Angew. Chem. 116, 41 (2004) 5656.
26 O. Oeckler, F. Stadler, T. Rosenthal, W. Schnick, Solid State Sci. 9 (2) (2007) 205.
27 W. Schnick, private communication.
28 A. Tücks, P. Schmidt, private communication.
29 S.H.M. Poort, A. Meijerink, G. Blasse, J. Phys. Chem. Solids 58,9 (1997) 1451.
30 C. Dujardin, B. Moine, C. Pedrini, J. Lumin. 54 (1993) 259.
31 J.S. Kim, P.E. Jeon, J.C. Choi, H.L. Park, Solid State Commun. 133 (3) (2005) 187.
32 Z. Barandiarán, L. Seijo, J. Chem. Phys. 119 (7) (2003) 3785.
33 Z. Barandiarán, N.M. Edelstein, B. Ordejón, F. Ruiperez, L. Seijo, J. Sol. Stat. Chem. 178 (2005) 464.
34 A. Meijerink, G. Blasse, J. Lumin. 43 (1989) 283.
35 P. Dorenbos, J. Phys.: Condens. Matter 17 (2005) 8103.

Chapter 4: Luminescence properties of $SrSi_2AlO_2N_3$ doped with divalent rare earth ions

The optical properties of $SrSi_2AlO_2N_3$ doped with Eu^{2+} and Yb^{2+} are investigated for the potential application in LEDs. The Eu^{2+} doped material shows emission in the green, peaking around 500 nm. The emission is ascribed to the $4f^6 5d^1$ to $4f^7$ transition on Eu^{2+}. In view of the too low quantum efficiency and the thermal quenching temperature around the operation temperature of high power LEDs the phosphor is less suitable for the use in phosphor converted LEDs. The Yb^{2+} emission shows an anomalously red-shifted emission compared to the one of Eu^{2+}, which is characterized by a larger FWHM, a larger Stokes Shift and lower thermal quenching temperature. The emission is ascribed to self-trapped exciton emission. The Yb^{2+} activated phosphor is found to be unsuitable for use in phosphor converted LEDs.

4.1 Introduction

The search for new phosphors for the conversion of the near UV to blue emission from (In,Ga)N LEDs into visible light opened an exciting new field in the development of luminescent materials. Luminescent compounds with activators showing allowed f-d transitions are investigated worldwide. Rare-earth elements with forbidden f-f absorption and emission are not suitable for this kind of application since their absorption strength in the near UV and visible part of the electromagnetic spectrum is too low and therefore cannot be excited with (In,Ga)N LEDs. Additionally, forbidden transitions cause long decay times, which may cause saturation of phosphors doped with f-f emitters. This is especially of importance considering the high light output of today's high power LEDs (HP-LEDs).

The lanthanide elements with allowed absorption into the 5d-states of their electronic configuration are highly sensitive to their chemical surrounding because the d-states are not shielded like the f-states and participate in the bonding. This is very useful as the f-d transitions of the free RE ions (both in absorption and emission) are located in the UV spectral range whereas LED phosphors have to show absorption in the near UV to blue spectral range, as this is the spectral position where LEDs emit. Two factors govern changes on the free ion's f-d absorption and emission upon introduction in a host lattice. First, the nephelauxetic effect where differences in electronegativity between the dopant and its surrounding can shift the charge density on the bond-axes and thereby cause changes in the covalency. Second, the crystal-field splitting of the 5d band can be varied, e.g. by differences in the charge of the surrounding ion ($O^{2-} \rightarrow N^{3-}$) or by varying the metal-ligand distance. Both a higher covalency and an increase in crystal-field splitting will shift the f-d transition to lower energies.

Most prominent for the use with near UV and blue LEDs are Ce^{3+} and Eu^{2+}. For example, oxides like $Y_3Al_5O_{12}:Ce^{3+}$ (YAG:Ce) or sulfides like $CaS:Eu^{2+}$ are currently applied in phosphor converted LEDs (pcLEDs) as luminescence converters [1,2]. Recently also Yb^{2+} has been proposed for the use in low power pcLEDs [3].

One of the well-known characteristics of LEDs is the long operational lifetime. This puts up high requirements for potential host lattices. Some of the currently used materials tend to hydrolyze, which limits their use in

LED lighting applications. In recent years much has been published on the high potential of nitridosilicates [4-6], oxonitridosilicates (siones) [3,7,8] and oxonitridoaluminosilicates (sialons) [9-11]. In these three material classes only the higher condensed lattices are highly covalent and stable towards oxidation and hydrolysis [12]. They also exhibit excellent thermal and mechanical properties [9]. This makes them very interesting for the use as host materials in LED phosphors.
The focus in this chapter is on a sialon material. The first sialon material found to be isostructural with pure nitridosilicates ($LnSi_3N_5$ (Ln = Ca, Ce, Pr, Nd)) was $SrSiAl_2O_3N_2$ [13]. This material contains only one crystallographic Sr-site. Doping with divalent rare-earth ions the Sr^{2+} will partially be substituted. It is one of few sialon materials, which has well defined crystallographic sites without intermixing of O- and N-, and Si- and Al-ions respectively [13]. Doped with Eu^{2+} it was patented by Ellens et al. [14]. Xie et al. [15] describe in some more details the concentration dependence of the Eu^{2+} emission in the lattice presented in [13]. Uheda et al. reported on the synthesis and luminescent properties of Eu^{2+} doped $LaSi_3N_5$ and gave examples for the introduction of O-ions in the lattice [16].
This chapter shortly describes the synthesis and presents a thorough examination on the optical properties of luminescent materials based on a $SrSi_2AlO_2N_3$ host lattice doped with divalent rare earth ions, viz. Eu^{2+} and Yb^{2+}. The luminescence properties are investigated and the luminescence mechanism is discussed.

4.2 Experimental methods

All samples were synthesized by a conventional solid-state reaction. Mixtures of $SrCO_3$ (Philips Lighting Components, 99.9%), α-Si_3N_4 (SN-E10, UBE Industries, Ltd.), AlN (Aldrich 98+%) and the rare earth dopants Eu_2O_3 (Alfa Aesar, REacton 99.999%) or Yb_2O_3 (Auer-Remy, 99.99%) were prepared by ball milling and fired for 2 to 6 hours at 1500 to 1700 °C in a reducing atmosphere (H_2/N_2) in a tube furnace. After milling the raw product powders were washed with KOH, water and isopropanol. XRD analysis was done on a Philips diffractometer PW 1729 at RT, using Cu K_α radiation. All samples under investigation showed to be single phase. The composition of the title compound was confirmed by elemental analysis.

Luminescence spectra were recorded between 4 K and 300 K on a Spex Fluorolog 2 spectrofluorometer equipped with a helium flow cryostat. The set-up is described in detail in Ref. [17]. To study thermal quenching between 300 and 600 K luminescence spectra were measured on the same set-up now equipped with a homemade heating cell connected to a temperature controller.
The decay measurements were performed using the third harmonic of a Quanta Ray DCR-2A Nd:YAG laser (355 nm). For temperatures between 4 K and 300 K the set-up was equipped with a helium flow cryostat, between 300 K and 600 K the homemade heating cell was used. The emission was focused on a monochromator and detected by a photomultiplier (RCA C31034). The decay curves were measured with a Tektronix 2430 digital oscilloscope, which was triggered by the laser pulse [18].

4.3 Results and Discussion

4.3.1 $SrSi_2AlO_2N_3:Eu^{2+}$

For dopants, which show f-d absorption and emission, the corresponding spectra are expected to show bands, rather than lines like for f-f transitions. In Figure 4-1 the room temperature excitation, emission and reflection spectra of $SrSi_2AlO_2N_3$ doped with 2% Eu^{2+} are shown. The emission spectrum was taken for excitation at 320 nm, the excitation spectrum for emission at 520 nm. Both spectra were measured at room temperature (RT). The emission band, which is assigned to the $5d^14f^6$ to $4f^7$ transition, has its maximum at 494 nm (20243 cm^{-1}) and the full width at half maximum (FWHM) of 3543 cm^{-1}. The latter is a typical value for Eu^{2+} f-d emission [19]. The quantum efficiency (QE) at 320 nm excitation wavelength is 0.61 with a reflectivity of 0.06. For excitation at 450 nm QE drops to 0.40 and reflectivity increases to 0.60. This is unexpectedly low. From [13] it is known that the cation (Sr^{2+}/Eu^{2+}) is coordinated by oxygen and nitrogen ions. Since in the material presented here the N/O ratio is inverse to the one in [13] the exact coordination scenario is not known. The emission wavelength maximum is somewhat longer than the typical values given for Eu^{2+} in silicates and aluminates and shorter than those given for pure nitride materials [19]. This

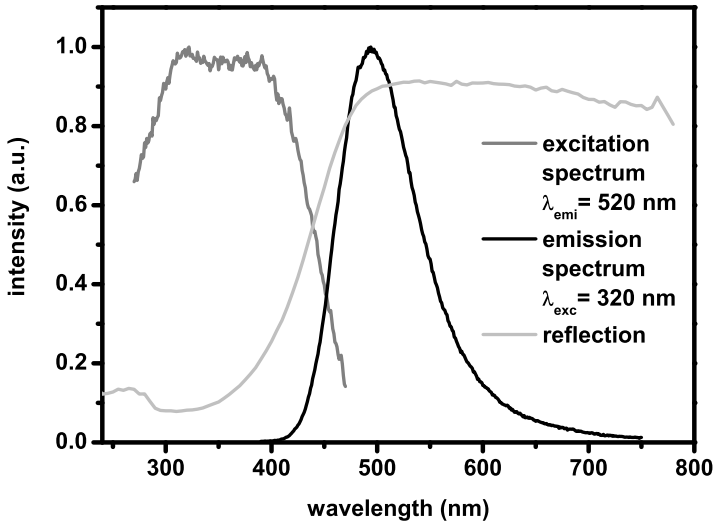

Figure 4-1 Luminescence excitation for 520 nm emission, emission for 320 nm excitation, and reflection spectrum $SrSi_2AlO_2N_3$ doped with 2% Eu^{2+}, recorded at 298 K.

is in line with the mixed O/N coordination. The color point in the 1931 C.I.E chromaticity diagram is x;y = 0.211;0.393. This is compared to Ref. [14] (FIG 4a). Ellens et al. present an emission spectrum of a sample with the composition $SrSiAl_2O_3N_2$ doped with 4% Eu^{2+}. The emission maximum in this spectrum is reported to be at 534 nm for an excitation at 400 nm. This is in contradiction to the data given by the authors in their tables 3 and 4. In table 3 they give an emission maximum of 497 nm, which is comparable to the maximum presented here. Their color coordinates are 0.304 and 0.432 for x and y, respectively. This means the emitted light is perceived as more yellowish by the human eye. For this the emission band is expected to be broader and to have more intensity in the yellow range than the spectrum presented by us in the present chapter. With 1% of Eu^{2+} in the same lattice as [14] Xie et al. present an emission spectrum with its maximum at 475 nm [15]. Xie et al. show color coordinates only in a diagram but it can be approximated that for Eu^{2+} concentrations between 0.5 and 10 at.% the x-coordinate varies between 0.15 and 0.2 and the y-coordinate between 0.2 and 0.4. The FWHM of their 1% doped sample is given with 78 nm [15], which is in line with the 89 nm found in the composition presented here. From the emission spectrum

for $SrSiAl_2O_3N_2:Eu^{2+}$ in [14] one can approximate the FWHM to 125 nm. The differences of the spectrum presented here and those of and Xie et al. can be understood in the different N/O ratio and the amount of activator doped into the lattice. More nitrogen and a higher degree of dopant shift our emission spectrum to longer wavelength. The differences in emission spectra between [14], [15] and the sample presented here can only partially be explained by the higher Eu^{2+} content. The large red-shift and the broadening in [14] are possibly due to a undetected second phase.

The Stokes Shift is approximated by the energy of twice the distance between the intersection of excitation and emission spectrum and the maximum of the emission spectrum [3]. The intersection of the two spectra is at 452 nm (22124 cm^{-1}). The Stokes Shift is 3762 cm^{-1}. This is within the range of Stokes Shifts typically found for Eu^{2+} emission [19].

The daylight color of the Si-rich powder is perceived as greenish-yellow. This is in line with the shape of the reflection spectrum presented in Figure 4-1. Figure 4-2 shows the reflection spectra of the undoped material investigated in this study. It gives information on its band gap, which is determined to 4.54 eV and by that is typical for a sialon [20]. The 5d-4f emission of Eu^{2+}

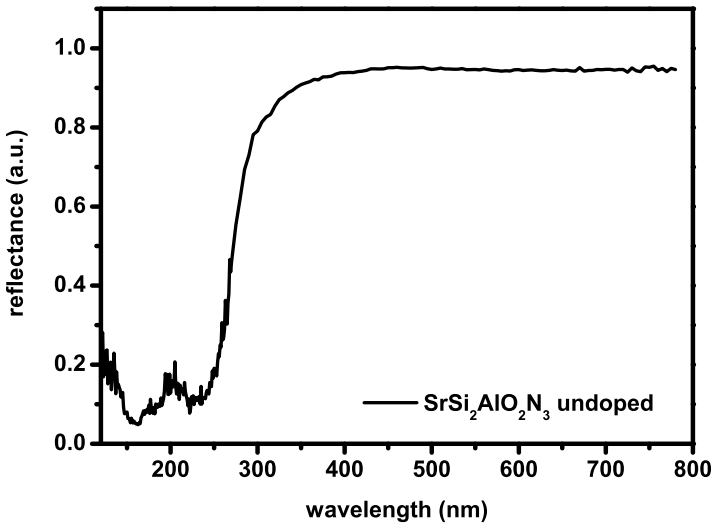

Figure 4-2 Diffuse reflection spectrum of undoped $SrSi_2AlO_2N_3$, recorded at 298 K.

has a short decay time, since it involves a parity allowed transition. Typical values are around 1 µs [18]. Decay curves of the sample were measured between 4 and 600 K. All decay curves show a single exponential behavior. The decay time $\tau_{1/e}$ is 0.65 µs between 4 and 260 K as shown in Figure 4-3. This is a typical value for the d-f emission from Eu^{2+}. Above 260 K the decay time decreases as shown in Figures 4-3. The decrease in decay time is accompanied by a decrease in emission intensity. This indicates that non-radiative relaxation sets in above 260 K. Both, decay time and emission intensity, are plotted as function of temperature in Figures 4-3. From the temperature dependence of the luminescent decay time and the emission intensity the luminescent quenching temperature $T_{50\%}$ (temperature at which half of the initial luminescent intensity is quenched) is determined to be 540 K and 420 K, respectively. The latter value being relevant for the industrial application of this phosphor.

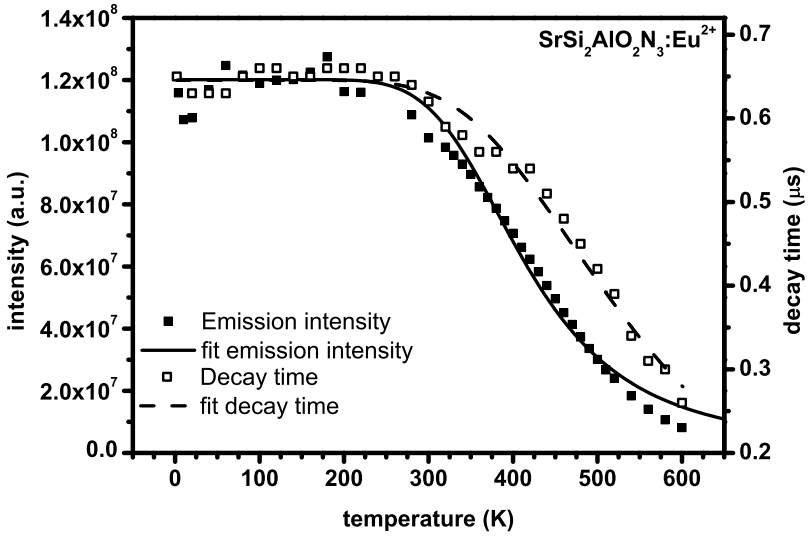

Figure 4-3 Temperature dependence of the integrated emission intensity (black squares) and luminescence decay times (open squares) of $SrSi_2AlO_2N_3:Eu^{2+}$. The lines through the data points are fits to Eq. 4-1 for the temperature dependent emission intensity (solid line) and the decay time (dashed line).

Two mechanisms can cause the quenching of the d-f luminescence of Eu^{2+}: first, quenching by thermally activated cross-over from the $4f^6 5d$ excited stated to the $4f^7$ ground state and second, thermally activated photoionization from the $4f^6 5d$ state to the conduction band. Historically the former is most widely used as an explanation. The Struck-Fonger model can be used for a proper analysis of the temperature dependence of the luminescent intensity [21]. More recently, for several host lattices it has been shown that thermally induced ionization of the 5d excited state is responsible for the quenching of the Eu^{2+} 4d to 5f luminescence [22]. Strong indications for this mechanism are the presence of a small Stokes Shift for 5d to 4f emission combined with a low quenching temperature at low Eu^{2+} concentrations for the luminescence. The ionization process has been confirmed by temperature dependent photoconductivity experiments [23]. For the composition presented here, there are indications that the latter described mechanism is responsible for the quenching of the 5d to 4f emission of Eu^{2+} (see below). It is likely that the Eu^{2+} excited 5d level is close to the conduction band, and that thermally induced ionization causes the thermal quenching of the d-f emission. A modified Arrhenius equation can be used to describe the temperature dependence of the emission intensity and the luminescent decay time. It takes the radiative and thermally activated non-radiative processes into account.

(eq. 4-1)
$$\tau(T) = \frac{\tau_0}{1 + C \cdot e^{\frac{-E_A}{kT}}}; I(T) = \frac{I_0}{1 + D \cdot e^{\frac{-E_A}{kT}}}$$

where $\tau(T)$ and $I(T)$ are luminescence decay time and intensity at temperature T [K] respectively, τ_0 and I_0 are decay time and intensity at 4.2 K, respectively, C and D being a constant for the thermally activated escape which contain τ_0 and I_0 as well, respectively, E_A being the activation energy for this process which represents the energy gap between the relaxed Eu^{2+} $4f^6$ $5d^1$-excited level and the bottom of the conduction band and k being the Boltzmann constant. Figure 4-3 contains the best fits to this equation for the emission intensity and the luminescent decay time. We found small discrepancies between the values for the measurements of decay time and emission intensities in the activation energy due to the difference in the shape of the two curves. The energy gap E_A results in 0.23 eV and 0.20 eV from emission intensity and decay

Table 4-1 Fitting parameters for the samples under investigation according to Eq. 1.

composition	E_A decay	C	τ_0	E_A intensity	D	I_0
$SrSi_2AlO_2N_3$:Eu	0.20 eV	68	0.65 µs	0.23 eV	613.2	1.2E+08
$SrSi_2AlO_2N_3$:Yb	-	-	-	0.16 eV	959.6	1.7E+08

time measurements, respectively. All fitting parameters are summarized in Table 4-1. This difference in the two curves can be explained by re-absorption, which influences the observed decay time to be longer than expected. This is a known process for the case of spectral overlap of excitation and emission spectrum.

In high brightness LEDs the color converting phosphors can be heated up to 450 K under continuous operation mode. With the given thermal quenching behavior the Eu^{2+} doped sialon material presented here would be operated beyond its $T_{50\%}$ temperature. For application in a pulsed operation mode or with low power LEDs the material could be used as color converter. From the position of the excitation spectrum and the small Stokes Shift the Eu^{2+} doped material complies well with an application as color converter in a UV-LED.

4.3.2 $SrSi_2AlO_2N_3:Yb^{2+}$

For a number of host lattices Eu^{2+} and Yb^{2+} show similar luminescent properties when doped into the same lattice [19,24-27]. Generally the Yb^{2+} 5d-4f emission is found to be slightly blue shifted compared to Eu^{2+} as the lowest $4f^{13}5d$ excited state is at an about 0.1 eV higher energy than the lowest excited Eu^{2+} state when comparing the energy differences between ground states and excited states. Figure 4-4 shows the excitation, emission and reflection spectra of the compound presented here doped with 2% Yb^{2+}. The position of the maximum in the excitation band is with 340 nm slightly red shifted compared to the one found for doping Eu^{2+} to the same lattice.

The emission spectrum is very different in shape and position compared to the Eu^{2+} emission bands found in the same lattice. The maximum of the emission band is at 560 nm. The point of intersection of excitation and emission spectrum is widely used to estimate the position of the zero-phonon-line

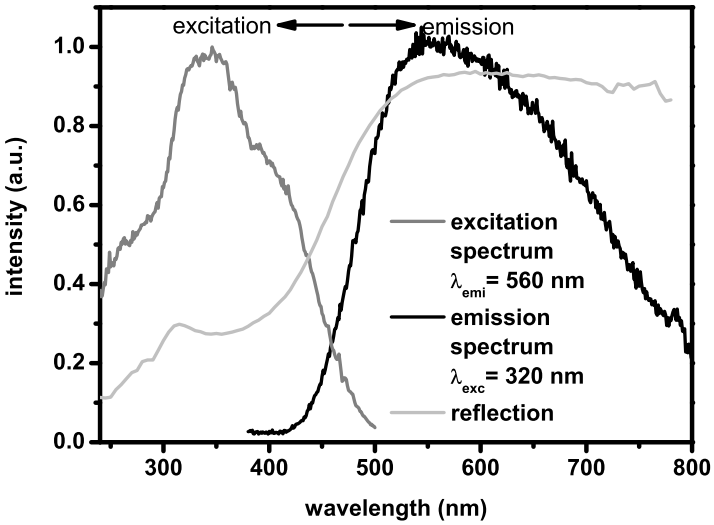

Figure 4-4 Luminescence excitation for 560 nm emission, emission for 340 nm excitation, and reflection spectrum for $SrSi_2AlO_2N_3$ doped with 2% Yb^{2+}, recorded at 298 K.

(ZPL) for compounds in which this line cannot be seen at low temperatures. The estimated ZPL is at 459 nm (21786 cm^{-1}). In contrast to the expectation the emission of Yb^{2+} is red shifted compared to Eu^{2+} and is characterized by a large FWHM. For $SrSi_2AlO_2N_3$:Yb^{2+} the Stokes Shift is 7858 cm^{-1} and FWHM is 7103 cm^{-1}. Compared to the Eu^{2+} emission the Stokes Shift and FWHM for Yb^{2+} are larger by a factor of two. The quenching temperature $T_{50\%}$ for the Yb^{2+} activated phosphor is around RT.

An anomalous red shift has been seen before for Yb^{2+}. For example, the fluoride host lattice CaF_2 shows quite similar emission for Eu^{2+} and Yb^{2+} doping while SrF_2 shows a red shift in Yb^{2+} emission, which additionally is characterized by a larger Stokes Shift and FWHM and lower luminescent quenching temperature [28]. To explain the anomalous luminescence properties for Yb^{2+} one has to consider the position of the lowest energetic excited d-state. If the lowest energetic d-state is situated above the conduction band edge anomalous red shifted emission is observed. In this mechanism the excitation into the d-state is followed by photoionization and trapping of the electron close to the lanthanide impurity, which forms an impurity trapped exciton state. Deexcitation from this impurity trapped exciton state

is observed as radiative luminescence. Photoconductivity experiments on CaF_2 and SrF_2 have been performed to convincingly proof this model [29]. Photoconductivity was clearly observed upon excitation into the lowest energy d-band in host lattices where Yb^{2+} or Eu^{2+} show the anomalous emission, proving that the lowest energetic d-state is positioned in the conduction band. Impurity trapped exciton emission is observed for Yb^{2+} and Eu^{2+} in a number of oxide and fluoride host lattices [30]. Moine and co-workers describe in Ref. [28] and [31] the temperature dependence of Yb^{2+} emission in SrF_2. Recently we reported on impurity trapped exciton emission of Yb^{2+} in a sion host lattice [3].

To provide further evidence for impurity trapped exciton emission and to probe the thermal quenching behavior of the Yb^{2+} emission the temperature dependence of the decay time and the emission intensity were measured. For a single type of emission site one would expect a similar behavior of decay time and emission intensity as function of temperature, which is the case for the above-described Eu^{2+} ion in the same host lattice. Figures 4-5 shows a

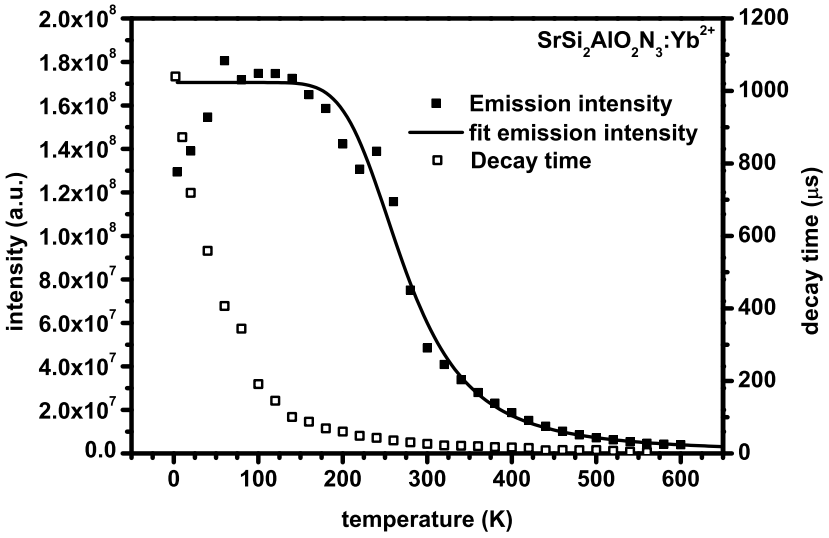

Figure 4-5 Temperature dependence of the integrated emission intensity (black squares) and luminescence decay times (open squares) of $SrSi_2AlO_2N_3:Yb^{2+}$. The line through the data points is the best fit to Eq. 4-1 for the temperature dependent emission intensity.

different temperature behavior of decay time and emission intensity in the Yb-doped compound. The temperature dependent emission spectra were measured between 5 K and 600 K. Between 5 K and 120 K the emission intensity increases. Upon increasing the sample temperature further the emission intensity starts to decrease to be almost completely quenched at 600 K. The shape of the curve emission intensity vs. temperature was fit according to equation 1 in the range from 120 K to 600 K. The best fit, also shown in Figures 4-5, gives an activation energy for the intensity quenching of E_A = 0.16 eV, this value is lower than the one found for the doping with Eu^{2+}. Further fitting-parameters are given in Table 4-1.
Decay times have been measured between 5 K and 600 K. They were measured at different wavelengths between 500 and 700 nm to verify whether there is one or more different emitting Yb^{2+} sites. The decay times proved to be independent of the excitation wavelength. To allow for comparison, Figure 4-5 contains only decay times measured on the long wavelength side of the emission spectrum. In the temperature range between 5 K and 120 K, comparable to the range of increasing emission intensity, the decay curves are not single exponential. To get an estimate of the average decay time $\tau_{1/e}$ the

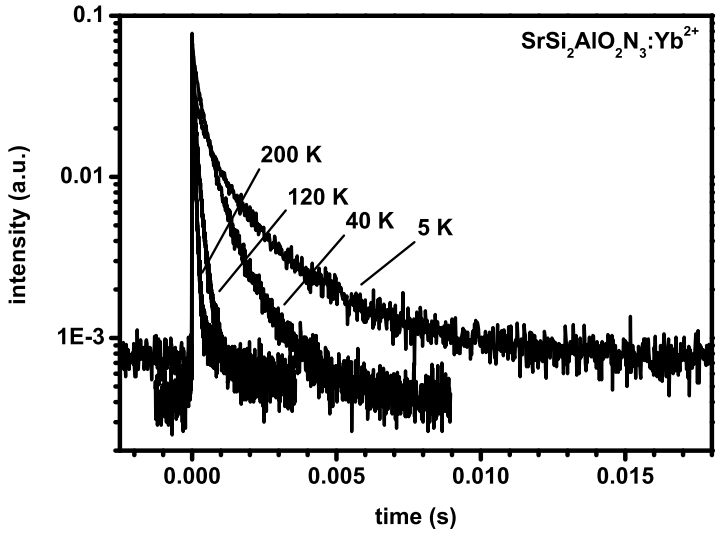

Figure 4-6 Temperature dependent decay curves of the Yb^{2+} emission (for 580 nm emission under 355 nm excitation) in $SrSi_2AlO_2N_3$.

time difference between the maximum intensity and the point where intensity has dropped to 1/e of the initial intensity was taken. A selection of decay curves of the sample doped with Yb^{2+} is depicted in Figure 4-6. From there it is visible that for temperatures above 120 K the decay behavior becomes single exponential. The initial decay time at 5 K is around 1 ms. This is too short for Yb^{2+} d-f-emission (typically ~ 10 ms [32]). At temperatures were the decay behavior becomes single exponential the decay time is found to be around 100 µs. This is in line with the decay times typically found for impurity (Yb) trapped exciton emission (50 – 500 µs) at low temperature [28]. With increasing temperature the decay times are quenched to around 10 µs at RT and to < 5 µs for temperatures above 500 K.

The following model can be used to understand the differences in the temperature dependent behavior of the emission intensity and the decay time. It supports the earlier made assumption that the origin of emission seen for Yb^{2+} in the here presented host lattice is a self-trapped exciton state (STE). The Yb^{2+} ion is a $4f^{14}$ system. Upon excitation one electron is promoted from the 4f state to the 5d state to form the configuration $4f^{13}5d^{1}$. It is proposed that the lowest 5d state of Yb^{2+} in this host lattice is situated in the conduction band as it was found in other host lattices showing anomalous red shifted Yb^{2+} emission. There the ion may ionize and form an impurity-trapped exciton, which consists of a bound electron-hole pair with the hole localized on the impurity and the electron on nearby lattice sites [28]. Hole and electron interact only via their opposite charge. The hole resides in well-shielded f-states, consequently it does not exchange interact with the electron, which is in host-lattice like states. Therefore there is no exchange induced splitting in the exciton energy levels.

For trapped exciton emission a splitting into two levels was found for Yb in SrF_2, a cubic lattice [33]. The site of the Yb-ion in the lattice presented here is nine-fold coordinated and has low symmetry. We however remark that the excitation spectrum shows the presence of two spectrally resolved d-levels only (Fig. 4). Based on the experimental results we deduce that the level of lowest energy is not the one with the fastest and most efficient radiative decay. A second level, which is close to the lowest, can be thermally populated. From this state faster radiative emission occurs. Since the activation energy for thermal quenching is small, < 0.2 eV, further split levels with higher energy are

thought to be localized in the conduction band. Experimental results indicate the participation of only two levels participating in the emission process. For very low temperatures the lowest level is preferably populated but the transition to the ground state is characterized by a small decay rate. With increasing temperature the energetically higher level is populated. Radiative emission from this level has a decay rate that is much larger than from the lowest one. The energy difference between the two excited levels described is small, which makes the decay time decrease rapidly when the emitting level is increasingly populated, whereas the emission intensity increases with increasing population of the emitting level. Beyond the maximum of the emission intensity the thermal quenching process sets in. This process is in analogy to the one described above for the host lattice activation with Eu^{2+} ions.

4.4 Conclusions

New phosphors for the potential use in phosphor-converted LEDs were presented. A sialon with the composition $SrSi_2AlO_2N_3$ doped with Eu^{2+} or Yb^{2+} was prepared and characterized. The Eu^{2+}-doped sample shows 5d to 4f band emission in the green spectral range with band maxima at 500 nm. Stokes Shift and FWHM are within the range typically found for Eu^{2+} activated phosphors. From temperature dependent measurements of the emission intensity the quenching temperature $T_{50\%}$ was calculated to be 420 K. Today's high power LEDs can reach chip temperatures of around 450 K. From this, the quenching behavior and also the position of the excitation band one has to draw the conclusion that the Eu^{2+} activated phosphor is only useful in phosphor converted high power LEDs in pulsed operation mode or in low power LEDs.

For the Yb^{2+} doped material we present for the second time a potential conversion material showing an anomalous red shifted emission. Stokes Shift and FWHM are large compared to the Eu^{2+} emission by a factor of two. The radiative emission is assigned to impurity trapped exciton (Yb^{2+}) emission. The assignment to ITE emission is supported by photoconductivity measurements for different materials showing the same anomalous red-shifted luminescence and thermal behavior as the material presented here. From the

emission intensity the quenching temperature $T_{50\%}$ is found to be around room temperature. Although scientifically interesting the Yb^{2+} activated phosphor is not suitable for the application as conversion phosphor in high power LEDs due to the low thermal quenching temperature.

References

1 P. Schlotter, J. Baur, Ch. Hielscher, M. Kunzer, H. Obloh, R. Schmidt, J. Schneider, Mater. Sci. Eng. B 59 (1999) 390.
2 Y. Hu, W. Zhuang, H. Ye, S. Zhang, Y. Fang, and X. Huang, J. Lumin. 111 (2005) 139.
3 V. Bachmann, T. Jüstel, A. Meijerink, C. Ronda, P.J. Schmidt, J. Lumin. 121 (2006) 441.
4 H. Huppertz and W. Schnick, Acta Crystallogr. C 53 (1997) 1751.
5 T. Schlieper, W. Milius, and W. Schnick, Z. Anorg. Allg. Chem. 621 (1995) 1380.
6 H.A. Höppe, H. Lutz, P. Morys, W. Schnick, and A. Seilmeier, J. Phys. Chem. Solids 61 (2000) 2001.
7 J.W.H. van Krevel, On new rare-earth doped M-Si-Al-O-N materials, Ph.D. thesis (Universiteitsdrukkerij TU Eindhoven, Eindhoven, 2000).
8 Y.Q. Li, A.C.A. Delsing, G. de With, H.T. Hintzen, Chem. Mater. 17 (2005) 3242.
9 S. Hampshire in Materials Science and Technology, Vol. 11 (Edt.: R.W. Cahn, P. Haasen, E.J. Kramer), VCH, Weinheim (1994) 119.
10 J.W.H. van Krevel, J.W.T. van Rutten, H. Manda, H.T. Hintzen, R. Metselaar, J. Solid State Chem. 165 (2002) 19.
11 K. Sakuma, N. Hirosaki, R.-J. Xie, Y. Yamamoto, T. Suehiro, Mater. Lett. 61(2) (2007) 547.
12 W. Schnick, Int. J. Inorg. Mat. 3 (2001) 1267.
13 R. Lauterbach, W. Schnick, Z. Anorg. Allg. Chem. 624 (1998) 1154.
14 A. Ellens, T. Fries, T. Fiedler, G. Huber, US Patent US6,670,748 B2.
15 R.-J. Xie, N. Hirosaki, Y. Yamamoto, T. Suehiro, M. Mitomo, K. Sakuma, J. Ceram. Soc. Japan 113, 7 (2005) 462.
16 K. Uheda, H. Takizawa, T. Endo, H. Yamane, M. Shimada, C.-M. Wang, M. Mitomo, J. Lumin. 87-89 (2000) 967.
17 J.F. Suyver, J. J. Kelly and A. Meijerink, J. Lumin. 104, 3 (2003) 187.
18 S.H.M. Poort, A. Meijerink, G. Blasse, J. Phys. Chem. Solids 58, 9 (1997) 1451.
19 P. Dorenbos, J. Lumin. 104 (2003) 239.
20 Y.Q. Li, G. de With, H.T. Hintzen, J. Electrochem. Soc. 153 (2006) G278.
21 C.W. Struck, W.H. Fonger, J. Lumin. 10 (1975) 1.

22 E.v.d. Kolk, P. Dorenbos, C.W.E. van Eijk, S.A. Basun, G.F. Imbusch, W.M. Yen, Phys. Rev. B 71 (2005) 165120/1.
23 U. Happek, S.A. Basun, J. Choi, J.K. Krebs, M. Raukas, J. Alloys Comp. 303-304 (2000) 198.
24 S. Lizzo, A. Meijerink and G. Blasse, J. Lumin. 59 (1994) 185.
25 S. Lizzo, A. Meijerink, G.J. Dirksen and G.Blasse, J. Lumin. 63 (1995) 223.
26 S. Lizzo, A.H.Velders, A. Meijerink, G.J. Dirksen and G. Blasse, J. Lumin. 65 (1995) 303.
27 J.W.M. Verwey, G.J. Dirksen and G. Blasse, J. Phys. Chem. Solids 53, 3 (1992) 367.
28 B. Moine, B. Courtois, C. Pedrini, J. Lumin. 48 & 49 (1991) 501.
29 B. Moine, C. Bruna and C. Pedrini, J. Lumin. 45 (1990) 248.
30 P. Dorenbos, J. Phys: Condensed Matter 15 (2003) 2645.
31 B. Moine, C. Pedrini, D.S. McClure and H. Bill, J. Lumin. 40&41 (1988) 299.
32 S. Lizzo, A. Meijerink, G. Blasse, J. Lumin. 59 (1994)185.
33 D.S. McClure, C. Pedrini, Phys. Rev. B. 32(12) (1985) 8465.

Chapter 5: Temperature Quenching of the yellow Ce^{3+} Luminescence in YAG:Ce

Yttrium aluminum garnet (YAG) doped with Ce^{3+} is the phosphor of choice for the conversion of blue to yellow light in the rapidly expanding market of white light LEDs. Luminescence temperature quenching is an important parameter, especially in high power LEDs, but surprisingly no systematic research has been done to measure and understand the temperature quenching of the yellow Ce-luminescence. Here we report on the luminescence temperature quenching in YAG:Ce. For a wide range of Ce-concentration (between 0.033% and 3.3%) the temperature dependence of the emission intensity and the luminescence life times are reported. The intrinsic quenching temperature of the Ce-luminescence is shown to be very high (>680 K). The lower quenching temperatures reported in the literature are explained by thermally activated concentration quenching (for highly doped systems) and the temperature dependence of the oscillator strength (for low doping concentrations). In addition, high resolution spectra are reported which provide insight in the position of the zero-phonon transition (20 450 cm^{-1}), the Stokes' shift (2400 cm^{-1}), the energy of the dominant phonon mode (200 cm^{-1}) and the Huang-Rhys parameter (S=6). These parameters can serve as input for comparison with *ab initio* calculations on the position of and relaxation in the excited 5d state of Ce^{3+} in YAG.

5.1 Introduction

Yttrium Aluminum Garnet ($Y_3Al_5O_{12}$ or YAG) doped with Ce^{3+} is a luminescent material with a rich history and a wide variety of applications. Recently, there is a renewed interest in this material due to its application in white light LEDs. The story of the garnet starts in 1928 when Menzer assigned the garnet structure to the space group Ia3d [1]. The unit cell consists of eight formula units with a single type of Y-site. Eight oxygen atoms in a distorted dodecahedron coordinate the Y atom giving it D_2 symmetry. Blasse and Bril were the first to report on Ce^{3+} doped YAG as a new phosphor for flying-spot cathode ray tubes (CRT). The combination of a high luminescence efficiency, a short luminescence life time and a relatively long wavelength (visible) emission made this material ideally suited for this application. A good estimate of the luminescence decay time was given (0.07-0.08 μsec) [2]. The fast emission was shown to be most efficiently excited in the blue (at 460 nm) but it was not until later that this feature was exploited. In a second publication Blasse and Bril reported more detailed spectroscopic results like the position of the first four (of the expected five) 4f-5d excitation bands, emission bands in the visible and the UV spectral range, the quantum efficiency for the emission from the lowest excited d-level and the Stokes' shift [3]. The use of the long wavelength excitation band centered around 460 nm was reported by Van Kemenade et al. [4]. They described the application of YAG:Ce in low-pressure mercury vapor discharge lamps to absorb the Hg-plasma lines in the blue/violet part of the spectrum, viz. 405 nm and 436 nm. The conversion of the violet and blue emission lines into yellow light adds to the white light emitted by the halophosphate phosphor (the commonly used phosphor in those days) to create a warmer white light. In the late 1970s some excellent papers were published by Robbins et al. on the fundamental aspects of the luminescence (and luminescence quenching) for Ce^{3+} in YAG [5-8]. In the nineties YAG:Ce (and the higher density analog LuAG:Ce) were proposed as fast and efficient scintillator materials which again triggered interest in this material. Here research was focused on the response time as a scintillator material and energy transfer from a self-trapped-exciton (STE) state to Ce^{3+}. Another recent application of the luminescence of YAG:Ce is the use of single crystalline disks of YAG:Ce to control the dose of VUV radiation in

wafer steppers. The dose applied for photoetching is measured by converting a small part of the VUV radiation from an excimer laser pulse into visible light.
In recent years YAG:Ce has received renewed interest for the use as color converter in InGaN based phosphor converted LEDs (pcLEDs) and at present it is the most widely applied phosphor in white light LEDs. Part of the blue light from the InGaN LED is absorbed by a thin layer of YAG:Ce and is converted into yellow light. The combination of blue and yellow gives a bright white light source with an overall energy efficiency exceeding that of the fluorescent lamp. One can observe the yellow phosphor when looking into the LED. In spite of the success of YAG:Ce, the rapidly expanding market for solid-state lighting has an urgent need for new phosphors with a higher conversion efficiency, a better coverage of the spectrum (including the orange/red spectral region) and an improved thermal quenching behavior. This becomes even more evident when one takes the fast development in the market of *high power* LEDs into account. For general lighting applications, high power LEDs are needed but by increasing power consumption the heat created at the p-n junction will increase as well, and the temperature of the phosphor layer will reach temperatures well above todays 450 K in commercially available products. At these high temperatures thermal quenching has been observed for YAG:Ce. For example, Tamura et al. give temperature dependent emission spectra of an InGaN white LED [9]. For increasing chip temperatures they observe an intensity decrease of the blue emission from the LED combined with a shift of the emission maximum to longer wavelength. They also observe a decrease of the YAG:Ce emission band [9]. The same observation has been reported by Sakuma et al. [10]. Setlur et al. reported on the temperature dependence of the Ce^{3+} emission intensity and observed a steady decrease above 400 K [11]. New luminescent materials with a better spectral coverage and temperature behavior are thoroughly investigated and this work has resulted in an impressive number of papers and patents in the past three years. Especially the Ce^{3+} and Eu^{2+} doped into nitrides and oxynitrides are promising candidates to replace YAG:Ce.
In spite of the general realization that the efficiency of YAG:Ce decreases at the high temperatures that are reached in high power LEDs, the understanding of the temperature quenching is limited. The work of Robbins was focused on the behavior between 4 K and 400 K [7]. The variation of the light output was

shown to be complex and to involve changes in the absorption strength of the (different) 4f-5d absorption bands and the (temperature dependent) energy transfer to defects. After this work, research on the fundamental understanding of the temperature quenching of the luminescence in YAG:Ce is limited. It is the aim of this chapter to provide a better understanding of the temperature quenching of the Ce^{3+} emission in YAG:Ce in the high temperature regime (above 400 K). To establish the intrinsic quenching temperature for the Ce-luminescence, temperature dependent measurements are performed on systems down to very low Ce^{3+} concentrations (0.033%) in the temperature range 4-650 K. For the isolated centers thermally activated cross-over to the ground state is probably responsible for the temperature quenching and the temperature dependence of the luminescence of isolated Ce^{3+} ions (i.e. no energy transfer) provides insight into the intrinsic thermal quenching for Ce^{3+} in YAG. It is shown that the intrinsic quenching temperature for the emission is high (> 680 K). The lower luminescence quenching temperature observed in the commercial (highly doped) YAG:Ce LED phosphors is explained by concentration quenching, which becomes more pronounced at elevated temperatures. In addition to establishing the intrinsic luminescence quenching temperature, low temperature studies are reported on the luminescence properties of the YAG:Ce samples. The observation of zero-phonon lines and vibrational structures makes it possible to accurately determine the true Stokes' shift (which is smaller than the Stokes' shift reported in the literature for more concentrated systems) which can be related to ongoing theoretical work (*ab initio* calculations) on the configurational coordinate diagram for Ce^{3+} in YAG [12].

5.2 Experimental

Research on YAG:Ce has been conducted on single crystals, ceramics and powders. Details on the preparation of single crystals can be found in [13,14], on ceramics in [15-17]. For powder samples several preparation routines have been described. A good overview of the different synthesis methods is provided by Pan et al. Four methods are described: solid-state reaction, co-precipitation method, sol-gel method, and combustion method [18]. Kang et al. described particle preparation by ultrasonic spray pyrolysis [19].

We used a co-precipitation method to prepare samples of YAG:Ce with 0.033, 0.33 and 1.0 at% Ce^{3+} (relative to Y^{3+}). $YCl_3 \cdot 6H_2O$ (Aldrich 99.99%), $AlCl_3$ (Aldrich 99.99%), $(NH_4)_2SO_4$ (Aldrich 99.999%), Urea (Aldrich, 99+%), and $CeCl_3 \cdot 7H_2O$ (Aldrich 99.999%) were dissolved in water. The solution was heated slowly to 90-100 °C until the precipitation started. The solution was kept constant at this temperature for two to three hours. The precipitate was filtered, washed with water and dried at 100 °C. For the firing the crucible was placed in a bed of active carbon to create a reducing atmosphere. It was fired twice, at 1300 °C and 1700 °C, respectively, each time for two hours with a milling step in between. Additionally a commercially available sample of YAG:Ce containing 3.33% Ce^{3+} (made by Philips Lighting Components) was used for this study. XRD analysis was done on a Philips diffractometer PW 1729 at RT, using Cu K_α radiation. All samples under investigation were single phase.
Luminescence spectra were recorded between 300 and 600 K on a modified spectrofluorometer system FL900 of Edinburgh Instruments using a Xe-lamp as excitation source. The spectra were measured with a spectral resolution of 0.5 to 1.0 nm. The complete set-up is described in Ref. [20]. Luminescence spectra between 4 and 300 K were recorded on a Spex Fluorolog 2 spectrofluorometer equipped with a helium flow cryostat. The set-up is described in detail in [21]. Luminescent lifetimes were obtained using a Pico Quant picosecond laser (λ_{exc} = 406 nm, pulse width 65 ps) with a repetition rate of 1 MHz using pulse height analysis (PHA) and time-to-amplitude conversion (TAC). The emitted photons were detected using a fast Hamamatsu photomultiplier. The emission wavelength was selected using a 0.1 m monochromator with a grating blazed at 536 nm. The details of the set-up are described in [22]. For measurements up to 680 K a home made heating cell connected to a temperature controller was used.

5.3 Results

5.3.1 Luminescence spectra

The normalized room temperature (RT) excitation and emission spectra of the YAG samples with the four different Ce-concentrations are depicted in Fig. 5-1a. Emission spectra were recorded for λ_{exc} = 450 nm, which

corresponds to excitation into the lowest energy d-level of Ce^{3+}. For increasing Ce^{3+} concentrations a significant red shift in the emission spectrum and its maximum is observed, viz. 536 nm for 0.033% to 558 nm for 3.33% Ce^{3+}. The emission is ascribed to the 5d to 4f transition on Ce^{3+}. Excitation spectra were taken for emission at 536 nm (for 0.033% and 0.33% Ce^{3+}), 546 nm (for 1% Ce^{3+}) and at 558 nm (for 3.33% Ce^{3+}), respectively. The spectra show two excitation bands which are assigned to transitions to the two lowest energy levels of the five crystal field levels expected in D_2 symmetry. The two bands are centered around 460 nm and 342 nm, which is in agreement with the observations reported in the literature, e.g. [3]. The relative intensity of the two bands changes with increasing Ce-concentration due to saturation of the absorption. Saturation sets in at lower concentrations for the stronger absorption band around 460 nm and as a result the relative intensity of the weaker absorption band increases. This is also observed in the diffuse reflection spectra (Fig. 5-1b) of the same four samples. The position of the absorption bands does not change with increasing Ce^{3+} concentration. In the reflection and excitation spectra also a third absorption band centered around 260 nm is observed. The origin of this band is under discussion in the literature and it is not clear whether it is a transition to the (third) 5d level or a transition related to a defect or impurity in the YAG host lattice [19]. For the present work the origin of this band is not important. The reflection spectrum of the sample with 1% Ce^{3+} shows a shoulder for wavelengths shorter than

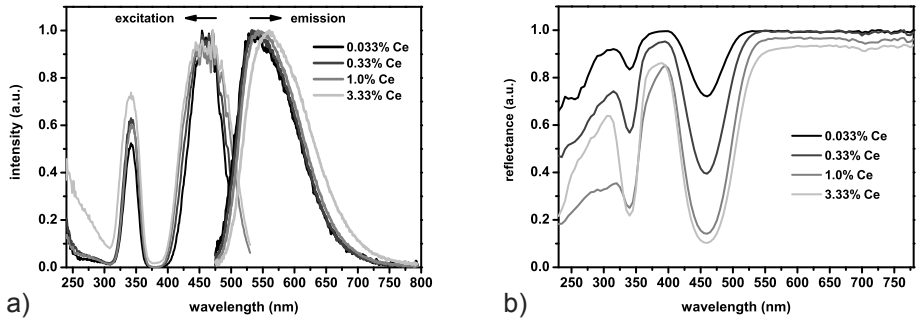

Figure 5-1 a) Excitation and emission spectra of $Y_3Al_5O_{12}$:Ce 0.033%, 0.33%, 1.0% and 3.33% at room temperature b) Reflection spectra of $Y_3Al_5O_{12}$:Ce 0.033%, 0.33%, 1.0% and 3.33% at room temperature.

400 nm. The origin of this absorption is not clear and may be related to a difference in the preparation conditions, even though the same synthesis procedure was followed as for the other samples.
The luminescence spectra are studied as a function of temperature in the ranges from 4 to 295 K (in a cryostat) and from 300 to 600K (in a high temperature cell). Since we are interested in the luminescence properties of the isolated Ce-ions, the spectra for the lowest Ce-concentration are studied in detail. For higher concentrations energy transfer and reabsorption of the emission can occur. This will influence the (temperature dependence of the) luminescence spectra and decay curves. As a result, the observations will not reflect the intrinsic luminescence properties of the isolated Ce-ions in YAG (see below). In Fig. 5-2a a selection of excitation and emission spectra is shown for the sample containing 0.033% Ce^{3+} in the range between 300 and 600 K. For this low Ce-concentration interaction between the Ce^{3+} ions will be negligible. The inset in Fig. 5-2a depicts a close up of area around the zero-phonon origin and shows the spectral overlap as a function of temperature. For the excitation spectra only the 460 nm band is shown. For both types of spectra the area of each spectrum was normalized to unity. The following is observed: both excitation and emission spectrum broaden with increasing temperature, which, due to the area normalization, leads to a decrease in height. Clearly, the spectral overlap between the excitation and emission band increases as the

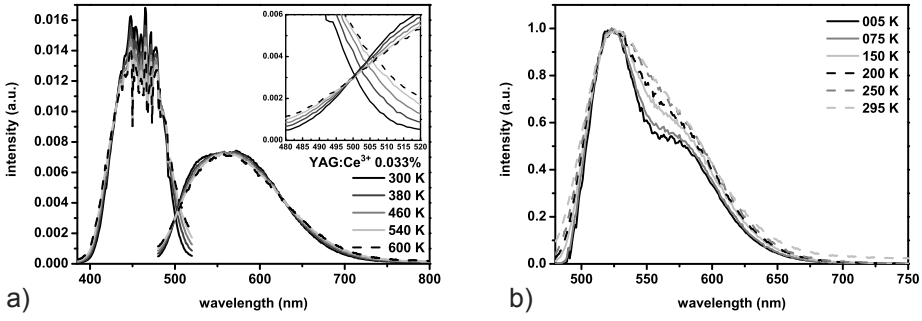

Figure 5-2 a) Excitation and Emission spectra for YAG:Ce 0.033% for λ_{exc} *= 450 nm taken at temperatures indicated; inset: magnification of the area of spectral overlap b) Emission spectra at temperatures indicated for the same sample as in (a).*

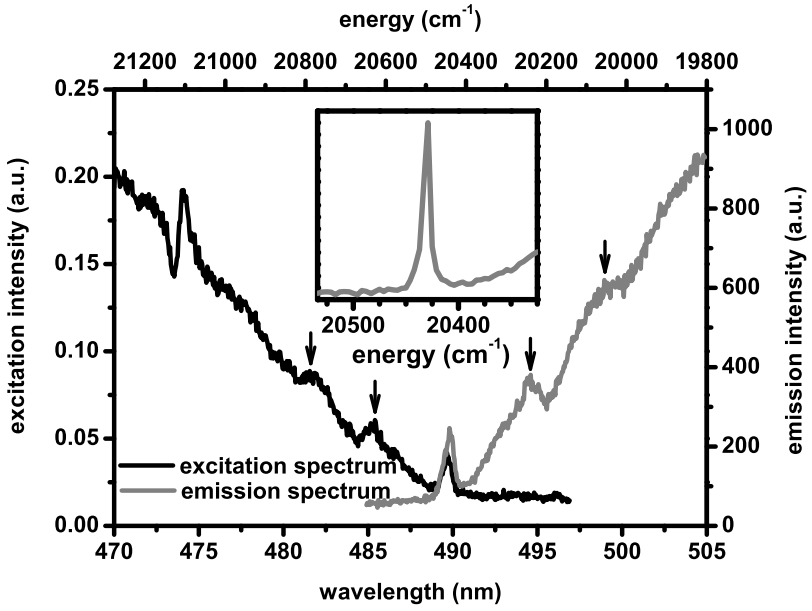

Figure 5-3 Emission spectrum for YAG:Ce 0.033% for λ_{exc} = 450 nm taken at 7 K; inset: detail of the emission spectrum measured with higher resolution.

temperature is raised. In the excitation spectra the position of the band does not change with increasing temperatures. The structure around 470 nm in the excitation bands is due to the variation in intensity of the Xe-lamp. The sharp Xe-lines around 470 nm result in sharp features in spite of the fact that the excitation spectrum is corrected for changes in the lamp intensity.

To accurately determine the Stokes' shift and the energy of the 5d excited state, luminescence spectra were recorded at 4 K. At low temperatures the emission spectrum shows the well-known double band structure of the Ce^{3+} emission (Fig. 5-2b). Upon raising the temperature the two emission bands, $5d^1 \rightarrow {}^2F_{5/2}$ and $5d^1 \rightarrow {}^2F_{7/2}$, broaden and start to overlap resulting in one broad emission band at 600 K. At the lowest temperatures fine structure is observed. In Fig. 5-3 the zero phonon line and vibrational structure are shown in more detail for the excitation and emission spectrum at 4K. The spectra show a zero-phonon line at 489.6 nm (20425 cm^{-1}). The inset shows the zero-phonon line in more detail. On the low energy side of the zero-phonon line vibronic

structure is observed in emission with phonon sidebands at 20259, 20065 and 19866 cm^{-1}. This indicates that there is a coupling with a 200 cm^{-1} vibrational mode. In the excitation spectrum a similar vibronic structure is observed. The present results on the fine-structure compare well with the low-temperature spectra reported by Robbins [7].

From the high resolution low temperature spectra we can accurately determine the Stokes' shift for the Ce^{3+} emission a well as the Huang-Rhys parameter *S*. The Stokes' shift can be determined by different methods. The simplest way is to determine the Stokes' shift from the energy difference between the excitation and emission maximum. It is important to realize that a reliable value is only obtained for low Ce^{3+} concentrations; at higher Ce-concentrations reabsorption of the high energy part of the emission occurs and the resulting redshift of the Ce-emission band results in a calculated Stokes' shift that is larger than the actual shift. Also, it is important to use the low temperature spectra where the double band structure is observed for the Ce^{3+} emission and the position of the reverse of the electronic transition in absorption ($^2F_{5/2} \rightarrow 5d$) can be observed rather than the position of the emission band corresponding to transitions to both the $^2F_{5/2}$ and $^2F_{7/2}$ levels. The luminescence spectra for the 0.033% Ce-sample at 5 K show an excitation maximum at 460 nm while the maximum of the higher energy emission band is at 520 nm. This yields a Stokes' shift of 2500 cm^{-1}. A slightly lower number is obtained by taking the Stokes' shift as twice the energy difference between the zero-phonon line (~489 nm) and the maximum of the emission band (520 nm) (SS = 2440 cm^{-1}). Finally, the Stokes' shift can be obtained by taking the Stokes' shift as ($2S\ \hbar\omega$) and determining the Huang-Rhys parameter *S* from the relative intensity of the zero-phonon line. The Huang-Rhys-Parameter *S* characterizes the electron-phonon coupling for an electronic transition. The intensity of the zero-phonon line (I_{ZPL}) with respect to the total emission intensity I_0 is given by $I_{ZPL} = I_0 * \exp(-S)$. The relative intensity of the zero phonon line is 0.27% of the total intensity of the higher energy emission band, giving a value of 6 for *S*. From $SS = 2S\hbar\omega$ and $\hbar\omega = 200\ cm^{-1}$ the Stokes' shift is determined to be 2400 cm^{-1}. The values obtained here with the various methods are consistent and show that for Ce^{3+} in YAG the Huang-Rhys factor *S* is 6 and the Stokes' shift is about 2400 cm^{-1}.

Now that the optical properties for isolated Ce^{3+} ions in YAG have been described we turn to the temperature dependence of the luminescence with a focus on understanding the luminescence temperature quenching. The total emission intensity was measured as a function of temperature for all four Ce^{3+} concentrations and for different excitation wavelengths. The results are shown in Fig. 5-4. For all concentrations temperature quenching is observed. The quenching is most pronounced for higher doping levels. For the (commercially applied) sample with 3.33% Ce^{3+} quenching sets in immediately above RT and at 520 K the intensity has dropped to half of the intensity at 300 K. For the higher dopant concentrations the temperature quenching is the same for the different excitation wavelengths, while for

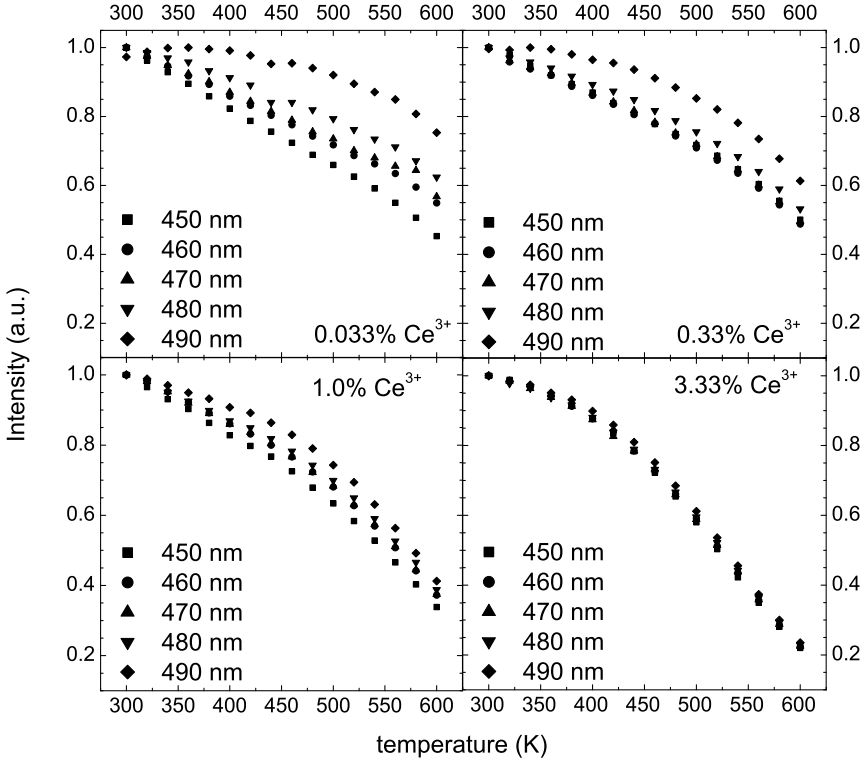

Figure 5-4 Emission intensity vs. temperature for YAG:Ce 0.033%, 0.33%, 1.0% and 3.33% taken at the five excitation wavelengths indicated.

the systems with low Ce-concentrations the temperature dependence of the emission intensity depends on the excitation wavelength. Below we will explain this complex behavior. Due to the complexity of the various factors that contribute to the temperature dependence of the luminescence intensity (e.g. temperature dependence of the absorption strength and temperature dependence of energy migration and reabsorption) luminescence life time measurements are performed to provide a better insight into the quenching temperature for the 5d-4f emission of Ce^{3+} in YAG.

5.3.2 Luminescence life time measurements

For an allowed transition the radiative life time usually does not change strongly with temperature. A well-established method to determine the temperature quenching is therefore to measure the luminescence life time of an emission band as a function of temperature. As quenching sets in, the luminescence life time shortens due to an additional non-radiative contribution to the decay process. To determine the luminescence quenching temperature for the Ce^{3+} luminescence in YAG luminescence life time measurements were performed as a function of temperature for the four different Ce^{3+} concentrations. As an example, luminescence decay curves are shown in Fig. 5-5a for the 560 nm emission of Ce^{3+} in YAG doped with 3.3% Ce^{3+} for different temperatures between 300 and 680 K. All decay curves are (close to) single exponential. In Fig. 5-5b the decay times (determined from a fit of the experimental data to a single exponential function) are plotted as a function of temperature for all four samples. Some interesting differences are observed. At room temperature the luminescence decay time is around 65 ns for all Ce-concentrations. There seems to be a slight increase in the experimentally determined luminescence life time upon increasing the Ce-concentration (from 63 ns for 0.033% Ce to 67 ns for 3.33% Ce). Most probably this is caused by reabsorption of the emission at the higher Ce-concentrations. It is well known that reabsorption of emission gives rise to a longer decay time [23]. This means that the true radiative life time of the 5d-4f emission from Ce in YAG is 63 ns, the life time measured for the lowest Ce-concentration. It compares well with the commonly reported value of 65 ns [5,24]. Note that in most reports the life times have been measured for relatively high Ce-concentrations (1-5%) or for

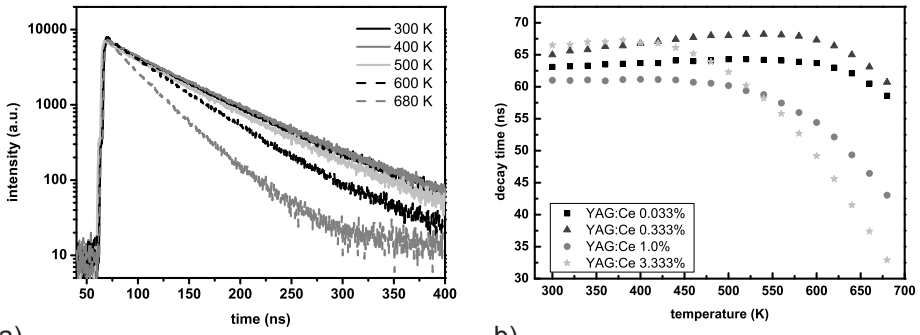

Figure 5-5 a) Luminescent decay curves for YAG:Ce 3.33% for λ_{exc} = 406 nm taken at temperatures indicated b) Decay time vs. temperature for YAG:Ce 0.033%, 0.33%, 1.0% and 3.33%.

single crystal where reabsorption may influence the experimentally observed decay time.

The most important observation in Fig. 5-5b is that the life time of the Ce^{3+} emission for the low dopant concentrations does not change in the temperature regime up to 600 K. Above 600 K the life time starts to decrease. Experimental limitations prevent the measurements of the life time at temperatures above 700 K and the quenching temperature $T_{50\%}$ cannot be determined. The present results show that the thermal quenching temperature for the Ce^{3+} emission in YAG:Ce is well above 600 K and is much higher than previously reported [11]. For the higher Ce-concentrations (1% or 3.3%) a shortening of the life time sets in above 400 K. The origin will be discussed below. The low temperature decay time, temperature of the onset of the shortening of the luminescence life time and the quenching temperature $T_{50\%}$ are summarized in Table 5-1 for YAG doped with 0.033, 0.333, 1 and 3.333% Ce^{3+}.

5.4 Discussion

The temperature and concentration dependent luminescence and luminescence decay time measurements provide new insights into the luminescence properties of Ce-ion in YAG and on the potential of this material to be applied as a phosphor in (high power) white light LEDs. These various aspects will be discussed below.

Table 5-1 Decay time at 4.2 K, onset of decay time quenching and quenching temperature $T_{50\%}$ for different Ce^{3+} concentrations in YAG

c(Ce^{3+})	0.033%	0.33%	1%	3.33%
$\tau_{4.2K}$ (ns)	63	65	61	67
onset quenching τ (K)	640	620	500	440
$T_{50\%}$ (K)	>>680	>>680	>680	680

5.4.1 Luminescence spectra

From the low temperature luminescence measurements on the YAG samples with the lowest Ce-concentration (0.033%) information is obtained on the Huang-Rhys parameter *S* for the electron-phonon coupling and the phonon energy. *S* is approximately 6, the energy of the dominant phonon mode coupling to the electronic 4f-5d transition is 200 cm^{-1} and the Stokes' shift of the emission is 2400 cm^{-1}. This Stokes' shift is smaller than Stokes' shifts that have previously been reported for the Ce^{3+} emission in YAG:Ce viz.3800 cm-1 [3], 3200 cm-1 [22] or 3770 cm-1 [11]. The discrepancy is explained by differences in the energy for the maximum of the emission band used to determine the Stokes' shift. In earlier work the maximum of the combined emission bands to the $^2F_{5/2}$ and $^2F_{7/2}$ levels was used or the emission maximum used was the value for the red-shifted emission band in a YAG:Ce sample with a higher (1-5%) Ce^{3+} concentration. The presently measured emission spectra show a shift of the emission maximum to longer wavelengths with increasing concentrations. Reabsorption of the high energy part of the emission and non-radiative energy transfer to Ce^{3+} ions which emit at a slightly lower energy can explain the continuous red-shift with increasing Ce-concentration. For the more accurate determination of the Stokes' shift the measurements for the lowest Ce-concentrations are used and the present data provide therefore a more accurate value for the Stokes' shift. Comparison with data in the literature, as collected by Dorenbos [25], shows that the Stokes' shift for the Ce-emission in YAG:Ce is smaller than for the Ce^{3+} emission in most other systems. Typically, Stokes' shift between 1000 and 8000 cm^{-1} are observed (although one has to keep in mind that not all the Stokes' shifts

have been determined correctly; just as for YAG:Ce, the Stokes' shifts are often overestimated). In view of the small Stokes' shift a high luminescence quenching temperature can be expected for the Ce^{3+} emission. This is in line with the high luminescence quenching temperature observed.
The present results on the phonon energy of the dominant vibrational mode coupling with the 4f-5d transition are in agreement with a recent paper by Grinberg et al. [26] where, based on the photoacoustic spectra of YAG:Ce, the phonon energy was estimated to be 200 cm^{-1}, in good agreement with the vibrational frequency observed in the low-temperature luminescence spectra. The Huang-Rhys parameter, deduced from the photoacoustic spectra in the same study, was however much higher, around 10, than the presently determined value of $S = 6$. From the parameters on the electron-phonon coupling a configurational coordinate diagram can be constructed for the 4f and 5d states of Ce^{3+} in YAG. It will be interesting to compare these experimental results to theoretical calculations on the excited 5d state of Ce^{3+} in YAG, which have recently been done [12].

5.4.2 Temperature dependence luminescence decay time

Now that we have determined the intrinsic luminescence properties of the Ce^{3+} ion in YAG, it is interesting to discuss the luminescence quenching behavior. At first sight the results are confusing: the observed temperature quenching behavior is different as a function of Ce-concentration, measuring technique (intensity or decay time) and excitation wavelength. To explain the various results shown in Figs. 5-4 and 5-5, first the intrinsic quenching temperature is established and after that the temperature dependence in the various Figures will be discussed. The most straightforward method to determine the luminescence quenching temperature is to measure the luminescence intensity as a function of temperature under identical experimental conditions as has been done for the results contained in Fig. 5-5. This method has however drawbacks, for example if the absorption strength is strongly temperature dependent. From the work of Robbins it is known that the absorption strength of the lower energy absorption band around 460 nm decreases with increasing temperature due to a redistribution over the different crystal field components of the $^2F_{5/2}$ ground state (the

transition from the second crystal field level of the $^2F_{5/2}$ level to lowest d-level being symmetry forbidden).

A more accurate determination of the intrinsic luminescence quenching temperature is possible by considering the temperature dependence of the luminescence decay time. The results in Fig. 5-5b show that for the sample with the lowest Ce-concentration the luminescence decay time is constant up to 600 K for the lowest doping level (0.033% Ce). This shows that indeed the luminescence decay time of this allowed 5d-4f emission band is not (strongly) temperature dependent and can be used to accurately determine the luminescence quenching temperature. The fact that the luminescence decay time is constant up to 600 K shows that the intrinsic quenching temperature for the Ce^{3+} in YAG is very high (well above 600 K), and is comparable or even better than that of the Eu^{2+} emission in Eu-doped nitride and oxonitride phosphors which have been introduced to replace YAG:Ce.

For the sample with 0.33% Ce, the luminescence decay time shows a small increase between 300 and 600 K and the decay time is slightly longer than for 0.033% sample (65 vs. 63 ns). These observations are explained by reabsorption. Because of the strongly allowed character of the 4f-5d transition, reabsorption may occur for the light emitted in the wavelength region where Ce^{3+} can reabsorb the emission (see the spectral overlap region in Fig. 5-2a). Reabsorption of emission leads to a lengthening of the experimentally measured life time. Since the spectral overlap increases with temperature, the reabsorption will also slightly increase with temperature and this can explain the small increase of the experimentally observed life time for the YAG sample doped with 0.33% of Ce^{3+} in the temperature regime between 300 and 600 K. For the samples with 1% and 3.33% of Ce^{3+} the luminescence quenching temperature is lower and quenching starts around 480 K (for the 1% sample) or 440 K (for the 3.33% sample). The lower quenching temperatures are explained by (thermally activated) concentration quenching. Thermal activation results from an increase of the spectral overlap with increasing temperature on the one hand (faster energy migration) and from a thermally activated trapping of the (migrating) excitation energy by defects (faster trapping) on the other hand. A quantitative analysis of the concentration quenching process is beyond the scope of the present chapter. Qualitatively, the observations

are well explained by this model. The lower quenching temperatures are observed for the more concentrated samples. The temperature dependence of the quenching due to thermally activated energy transfer to defects is also consistent with the work of Robbins [5-7].

5.4.3 Temperature dependence luminescence intensity

The measurements depicted in Fig. 5-4 show that the temperature dependence of the luminescence is complex: it varies as a function of both the Ce-concentration and excitation wavelength. Based on the discussion above it is clear that the intrinsic quenching temperature of the Ce-emission is well above 600 K. To explain the decrease in the emission intensity below 600 K several factors need to be considered.
For the lowest concentration the main contribution is from the temperature dependence of the oscillator strength. At higher temperatures the absorption strength decreases due to thermal population of the higher crystal field components of the $^2F_{5/2}$ ground state (see above). The lower absorption strength results in a lower light output, even though the quantum efficiency is constant. This explanation is consistent with both the wavelength dependence and the concentration dependence of the emission intensity as a function of temperature. For the lower concentrations the temperature quenching is less pronounced for excitation at longer wavelengths (as the excitation shifts from the maximum of the absorption band to the wings, from 450 to 490 nm, the “quenching temperature” increases). This is explained by the fact that in the center of the band, the absorption strengths decreases (as discussed above) but for the longer wavelengths this decrease is partially compensated by thermal broadening of the absorption band (see also Fig. 5-2) which increases the absorption strength in the long wavelength tail of the absorption band. The influence of the excitation wavelength is strongest for the lowest concentrations where the fraction of the light absorbed is proportional to the oscillator strength. For higher concentrations we move into the saturation regime where the fraction of absorbed light increases no longer linearly with the oscillator strength. For the highest concentration (3.33% of Ce) there is hardly any wavelength dependence observed indicating that for this concentration there is (almost)

complete saturation and the fraction of excitation light that is absorbed is close to 100% over the full width of the absorption band. The presently observed decrease of the luminescence intensity with increasing temperature is the opposite of the increase of the intensity that has been reported by Robbins for excitation in the higher energy 5d absorption band (excitation at 340 nm) upon increasing the temperature. Indeed, for this transition (to the higher energy 5d level) the oscillator strength increases upon increasing the temperature and for a (low concentration) YAG:Ce crystal an increase of the luminescence intensity is observed.

In addition to the influence of the oscillator strength, a second factor responsible for the decrease in luminescence intensity upon raising the temperature is thermally activated concentration quenching. As discussed above this gives rise to temperature quenching of the emission for the higher doped samples where energy migration to defects occurs. This observation is in line with the decrease in luminescence life time observed for the higher doped (1 and 3.33% Ce) samples in this temperature regime. For these higher concentrations the temperature quenching due to thermally activated concentration dominates.

From the discussion above it is clear that the low quenching temperature reported in the literature for the commercial YAG:Ce phosphor is not related to the intrinsic quenching temperature of the Ce^{3+} luminescence. For commercial YAG:Ce phosphors with relatively high Ce^{3+} concentration (1-5%) the mechanism behind the temperature quenching is thermally activated concentration quenching and is observed at temperatures above 400 K. For example, the temperature quenching reported by Setlur et al. [11] is very similar to the temperature dependence of the luminescence intensity shown in Fig. 5-2 for the sample with 3.3%. The fact that the temperature quenching of the luminescence in commercial YAG:Ce is due to thermally activated concentration quenching has important implications for industrial applications. With its intrinsic quenching temperature above 600 K for low activator concentrations, the temperature quenching behavior of YAG:Ce compares favorably to those of rare-earth activated nitride and oxonitride materials. In [27] we reported on the thermal quenching behavior of Eu^{2+} activated $SrSi_2O_2N_2$. The onset of thermal quenching was determined to be around 500 K. In the class of nitride materials the system $M_2Si_5N_8:Eu^{2+}$

(M = Ca, Sr, Ba) plays an important role [28-30]. In this material the emission intensity at 470 K was thermally quenched to about 90% of the initial emission intensity at RT [30]. Both the oxonitride and the nitride materials are discussed by Müller-Mach et al. for the use in an all-nitride white LED [30]. The present results show that the intrinsic quenching temperature of the Ce-luminescence is in fact higher than for some of the alternative LED phosphors suggested. In commercial YAG powder phosphors with Ce^{3+} concentrations above 1% thermal quenching by energy migration occurs. The same may be true for nitride and oxonitride phosphors doped with relatively high Eu^{2+} concentrations. To make use of the high thermal quenching temperature of YAG:Ce, one may use translucent ceramic YAG:Ce plates for color conversion [31,32]. Here one can choose smaller amounts of activator ions and compensate the loss in absorption strength by a longer optical path way, e.g. by increasing the thickness of the YAG:Ce ceramic disk.

5.5 Conclusion

Systematic research on the temperature dependence of the intensity and life time of the Ce^{3+} luminescence is reported for the widely applied YAG:Ce phosphor. Temperature dependent luminescence life time measurements for low Ce-concentrations (0.033%) show that the intrinsic quenching temperature of the Ce^{3+} is high (well above 680 K). The lower quenching temperatures reported for the commercial YAG:Ce phosphor is explained by thermally activated concentration quenching. The high luminescence quenching temperature offers possibilities for YAG:Ce to be applied in high power LEDs, provided that lower dopant concentrations are used. In addition, low temperature luminescence spectra are reported. For YAG doped with low Ce^{3+} concentrations zero-phonon lines and vibrational structure are observed in the excitation and emission spectra. Based on these measurements the Stokes' shift (~2400 cm^{-1}), Huang-Rhys parameter (S=6) and phonon energy (~200 cm^{-1}) have been determined for the 4f-5d luminescence. These parameters may be compared with results from theoretical calculations on the 5d excited state for Ce^{3+} in YAG.

References

1 G. Menzer, Z. Kristallogr. 69 (1928) 300.

2 G. Blasse, A. Bril, Appl. Phys. Lett. 11 (1967) 53.

3 G. Blasse, A. Bril, J. Chem. Phys. 47, 12 (1967) 5139.

4 J.T.C. Van Kemenade, J.T.W. De Hair, E.G. Berns, Patent EP0124175B1.

5 D.J. Robbins, B. Cockayne, J.L. Glasper, B. Lent, J. Electrochem. Soc. 126 (7) (1979) 1213.

6 D.J. Robbins, B. Cockayne, J.L. Glasper, B. Lent, J. Electrochem. Soc. 126 (7) (1979) 1221.

7 D.J. Robbins, J. Electrochem. Soc. 126 (9) (1979) 1550.

8 D.J. Robbins, B. Cockayne, B. Lent, J.L. Glasper, J. Electrochem. Soc. 126 (9) (1979) 1556.

9 T. Tamura, T. Setomoto, T.Taguchi, J. Lumin. 87-89 (2000) 1180.

10 K. Sakuma, N. Hirosaki, N. Kimura, M. Ohashi, R.-J. Xie, Y. Yamamoto, T. Suehiro, K. Asano, D. Tanaka, IEICE Trans. Electron., E88-C (2005) 2057.

11 A.A. Setlur, A.M. Srivastava, H.A. Comanzo, G. Chandran, H. Aiyer, M.V. Shankar, S.E. Weaver, Proceedings of SPIE Vol. 5187 (2004) 142.

12 L. Seijo, private communication.

13 J. Barzowska, A. Kubicki, M. Grinberg, S. Kaczmarek, Z. Łuczyński, A.J. Wojtowicz, Cz. Koepke, Acta Phys. Pol. A95 (1999) 395.

14 S.M. Kaczmarek, D.J. Sugak, A.O. Matkowskii, Z. Moroz, M. Kwaśny, A.N. Durygin, Nucl. Instrum. Methods D132 (1997) 647.

15 E. Zych, C. Brecher, J. Alloy. Comp. 300-301 (2000) 495.

16 E. Zych, C. Brecher, H. Lingertat, in: G.E. Matthews, R.T. Williams (Eds.), ICDIM96, Proc. 13th Int'l. Conf. on Defects in Insulating Materials, Trans Tech Publ, Switzerland, 1997, p. 257.

17 E. Zych, C. Brecher, H. Lingertat, in: C.R. Ronda, T.Welker (Eds.), Proc. 6th Intl. Conf. Lumin. Mat'l., Paris Jt. Mtg. 1997, Electrochem. Soc. Proc., Vol. 97-29, The Electrochemical Society Inc, 1998, p. 177.

18 Y. Pan, M. Wu, Q. Su, Mater. Sci. Eng. B 106 (2004) 251.

19 Y.C. Kang, I.W. Lenggoro, S.B. Park, K. Okuyama, Mater. Res. Bull. 35 (2000) 789.

20 T. Jüstel, J.-C. Krupa, D.U. Wiechert, J. Lumin. 93 (2001) 179.

21 J.F. Suyver, J. J. Kelly, A. Meijerink, J. Lumin. 104, 3 (2003) 187.

22 A.F. van Driel, G. Allan, C. Delerue, P. Lodahl, W.L. Vos, D. Vanmaekelbergh, Phys. Rev. Lett. 95 (2005) 236804.

23 S. Bigotta, D. Parisi, L. Bonelli, A. Toncelli, M. Tonelli, A. Di Lieto, J. Appl. Phys. 100 (2006) 013109.

24 J. Mareš, Czech. J. Phys. B 35 (1985) 883.
25 P. Dorenbos, J. Lumin. 91 (2000) 91.
26 M. Grinberg, A. Sikorska, S. Kaczmarek, J. Alloy. Comp. 300-301 (2000) 158.
27 V. Bachmann, T. Jüstel, A. Meijerink, C. Ronda, P.J. Schmidt, J. Lumin. 121 (2006) 441.
28 H. Huppertz, W. Schnick, Acta Crystallogr. C 53 (1997) 1751.
29 T. Schlieper, W. Milius, W. Schnick, Z. Anorg. Allg. Chem. 621 (1995) 1380.
30 R. Mueller-Mach, G. Mueller, M.R. Krames, H.A. Höppe, F. Stadler, W. Schnick, T. Juestel, P. Schmidt, phys. stat. sol. (a) 202 (No. 9) (2005) 1727.
31 W. Rosser, B. Wessler, Patent US 2004/0145308 A1
32 P. Schmidt, H. Bechtel, J. Meyer, Patent WO 2006/035353 A2

Chapter 6:
Thermal quenching and color tuning studies for $(Y,Gd)_3Al_5O_{12}$:Ce

For the widely applied white light LED-phosphor $Y_3Al_5O_{12}$:Ce (YAG:Ce) the influence of partial substitution of Y by Gd on the Ce^{3+} luminescence and temperature quenching is reported. Low Ce-doping concentrations (0.03 and 0.3%) are used to avoid concentration quenching or radiative reabsorption. The luminescence shows a pronounced red shift from 536 nm (for YAG:Ce) to 579 nm (for $Y_{0.25}Gd_{0.75}Al_5O_{12}$:Ce) while the quenching temperature decreases. The results are explained by an increase in the crystal field splitting and Stokes' shift upon substitution of Y^{3+} by Gd^{3+} ions in the YAG host lattice. In spite of the lower luminescence quenching temperature, (Y,Gd)AG:Ce is a promising phosphor for realizing white light LEDs with a lower color temperature.

6.1 Introduction

The rapidly expanding market for solid-state lighting creates a need for new phosphors with high conversion efficiencies, excellent thermal quenching behavior and emission in a spectral range that will make it possible to adapt the color points of the emitted light over a wide range (from 'cool' to 'warm' white). This becomes even more important in view of the fast development in the field of high power LEDs. Yttrium Aluminum Garnet ($Y_3Al_5O_{12}$ or YAG) doped with Ce^{3+} is at present one of most important luminescent materials that is applied in white light LEDs. YAG:Ce was first introduced as phosphor for fast cathode ray tubes [1]. In recent years the commercial and scientific interest in YAG:Ce has increased in view of its use as color converter in (In,Ga)N based phosphor converted LEDs (pcLEDs) [2,3]. The blue light emitted by the semiconductor chip is partly absorbed and efficiently converted to yellow light. The combination of the two colors yields white light with a high color temperature ('cool white'). This is acceptable for many applications but there is a strong need for LEDs generating light with a lower color temperature in general (home) lighting applications.

We recently investigated the luminescence quenching and the influence of the Ce^{3+} concentration in YAG:Ce on the thermal quenching behavior [4]. The thermal quenching was found to be strongly dependent on the Ce^{3+} concentration while the intrinsic luminescence quenching temperature for the Ce^{3+} luminescence was shown to be high (>700 K). In view of the demand for new luminescent materials for creating warm white light with pc-LEDs [5] here we report on investigations to spectrally shift the emission band in Gd^{3+}-co-doped (Y,Gd)AG:Ce phosphors. It is well known that changes in the chemical composition of YAG can be used to shift the emission spectrum. Pan et al. already reported on the effect of Gd^{3+} co-doping in YAG:Ce [6]. They observe a red shift in emission that was accompanied by a decrease in emission intensity. This was attributed to the difference in ionic radius between Y^{3+} (116 pm) and Gd^{3+} (119 pm). Their explanation for the red shift was based on a higher crystal field splitting due to the lattice expansion upon substitution of the smaller Y^{3+} ions by the larger Gd^{3+} ion. This is however not in line with the opposite behavior that is commonly reported in case of an expansion of a host lattice. This usually gives rise to a decrease of the crystal

field splitting, which will shift the 5d-4f emission to shorter wavelengths. An alternative explanation for the unexpected red shift in emission is given in Ref. [7] and references therein. There the red shift is attributed to an increase in local dopant-host interaction leading to a larger covalence on the Ce^{3+}-O^{2-} bond, which also increases the crystal field strength. The higher covalency is explained by the difference in electronegativity between the Y^{3+} and Gd^{3+} ions (Y_{EN} = 1.22, Gd_{EN} = 1.20). Reference [7] also shows thermal quenching data for the emission of Ga^{3+} and Tb^{3+} doped YAG:Ce. Their pure YAG compounds quench to about 60% of RT emission intensity at 250 °C while for co-doping 20% and more the intensity drops to values below 40% compared to RT.
In the work reported in the literature relatively high Ce^{3+} concentrations are used. Pan et al. used (Y,Gd)AG samples with 2% Ce^{3+} [6] while in Ref. [7] the concentration is probably around 1% Ce^{3+}, based on the thermal quenching behavior. Recently we have reported on the luminescence of YAG:Ce and shown that at higher Ce-concentrations the luminescence properties and luminescence quenching behavior are influenced by effects like reabsorption of the emission and concentration quenching. As a result, the luminescence properties do not reflect the luminescence of the isolated Ce^{3+} ions. In this chapter we investigate the influence of Gd co-doping in YAG:Ce by (temperature dependent) luminescence studies on $(Y,Gd)_3Al_5O_{12}:Ce^{3+}$ for low Ce-concentrations (0.03 and 0.3%). In addition to luminescence measurements over a wide temperature range (4-600 K) also temperature dependent luminescence life time measurements are reported to provide a better understanding on the influence of Gd co-doping on the luminescence and the luminescence quenching mechanism for Ce^{3+} in YAG.

6.2 Experimental

Samples were prepared using a precipitation method with urea and ammonium sulfate. Y_2O_3 (Aldrich 99.999 %) and Gd_2O_3 (Aldrich 99.99+ %) were dissolved in hydrochloric acid resulting in aqueous solutions of YCl_3 and $GdCl_3$ (each 0.5 mol/l). $AlCl_3$ (Aldrich 99.99%), $(NH_4)_2SO_4$ (Aldrich 99.999%), Urea (Aldrich, 99+%), and $CeCl_3{\cdot}7H_2O$ (Aldrich 99.999%) were dissolved in water. Different ratios of the Y^{3+} and Gd^{3+} solutions were added. The solution was heated slowly to 90-100 °C where precipitation started. The

solution was kept constant at this temperature for two to three hours. The precipitate was filtered, washed with water and dried at 100 °C. The crucible was placed in a bed of active carbon to create a reducing atmosphere. It was fired twice, at 1300 °C and 1700 °C, respectively, each time for two hours with a milling step in between. XRD analysis was done on a Philips diffractometer PW 1729 at RT, using Cu K_α radiation. All samples under investigation were single phased.
Luminescence spectra were recorded between 4 K and 300 K on a Spex Fluorolog 2 spectrofluorimeter equipped with a helium flow cryostat [8]. Luminescence spectra were recorded between 300 and 600 K on a modified spectrofluorimeter system FL900 of Edinburgh Instruments using a Xe-lamp as excitation source. The spectra were measured with a spectral resolution of 0.5 to 1.0 nm. The complete set-up is described in more detail in [9]. Luminescence lifetimes were obtained using a Pico Quant picosecond laser (λ_{exc} = 406 nm) with a repetition rate of 1 MHz. The signal was detected using a fast Hamamatsu photomultiplier tube. The details of the set-up are described in [10]. For life time measurements up to 700 K a homemade heating cell connected to a temperature controller was used.

6.3 Results and Discussion

6.3.1 Luminescence properties

In Fig. 6-1 the room temperature (RT) emission spectra are shown for $(Y_{1-x}Gd_x)_3Al_5O_{12}:Ce^{3+}$ 0.3%. A broad 5d-4f emission band is observed for all samples. The RT the emission spectra do not resolve the spin-orbit split Ce^{3+} ground state ($^2F_{5/2}$, $^2F_{7/2}$) [4]. The 5d-4f emission band of Ce^{3+} shifts to longer wavelengths as the Gd-concentration increases, in agreement with the shifts reported in Refs. [6] and [7]. In the presently studied series the emission maxima shift from 536 nm (x = 0) to 579 nm (x = 0.75) for excitation at 450 nm. Also the full width at half maximum (FWHM) increases from 3464 to 3863 cm^{-1} for x = 0 and 0.75, respectively. The emission maximum for pure YAG:Ce is in agreement with the emission maximum reported in [11].
For the as-prepared samples relative quantum efficiencies (QE) were measured and found to be 1.0, 0.86, 0.91 and 0.71 for 0, 25, 50 and 75%

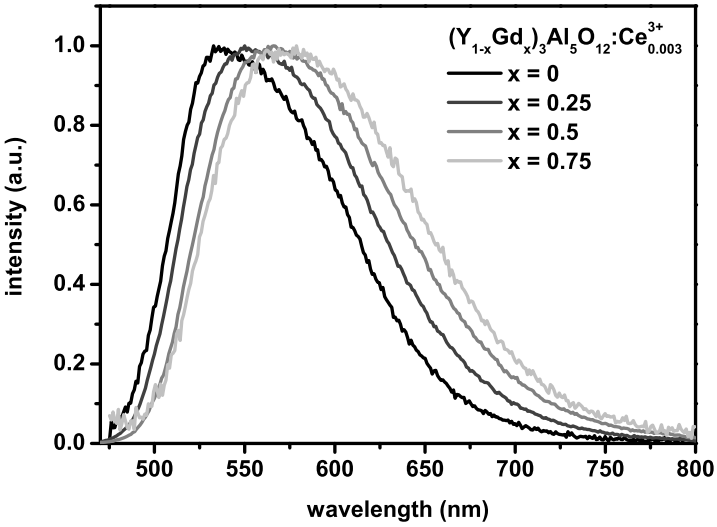

Figure 6-1 Normalized emission spectra of $(Y_{1-x}Gd_x)_3Al_5O_{12}:Ce^{3+}$ 0.3% (x = 0, 0.25, 0.5, 0.75) recorded for an excitation wavelength of 450 nm at RT.

Gd^{3+}, respectively. The quantum efficiency of the reference sample (the one without Gd^{3+}) was set to 1.0. The actual quantum efficiency of this sample was compared to and found to equivalent with commercial phosphors. The synthesis used was not optimized for yield, morphology or particle size distribution. The results show that even without these efforts highly efficient phosphors can be obtained.

In Figure 6-2 the excitation spectra for the emission of 0.3% Ce^{3+} in the four samples are depicted. All spectra show two broad excitation bands, which are attributed to the excitation from the 4f ground level into the two lowest 5d-sublevels. Additionally, for the samples containing Gd^{3+} sharp excitation peaks centered at 277 and 310 nm (the latter very weak) are seen. The sharp features are attributed to 4f-4f transitions in Gd^{3+}, viz. excitation from the $^8S_{7/2}$ ground state to the ^6I_J and ^6P_J excited states, respectively. The RT excitation spectra were recorded for the emission maxima (wavelengths of 536, 555, 555 and 579 nm for 0, 25, 50 and 75% Gd^{3+}, respectively). As for the emission spectra shown in Fig. 6-1 the widths of the excitation bands increases for higher Gd-concentrations. The positions of the maxima of the two d-sublevel shift in opposite directions

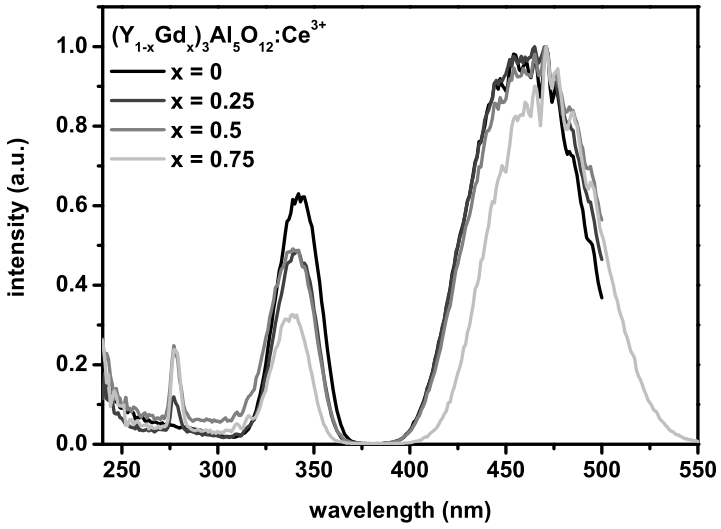

Figure 6-2 Normalized excitation spectra of $(Y_{1-x}Gd_x)_3Al_5O_{12}:Ce^{3+}$ 0.3% (x = 0, 0.25, 0.5, 0.75) recorded at an emission wavelength of 536 nm, 555 nm, 555 nm and 579 nm for x = 0, 0.25, 0.5 and 0.75, respectively; all taken at RT.

upon raising the Gd^{3+} concentration. The energy difference between the d_1- and d_2-sublevels, $\Delta_{d1\text{-}d2}$, was determined to be 7549 cm^{-1} for the pure YAG:Ce^{3+} and to increase upon introducing Gd^{3+} to the lattice to 7728, 8040 and 8309 cm^{-1} for 25, 50 and 75% Gd^{3+}, respectively. Also the Stokes' shift (SS) increases. For an accurate determination of the Stokes' shift, low temperature excitation and emission spectra are required as discussed in Ref. [4] where the Stokes' shift was determined to be 2400 cm^{-1} for the $5d_1$-$^2F_{5/2}$ luminescence. Here, we estimate the Stokes' shift by taking the energy difference between the maximum of the d_1 excitation band and the $5d_1$-($^2F_{5/2}$,$^2F_{7/2}$) emission band maximum, which leads to somewhat larger values then the actual SS. From the RT spectra this Stokes' shift was determined to 3035, 3416, 3791 and 4006 cm^{-1} for increasing Gd^{3+} concentrations from $x = 0$ to 0.75.

In Figure 6-3 the diffuse reflection spectra between 300 and 600 nm of the four samples are shown. The absorption bands for f-d transitions to the two lowest d-sublevels are shown. The splitting between the d_1 and the d_2 bands increases while also broadening is observed, in agreement with the trends observed in the excitation spectra shown in Fig. 6-2.

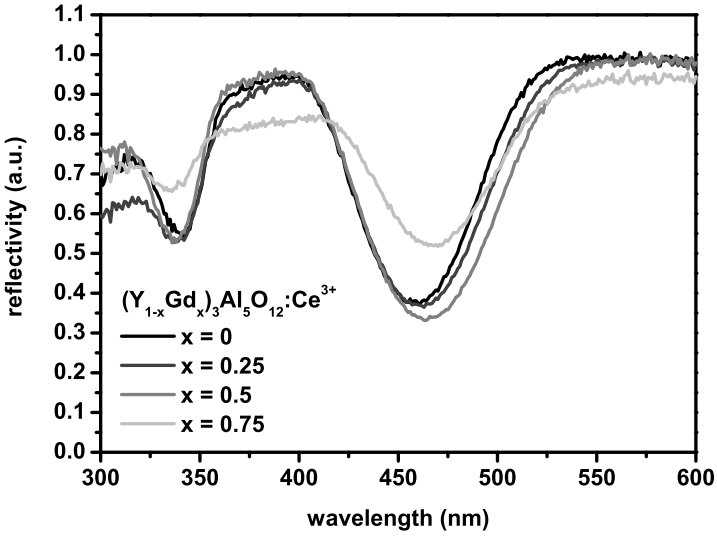

Figure 6-3 Reflection spectra of $(Y_{1-x}Gd_x)_3Al_5O_{12}:Ce^{3+}$ 0.3% (x = 0, 0.25, 0.5, 0.75) recorded between 300 and 600 nm at RT.

6.3.2 Thermal quenching behavior

To investigate the thermal quenching behavior of the various compounds, luminescence spectra and luminescence decay curves were recorded over a wide temperature range, between 25 and 600 K for the emission intensities and between 300 and 600 K for the luminescence decays. Previously, we reported on the temperature quenching for Ce-luminescence in pure YAG [4]. The results for this compound are compared to the results for the samples containing 25, 50 and 75% Gd^{3+} to analyze the influence of the co-dopant on the thermal quenching behavior. Temperature dependent emission spectra were recorded for excitation wavelengths of 465 and 340 nm, into the d_1- and the d_2-sublevel, respectively. The decay times were measured for an excitation wavelength of 406 nm. This wavelength was set by the (In,Ga)N picosecond-diode laser and corresponds to excitation in the high energy tail of the d_1 level. All decay curves measured were found to be single exponential.
Figure 6-4 shows the emission intensities (both for d_1 and d_2 excitation) and the decay times as a function of temperature for the sample containing 0.3% Ce^{3+} and 50% Gd^{3+}. The emission intensity upon 465 nm (d_1) excitation at 25 K was set to unity. In the temperature range 25 to 400 K there is a

clear difference in the temperature dependence of the emission intensity for d_1 and d_2 excitation. For excitation in the d_2 band, the intensity increases upon raising the temperature to 300 K. For excitation into the d_1 level a small decrease is observed. This behavior was observed and explained before by Robbins [12]. It is caused by the temperature dependence of the absorption strength for transitions to the two d-sublevels and originates from a temperature dependent population of the lowest crystal field components of the $^2F_{5/2}$ ground state multiplet (see also Refs. [4] and [12]). This behavior is not related to luminescence quenching. For an accurate determination of the luminescence quenching temperature, temperature dependent luminescence life time measurements give more insight.

The luminescence decay times of the Ce^{3+} emission were measured between RT and 700 K. The results are shown in Fig. 6-4. Shortening of the decay is indicates the onset of non-radiative decay processes (luminescence quenching). The shortening of the decay time starts above 400 K. The luminescence quenching temperature $T_{50\%}$ (defined as the temperature at which the intensity of decay time has dropped to 50% of the low temperature

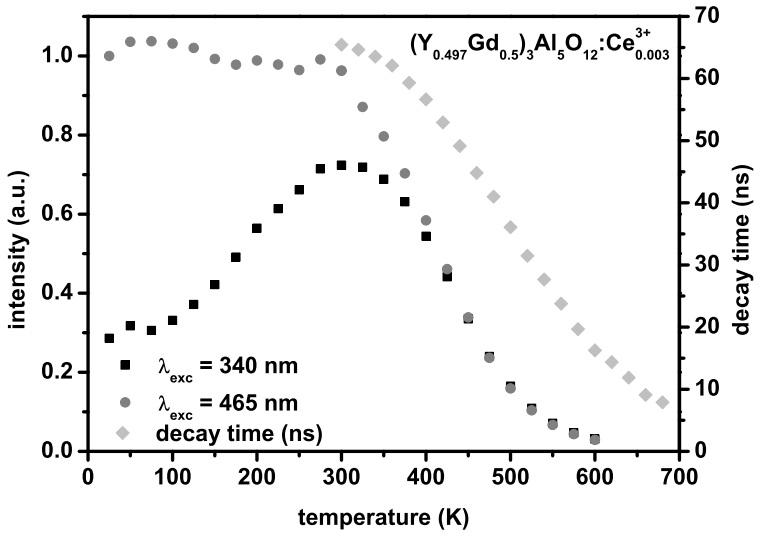

Figure 6-4 Temperature dependent decay times (light gray diamonds) and emission intensities for excitation wavelengths of 340 nm (black squares) and 465 nm (gray circles).

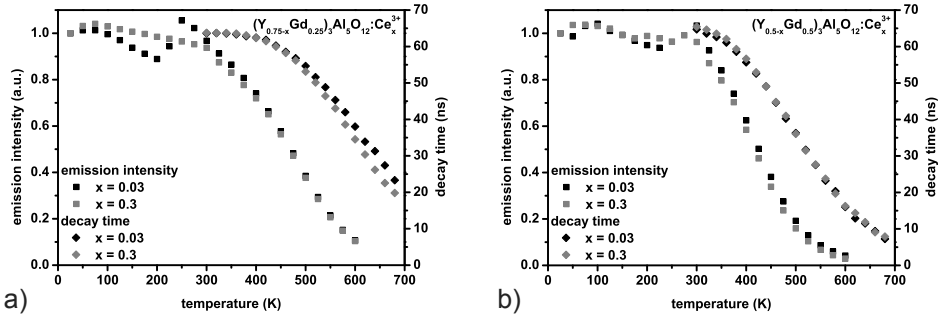

Figure 6-5 Temperature dependent emission intensities (quares) and luminescent decay times (diamonds) for 0.03% (black) and 0.3% (gray) Ce^{3+} in (a) $(Y_{0,75-x}Gd_{0,25})_3Al_5O_{12}$ and (b) $(Y_{0,5-x}Gd_{0,5})_3Al_5O_{12}$, respectively.

value) determined from the temperature dependent life time measurements is about 500 K. The fact that the luminescence intensity starts to drop at lower temperatures ($T_{50\%}$ = 425 K) is probably related to (thermally activated) energy transfer to quenching centers for part of the Ce^{3+} ions, although the origin for the discrepancy is not completely clear [4,12].

To investigate if the thermal quenching behavior is different for a lower Ce^{3+} concentration, luminescence life times and the emission intensity were recorded as a function of temperature for $(Y_{0.75},Gd_{0.25})_3Al_5O_{12}$ and $(Y_{0.5},Gd_{0.5})_3Al_5O_{12}$ doped with 0.03% Ce^{3+} and 0.3% Ce^{3+}. The results show that there is no significant difference for the two Ce^{3+} concentrations (Figure 6-5). The luminescence quenching temperatures determined from the emission intensities is about 470 K while the $T_{50\%}$ determined from the decay times is around 620 K for the sample with 25% Gd^{3+}. For the samples with 50% Gd^{3+} the quenching temperatures are lower, 510 K from the luminescence life time measurements and 420 K from the temperature dependence of the emission intensities. Again, no significant difference is observed between the results for the two (low) Ce-concentrations, indicating that temperature dependent energy migration does not play an important role at these low concentrations. Note that the lower quenching temperatures for the Ga and Tb co-doped systems as reported in Ref. [7] can be explained by thermally activated concentrations quenching in these higher doped systems [4].

In Figure 6-6 the temperature dependence of the emission intensity for the four samples with 0.3% Ce^{3+} and different Gd^{3+} concentrations is shown. The

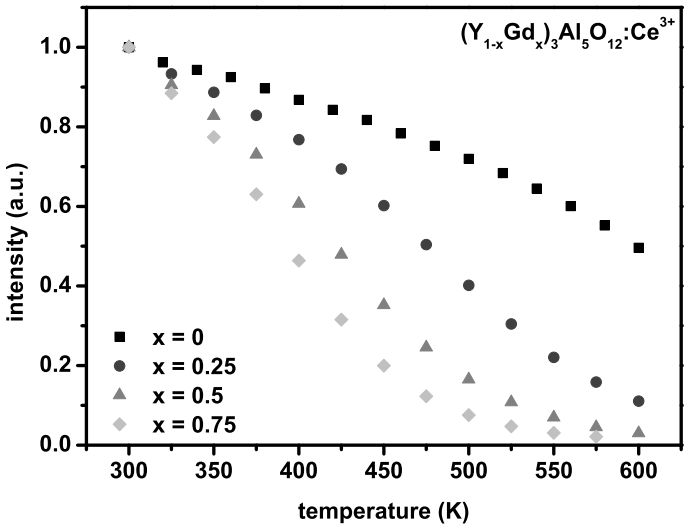

Figure 6-6 Temperature dependent emission intensities for $(Y_{1-x}Gd_x)_3Al_5O_{12}:Ce^{3+}$ 0.3% (x = 0, 0.25, 0.5, 0.75) recorded between 300 and 600 K excited at 465 nm.

emission intensity at 300 K was normalized to unity for all samples. The quenching temperatures $T_{50\%}$ are 600, 475, 420 and < 400 K for 0, 25, 50 and 75% Gd^{3+}, respectively.

The results from both the temperature dependence of the luminescence life times and emission intensities show that the quenching temperature decreases upon substitution Y by Gd. This trend can be explained by the simple configurational coordinate model [13]. The luminescence spectra show that the Stokes' shift increases for the Ce^{3+} emission in the compounds with a higher Gd^{3+} concentration. A larger Stokes' shift indicates that the relaxation in the excited state is larger: for higher Gd^{3+} co-doping levels, ΔR (the difference between the equilibrium metal-ligand distance of the ground state R_0 and the excited state R_0') is larger. It is well known that a larger relaxation in the excited state leads to lower luminescence quenching temperatures. The quenching mechanism is thermally activated cross-over from higher vibrational levels of the excited state to the ground state and not thermally activated photoionization. Further evidence for this quenching mechanism may be obtained from thermally activated photoconductivity measurements. If thermally activated cross-over is the operative quenching

mechanism, the luminescence quenching is not expected to coincide with an onset of photoconductivity.

6.4 Conclusion

The luminescence properties of $(Y_{1-x}Gd_x)_3Al_5O_{12}:Ce^{3+}$ have been investigated for x = 0, 0.25, 0.5 and 0.75 for low Ce^{3+} doping levels (0.03 and 0.3%). The partial substitution of Y by Gd in YAG:Ce causes a significant red shift of the emission (from 536 to 579 nm) and lower luminescence quenching temperatures. The red shift is explained by an increase of both the Stokes' shift and the crystal field splitting for systems with a higher Gd-content. The decrease in the luminescence quenching temperature is related to the increase in Stokes' shift, indicating a larger relaxation in the excited 5d state. In spite of the lower quenching temperature of the Ce^{3+} emission for higher Gd-concentrations, the substitution of Y by Gd is a promising method to obtain warmer white light LEDs.

References

1 G. Blasse, A. Bril, Appl. Phys. Lett. 11 (2) (1967) 53.
2 T. Tamura, T. Setomoto, T.Taguchi, J. Lumin. 87-89 (2000) 1180.
3 P. Schlotter, J. Baur, Ch. Hielscher, M. Kunzer, H. Obloh, R. Schmidt, J. Schneider, Mater. Sci. Eng. B 59 (1999) 390.
4 V. Bachmann, C. Ronda, A. Meijerink, to be published.
5 R. Mueller-Mach, G. Mueller, M.R. Krames, H.A. Höppe, F. Stadler, W. Schnick, T. Juestel, P. Schmidt, phys. stat. sol. (a) 202 (2005) 1721.
6 Y. Pan, M. Wu, Q. Su, J. Phys. Chem. Sol 65 (2004) 845.
7 A.A. Setlur, A.M. Srivastava, H.A. Comanzo, G. Chandran, H. Aiyer, M.V. Shankar, S.E. Weaver, Proceedings of SPIE Vol. 5187 (2004) 142.
8 S.H.M. Poort, J.W.H. van Krevel, R. Stomphorst, A.P. Vink, G. Blasse, J. Solid State Chem. 122 (1996) 432.
9 T. Jüstel, J.-C. Krupa, D.U. Wiechert, J. Lumin. 93 (2001) 179.
10 A.F. van Driel, G. Allan, C. Delerue, P. Lodahl, W.L. Vos, D. Vanmaekelbergh, Phys. Rev. Lett. 95 (2005) 236804.
11 P. Dorenbos, J. Lumin. 91 (2000) 155.

12 D.J. Robbins, J. Electrochem. Soc. 126 (9) (1979) 1550.

13 G. Blasse, B.C. Grabmaier, Luminescent Materials (1994) Springer, Berlin.

Samenvatting

Dit proefschrift gaat over luminescerende materialen, ook wel fosforen genoemd, die in licht emitterende dioden (LEDs) licht van kleur veranderen. In het proefschrift wordt optisch onderzoek aan nieuwe en bekende materialen beschreven. Het doel van het onderzoek was het verklaren van de luminescentiemechanismen en van de processen die tot doven van de emissie leiden. Deze informatie is belangrijk voor de ontwikkeling van betere fosforen voor toepassing in het zich snel ontwikkelende veld van de vaste stof verlichting.

In het proefschrift kunnen twee delen worden onderscheiden. Het eerste deel bestaat uit de hoofdstukken 2, 3 en 4. Deze hoofdstukken gaan over oxonitridosilikaten (sion) en aluminooxonitridosilikaten (sialon), gedoteerd met Eu^{2+} en Yb^{2+}. Het tweede deel omvat de hoofdstukken 5 en 6. Deze gaan over yttrium aluminium granaat (YAG), gedoteerd met Ce^{3+} en/of Gd^{3+}.

In hoofdstuk 2 worden de optische eigenschappen van $Sr_2Si_2O_2N_2$ gedoteerd met Eu^{2+} en Yb^{2+} onderzocht. Het Eu^{2+} gedoteerde materiaal laat efficiente groene emissie zien met een maximum bij 540 nm. Dit is consistent met een $4f^65d^1 \rightarrow 4f^7$ overgang op Eu^{2+}. Het quantum rendement en de thermische dooftemperatuur van de luminescentie zijn erg hoog (respectievelijk 90% en > 500 K). Daarom is dit een veelbelovend materiaal voor toepassing in fosforgeconverteerde LEDs. De Yb^{2+} emissie verschilt erg van die van Eu^{2+} en wordt gekenmerkt door een grotere Stokes' shift en een lagere dooftemperatuur. The anomale luminescentie eigenschappen worden toegeschreven aan emissie van een exciton dat aan een onzuiverheid gebonden is. Gebaseerd op temperatuur- en tijdsafhankelijke luminescentiemetingen zijn de energieniveaus voor zowel Eu^{2+} als Yb^{2+} t.o.v. de valentie- en geleidingsband van het oxonitridosilikaat afgeleid.

In hoofdstuk 3 wordt beschreven hoe de emissiekleur van de LED fosfor $Sr_{1-x-y-z}Ca_xBa_ySi_2O_2N_2:Eu_z^{2+}$ ($0 \leq x, y \leq 1$; $0.005 \leq z \leq 0.16$) kan worden afgestemd. De emissiekleur kan op twee manieren worden gevarieerd: door het veranderen van de Eu^{2+} concentratie en door de substitutie van het moederrooster kation Sr^{2+} door of Ca^{2+} of Ba^{2+}. Het verhogen van de Eu^{2+} concentratie resulteert in een roodverschuiving van de emissie voor Eu^{2+} concentraties hoger dan 2% De roodverschuiving wordt verklaard

door energie migratie en energieoverdracht naar Eu^{2+} ionen die bij langere golflengten licht uitzenden. Gekoppeld aan de (gewenste) roodverschuiving treedt er ook een (ongewenste) verlaging op van het quantum rendement en de thermische dooftemperatuur. Dit is het gevolg van concentratiedoving. Gedeeltelijke vervanging van Sr^{2+} door Ca^{2+} of Ba^{2+} resulteert eveneens in een roodverschoven Eu^{2+} emissie. Voor Ca^{2+} is dit in lijn met de verwachting en wordt de roodverschuiving verklaard door een sterkere kristalveldsplitsing voor Eu^{2+} op de (kleinere) Ca^{2+} kation roosterplaats. Voor Ba^{2+} is de roodverschuiving verrassend. Vaak wordt een blauwverschuiving van de d-f emissie waargenomen wanneer Sr^{2+} door het grotere Ba^{2+} vervangen wordt. Temperatuur afhankelijke luminescentiemetingen laten zien dat de dooftemperatuur lager wordt wanneer Sr door Ca wordt vervangen, terwijl bij Ba substitutie de dooftemperatuur hoog blijft. Het afstemmen van de kleur door gedeeltelijke vervanging van Sr^{2+} door Ba^{2+} is daarom een veelbelovende weg om het kleurpunt van LEDs te verschuiven met behoud van het hoge quantumrendement en de hoge thermische dooftemperatuur.

Tot slot van het eerste gedeelte van het proefschrift beschrijft hoofdstuk 4 de optische eigenschappen van $SrSi_2AlO_2N_3$, gedoteerd met Eu^{2+} and Yb^{2+}, voor mogelijke toepassing in LEDs. Het materiaal, gedoteerd met Eu^{2+}, laat groene emissie met een maximum rond de 500 nm zien. De emissie wordt toegeschreven aan de $4f^65d^1 \rightarrow 4f^7$ overgang op Eu^{2+}. In verband met het te lage quantumrendement bij de high power LED bedrijfstemperatuur en de te lage dooftemperatuur is deze fosfor minder geschikt voor toepassing in fosforgeconverteerde LEDs. The Yb^{2+} emissie laat dezelfde anomalie zien als die van Eu^{2+} zoals beschreven in hoofdstuk 2: een roodverschoven emissie, een grotere breedte van de emissieband, een grote Stokes' shift en ook een lagere dooftemperatuur. De emissie wordt toegeschreven aan een self-trapped exciton emissie. De Yb^{2+} geaktiveerde fosfor is niet geschikt voor toepassing in fosforgeconverteerde LEDs.

Het tweede deel van dit proefschrift gaat over YAG gedoteerd met gadolinium en/of cerium. In hoofdstuk 5 wordt de thermische doving van de luminescentie van YAG:Ce beschreven. De temperatuurafhankelijkheid van de emissie intensiteit en de luminescentie vervaltijden in een breed Ce-concentratie gebied (tussen 0.033% en 3.3%) worden gerapporteerd. Er wordt aangetoond dat de intrinsieke dooftemperatuur van de Ce-emissie erg hoog is

(> 680 K). De lagere dooftemperaturen die in de literatuur worden vermeld, worden verklaard m.b.v. thermisch geaktiveerde concentratiedoving (voor hoog gedoteerde systemen) en een temperatuurafhankelijke oscillatorsterkte (voor laag gedoteerde systemen). Bovendien worden hoge resolutie spectra getoond waaruit de positie van de zero-phonon lijn (20450 cm^{-1}), de Stokes' shift (2400 cm^{-1}), de energie van de dominante vibratie (200 cm^{-1}) en de Huang-Rhys parameter (S= 6) bepaald zijn. Deze parameters kunnen als basis dienen voor de vergelijking van deze resultaten met die van *ab initio* berekeningen van de positie en de relaxatie van de aangeslagen 5d toestand van Ce^{3+} in YAG.

Tenslotte wordt in het laatste hoofdstuk (hoofdstuk 6) van dit proefschrift de invloed beschreven van gedeeltelijke vervanging van Y door Gd in de veelvuldig toegepaste fosfor $Y_3Al_5O_{12}$:Ce (YAG:Ce) op de Ce^{3+} luminescentie en de thermische doving daarvan. Lage Ce concentraties (0.03% en 0.3%) werden gebruikt om concentratiedoving of reabsorptie te vermijden. De emissie laat een grote roodverschuiving zien van 536 nm (voor YAG:Ce) naar 579 nm (voor $Y_{0.25}Gd_{0.75}Al_5O_{12}$:Ce), waarbij de thermische dooftemperatuur lager wordt. De resultaten worden verklaard door een toename van de kristalveldsplitsing en de Stokes' shift wanneer Y^{3+} door Gd^{3+} wordt vervangen in het YAG grondrooster. Ondanks de lagere thermische dooftemperatuur is (Y,Gd)AG:Ce een veelbelovende fosfor om witte LEDs met een lagere kleurtemperatuur te realiseren.

Acknowledgements

This is the part where it's on me to say thanks to a number of people that helped me in accomplishing the work presented in this thesis. Of course there are many of the named ones that would need to stand first. Since this is not possible the position at which one stands has nothing to do with the importance of his or her contribution. Since I worked in two places, University Utrecht and Philips Research Aachen, two groups are to be thanked.
My first thanks go to Andries Meijerink and Cees Ronda as my promoters. In the last years you have taught me a lot, showed me a lot and sometimes nearly drove me crazy. But for the latter I am very thankful, since it broadened my horizon in more terms than just science.
I am thankful to Professors John Kelly, Daniël Vanmaekelbergh and Jaap Dijkhuis of the University Utrecht and Professor Pieter Dorenbos of the Technical University Delft for being part of my reading committee.
Where would we (Ph.D.) students stand without the support of technicians? Hans Ligthart and Stephan Zevenhuizen, thanks for helping out if something broke or didn't work for whatever reason.
Much of my time in Utrecht I spent with measuring spectra and decay times. It took me a while to get familiar with all the different setups, therefore thanks to Celso de Mello Donegá, Peter Vergeer and Arjan Houtepen for showing me how to operate all the lasers, spectroscopes and cryostats.
Sven Rühle and Harald de Wijn, I thank you for the hospitality in sharing the room with me whenever work had to be done in Utrecht.
Finally I like to thank all the other current and former Ph.D. students who always made me feel welcome on my visits to Utrecht.
In my Aachen work place I first like to thank Prof. Thomas Jüstel for making it possible in the first place that I was given the chance to do my Ph.D. thesis in corporation with Philips Research Laboratories.
Peter Schmidt, Jörg Meyer and Andreas Tücks thanks for valuable discussion on different topics of my work. The spectroscopy cluster, namely Detlef Wiechert, Dieter Wädow, Petra Huppertz and Henning Ohland – thanks for numerous measurements and for discussions regarding the interpretation of the results. Hans-Dieter Bausen is acknowledged for the help regarding XRD measurements.

Preparing samples of luminescent materials was one of the keys in my thesis. Baby Schreinemacher, Walter Mayr and Herbert Schreinemacher it was a great pleasure to get to know you and to learn from you.
The discussions with Professor Wolfgang Schnick and Florian Stadler, both of the University Munich, are acknowledged as well.
The workshop organized around Helmut Grosche and Peter Falter cannot be thanked enough. Whenever there was something to do or something broke everyone in the whole team was very helpful in fixing the problem. The same is true for the warehouse crew.
Throughout my work I had mainly two room mates, Carolina Ribbing and Baby Schreinemacher. Thanks for the good time and nearly endless amounts of Gummibärchen.
Of course there are many more people that belong or used to belong to the group Solid State Lighting. Thanks for being there if there were questions I really enjoyed my time as part of your group. The Carnival organization committee around Eberhard Waffenschmidt, Christoph Martiny and Stephan Borucki-Häfner, I had a blast being part of the Carnival band 2007 – to you and all the others involved: Drei Mal Oche - Alaaf, PFL – Alaaf, Oche – Alaaf.
Since no one can deliver good work without friends and a hobby that makes the spare time more pleasant my thanks go out to the Korneliusbläser and the Musikverein Hahn for a lot of fun and good music. Bernd und Claudia thanks for being there whenever I needed you and I hope our friendship will last regardless of the distance that separates us.
Zum guten Schluss bleibt noch der Dank an meine Familie. Es war eine lange Zeit hier in Aachen und sie war nicht immer einfach. Trotzdem habt ihr mich in jeder nur erdenklichen Weise unterstützt und ohne euch wäre ich sicher jetzt nicht an diesem Punkt angekommen.

To all: thank you, Dankeschön and bedankt.

List of publications

Chapter 2:
V. Bachmann, T. Jüstel, A. Meijerink, C. Ronda, P.J. Schmidt – Luminescence properties of $SrSi_2O_2N_2$ doped with divalent rare earth ions – J. Lumin. 121 (2006) 441

Chapter 3:
V. Bachmann, C. Ronda, A. Meijerink – Color point tuning for $Sr_{1-x-y-z}Ca_xBa_ySi_2O_2N_2:Eu_z^{2+}$ ($0 \leq x, y \leq 1$; $0.005 \leq z \leq 0.16$) – in preparation

Chapter 4:
V.Bachmann, A. Meijerink, C. Ronda – Luminescence properties of $SrSi_2AlO_2N_3$ doped with divalent rare earth ions – submitted to J. Lumin.

Chapter 5:
V.Bachmann, C. Ronda, A. Meijerink – Temperature Quenching of the yellow Ce^{3+} Luminescence in YAG:Ce – to be submitted

Chapter 6:
V. Bachmann, A. Meijerink, C. Ronda – Thermal quenching and color tuning studies for $(Y,Gd)_3Al_5O_{12}$:Ce – to be submitted

Curriculum Vitae

Volker Bachmann was born on 21st of June 1977 in Leipzig, Germany. In 1998 he got his Abitur („High School Diploma“) from the Städtisches Gymnasium Schmallenberg (Schmallenberg, Germany). He went on to study Chemical Engineering at the University of Applied Sciences Münster, located in Steinfurt, Germany. The main course of studies was focused on Applied Material Science and Plastics Technology. He served as a student assistant in the field of luminescent materials. His diploma thesis in 2002 was on „Synthesis and Optical Properties of Gallium doped Zeolites“. This work was supervised by Prof. dr. Ulrich Kynast. Starting in the second year of studies he became a scholar of the German Merit Foundation (Studienstiftung des deutschen Volkes) until finishing the course of studies. During this time he held internship positions in Japan, Germany and the USA.

Starting in 2003 he became Ph.D. student at the University Utrecht on assignment at the Philips Research Laboratories in Aachen, Germany. The Ph.D. project was supervised by Prof. dr. Andries Meijerink and Prof. dr. Cees Ronda. Most of the results from this project are described in this thesis and are or will be published in scientific journal.

Since August 2007 he holds a position as a scientist at the Centrum für Angewandte Nanotechnologie (CAN) GmbH in Hamburg, Germany.